VEHICLE DYNAMICS

FACHHOCHSCHULE REGENSBURG
UNIVERSITY OF APPLIED SCIENCES
HOCHSCHULE FÜR
TECHNIK
WIRTSCHAFT
SOZIALES

LECTURE NOTES

Prof. Dr. Georg Rill

download: http://homepages.fh-regensburg.de/%7Erig39165/

Contents

1 Introduction

1.1 Terminology

1.1.1 Vehicle Dynamics

The Expression ’Vehicle Dynamics’ encompasses the interaction of

- driver,
- vehicle
- load and
- environment

Vehicle dynamics mainly deals with

- the improvement of active safety and driving comfort as well as
- the reduction of road destruction.

In vehicle dynamics

- computer calculations
- test rig measurements and
- field tests

are employed.

The interactions between the single systems and the problems with computer calculations and/or measurements shall be discussed in the following.

1.1.2 Driver

By various means of interference the driver can interfere with the vehicle:

$$\text{driver} \left\{ \begin{array}{ll} \text{steering wheel} & \text{lateral dynamics} \\ \left.\begin{array}{l}\text{gas pedal}\\ \text{brake pedal}\\ \text{clutch}\\ \text{gear shift}\end{array}\right\} & \text{longitudinal dynamics} \end{array} \right\} \longrightarrow \text{vehicle}$$

The vehicle provides the driver with some information:

$$\text{vehicle} \left\{ \begin{array}{ll} \text{vibrations:} & \text{longitudinal, lateral, vertical} \\ \text{sound:} & \text{motor, aerodynamics, tires} \\ \text{instruments:} & \text{velocity, external temperature, ...} \end{array} \right\} \longrightarrow \text{driver}$$

The environment also influences the driver:

$$\text{environment} \left\{ \begin{array}{l} \text{climate} \\ \text{traffic density} \\ \text{track} \end{array} \right\} \longrightarrow \text{driver}$$

A driver's reaction is very complex. To achieve objective results, an "ideal" driver is used in computer simulations and in driving experiments automated drivers (e.g. steering machines) are employed.

Transferring results to normal drivers is often difficult, if field tests are made with test drivers. Field tests with normal drivers have to be evaluated statistically. In all tests, the driver's security must have absolute priority.

Driving simulators provide an excellent means of analyzing the behavior of drivers even in limit situations without danger.

For some years it has been tried to analyze the interaction between driver and vehicle with complex driver models.

1.1.3 Vehicle

The following vehicles are listed in the ISO 3833 directive:

- Motorcycles,
- Passenger Cars,
- Busses,
- Trucks

- Agricultural Tractors,
- Passenger Cars with Trailer
- Truck Trailer / Semitrailer,
- Road Trains.

For computer calculations these vehicles have to be depicted in mathematically describable substitute systems. The generation of the equations of motions and the numeric solution as well as the acquisition of data require great expenses.

In times of PCs and workstations computing costs hardly matter anymore.

At an early stage of development often only prototypes are available for field and/or laboratory tests.

Results can be falsified by safety devices, e.g. jockey wheels on trucks.

1.1.4 Load

Trucks are conceived for taking up load. Thus their driving behavior changes.

$$\text{Load} \left\{ \begin{array}{l} \text{mass, inertia, center of gravity} \\ \text{dynamic behaviour (liquid load)} \end{array} \right.$$

In computer calculations problems occur with the determination of the inertias and the modelling of liquid loads.

Even the loading and unloading process of experimental vehicles takes some effort. When making experiments with tank trucks, flammable liquids have to be substituted with water. The results thus achieved cannot be simply transferred to real loads.

1.1.5 Environment

The Environment influences primarily the vehicle:

$$\text{Environment} \left\{ \begin{array}{ll} \text{Road:} & \text{irregularities, coefficient of friction} \\ \text{Air:} & \text{resistance, cross wind} \end{array} \right\} \longrightarrow \text{vehicle}$$

but also influences the driver

$$\text{Environment} \left\{ \begin{array}{l} \text{climate} \\ \text{visibility} \end{array} \right\} \longrightarrow \text{driver}$$

Through the interactions between vehicle and road, roads can quickly be destroyed.

The greatest problem in field test and laboratory experiments is the virtual impossibility of reproducing environmental influences.

The main problems in computer simulation are the description of random road irregularities and the interaction of tires and road as well as the calculation of aerodynamic forces and torques.

1.2 Wheel/Axle Suspension Systems

1.2.1 General Remarks

The Automotive Industry uses different kinds of wheel/axle suspension systems. Important criteria are costs, space requirements, kinematic properties and compliance attributes.

1.2.2 Multi Purpose Suspension Systems

The Double Wishbone Suspension, the McPherson Suspension and the Multi-Link Suspension are multi purpose wheel suspension systems, Fig. 1.1.

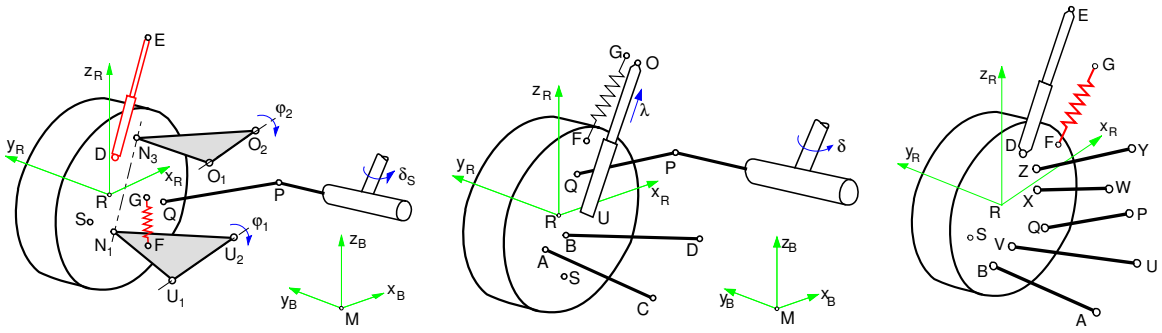

Figure 1.1: Double Wishbone, McPherson and Multi-Link Suspension

They are used as steered front or non steered rear axle suspension systems. These suspension systems are also suitable for driven axles.

In a McPherson suspension the spring is mounted with an inclination to the strut axis. Thus bending torques at the strut which cause high friction forces can be reduced.

At pickups, trucks and busses often solid axles are used. Solid axles are guided either by leaf

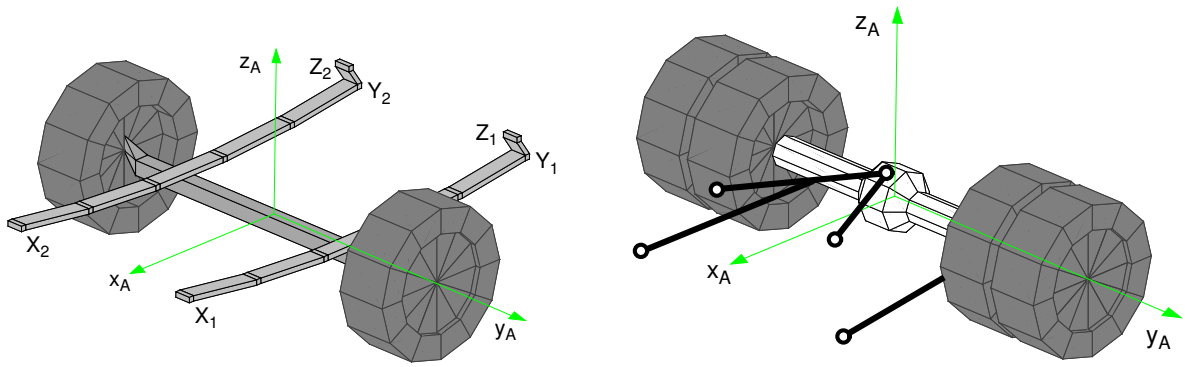

Figure 1.2: Solid Axles

springs or by rigid links, Fig. 1.2. Solid axles tend to tramp on rough road.

Leaf spring guided solid axle suspension systems are very robust. Dry friction between the leafs leads to locking effects in the suspension. Although the leaf springs provide axle guidance on some solid axle suspension systems additional links in longitudinal and lateral direction are used. Thus the typical wind up effect on braking can be avoided.

Solid axles suspended by air springs need at least four links for guidance. In addition to a good driving comfort air springs allow level control too.

1.2.3 Specific Suspension Systems

The Semi-Trailing Arm, the SLA and the Twist Beam axle suspension are suitable only for non steered axles, Fig. 1.3.

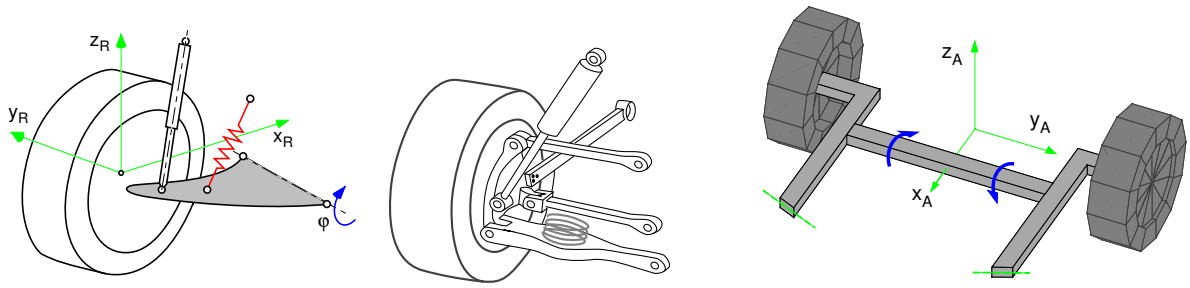

Figure 1.3: Specific Wheel/Axles Suspension Systems

The semi-trailing arm is a simple and cheap design which requires only few space. It is mostly used for driven rear axles.

The SLA axle design allows a nearly independent layout of longitudinal and lateral axle motions. It is similar to the Central Control Arm axle suspension, where the trailing arm is completely rigid and hence only two lateral links are needed.

The twist beam axle suspension exhibits either a trailing arm or a semi-trailing arm characteristic. It is used for non driven rear axles only. The twist beam axle provides enough space for spare tire and fuel tank.

1.3 Steering Systems

1.3.1 Requirements

The steering system must guarantee easy and safe steering of the vehicle. The entirety of the mechanical transmission devices must be able to cope with all loads and stresses occurring in operation.

In order to achieve a good maneuverability a maximum steer angle of approx. $30°$ must be provided at the front wheels of passenger cars. Depending on the wheel base busses and trucks need maximum steer angles up to $55°$ at the front wheels.

Recently some companies have started investigations on 'steer by wire' techniques.

1.3.2 Rack and Pinion Steering

Rack and pinion is the most common steering system on passenger cars, Fig. 1.4. The rack may be located either in front of or behind the axle. The rotations of the steering wheel δ_L are

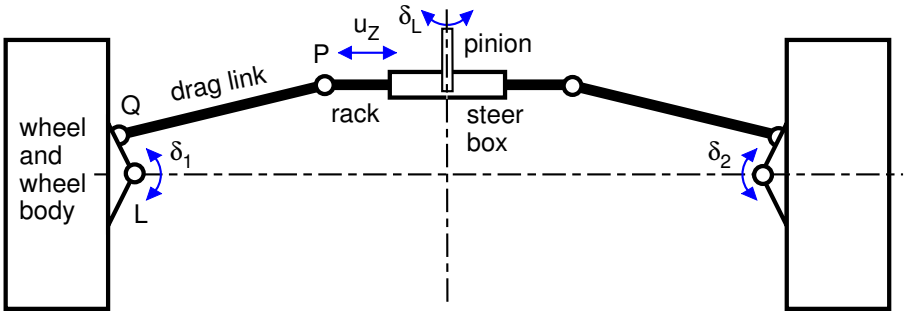

Figure 1.4: Rack and Pinion Steering

firstly transformed by the steering box to the rack travel $u_Z = u_Z(\delta_L)$ and then via the drag links transmitted to the wheel rotations $\delta_1 = \delta_1(u_Z)$, $\delta_2 = \delta_2(u_Z)$. Hence the overall steering ratio depends on the ratio of the steer box and on the kinematics of the steer linkage.

1.3.3 Lever Arm Steering System

Using a lever arm steering system Fig. 1.5, large steer angles at the wheels are possible. This

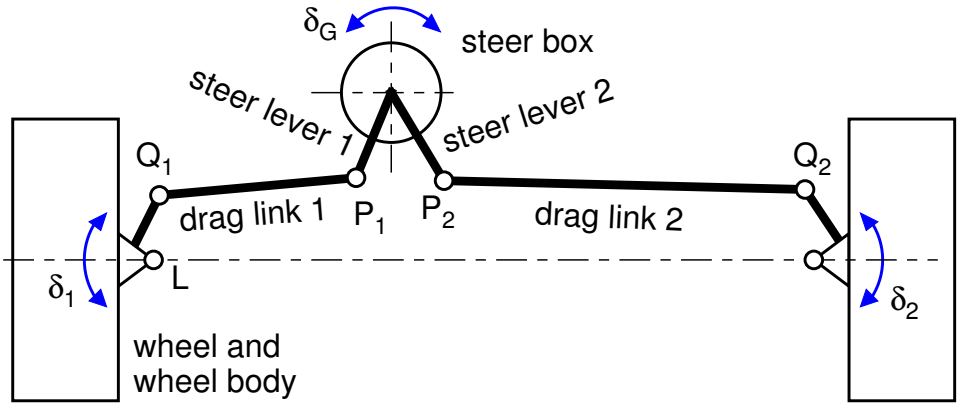

Figure 1.5: Lever Arm Steering System

steering system is used on trucks with large wheel bases and independent wheel suspension at the front axle. Here the steering box can be placed outside of the axle center.

The rotations of the steering wheel δ_L are firstly transformed by the steering box to the rotation of the steer levers $\delta_G = \delta_G(\delta_L)$. The drag links transmit this rotation to the wheel $\delta_1 = \delta_1(\delta_G)$, $\delta_2 = \delta_2(\delta_G)$. Hence, again the overall steering ratio depends on the ratio of the steer box and on the kinematics of the steer linkage.

1.3.4 Drag Link Steering System

At solid axles the drag link steering system is used, Fig. 1.6.

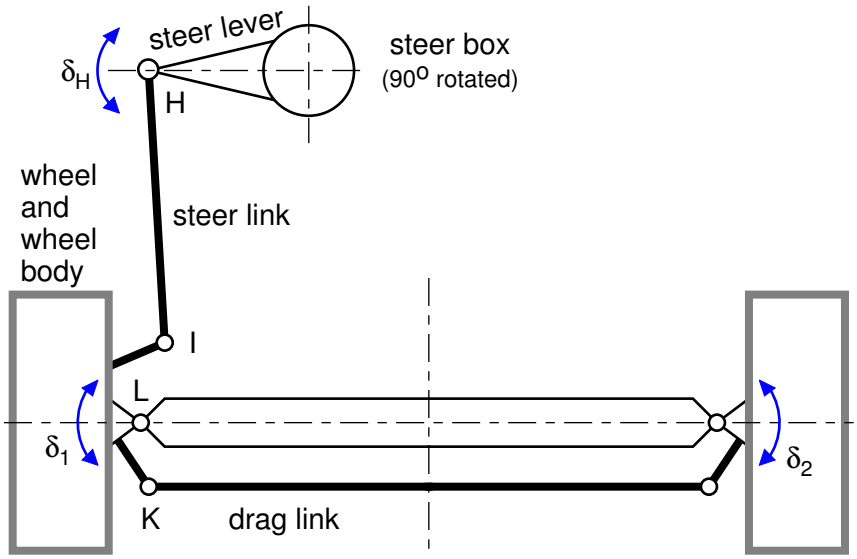

Figure 1.6: Drag Link Steering System

The rotations of the steering wheel δ_L are transformed by the steering box to the rotation of the steer lever arm $\delta_H = \delta_H(\delta_L)$ and further on to the rotation of the left wheel, $\delta_1 = \delta_1(\delta_H)$. The drag link transmits the rotation of the left wheel to the right wheel, $\delta_2 = \delta_2(\delta_1)$. The steering ratio is defined by the ratio of the steer box and the kinematics of the steer link. Here the ratio $\delta_2 = \delta_2(\delta_1)$ given by the kinematics of the drag link can be changed separately.

1.3.5 Bus Steer System

In busses the driver sits more than $2\ m$ in front of the front axle. Here, sophisticated steer systems are needed, Fig. 1.7.

The rotations of the steering wheel δ_L are transformed by the steering box to the rotation of the steer lever arm $\delta_H = \delta_H(\delta_L)$. Via the steer link the left lever arm is moved, $\delta_H = \delta_H(\delta_G)$. This motion is transferred by a coupling link to the right lever arm. Via the drag links the left and right wheel are rotated, $\delta_1 = \delta_1(\delta_H)$ and $\delta_2 = \delta_2(\delta_H)$.

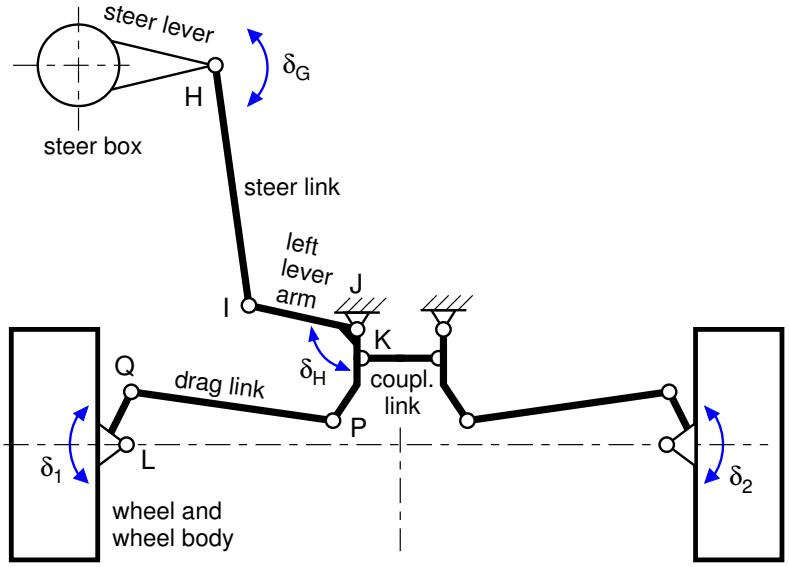

Figure 1.7: Bus Steer System

1.4 Definitions

1.4.1 Coordinate Systems

In vehicle dynamics several different coordinate systems are used, Fig 1.8.

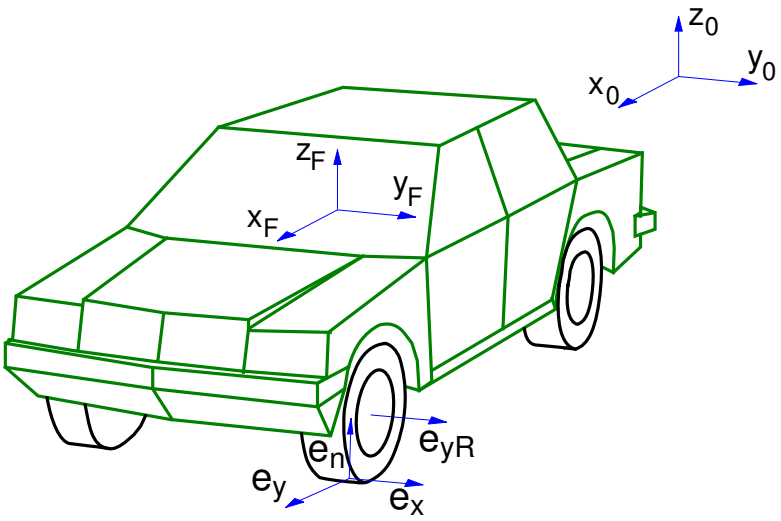

Figure 1.8: Coordinate Systems

The inertial system with the axes x_0, y_0, z_0 is fixed to the track. Within the vehicle fixed system the x_F-axis is pointing forward, the y_F-axis left and the z_F-axis upward. The orientation of the wheel is given by the unit vector e_{yR} in direction of the wheel rotation axis.

The unit vectors in the directions of circumferential and lateral forces e_x and e_y as well as the track normal e_n follow from the contact geometry.

1.4.2 Toe and Camber Angle

1.4.2.1 Definitions according to DIN 70 000

The angle between the vehicle center plane in longitudinal direction and the intersection line of the tire center plane with the track plane is named toe angle. It is positive, if the front part of the wheel is oriented towards the vehicle center plane, Fig. 1.9.

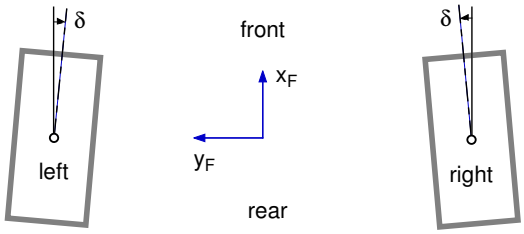

Figure 1.9: Positive Toe Angle

The camber angle is the angle between the wheel center plane and the track normal. It is positive, if the upper part of the wheel is inclined outwards, Fig. 1.10.

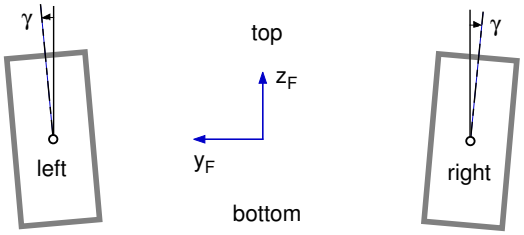

Figure 1.10: Positive Camber Angle

1.4.2.2 Calculation

The calculation of the toe angle is done for the left wheel. The unit vector e_{yR} in direction of the wheel rotation axis is described in the vehicle fixed coordinate system F, Fig. 1.11

$$e_{yR,F} = \left[\begin{array}{ccc} e_{yR,F}^{(1)} & e_{yR,F}^{(2)} & e_{yR,F}^{(3)} \end{array} \right]^T , \tag{1.1}$$

where the axis x_F and z_F span the vehicle center plane. The x_F-axis points forward and the z_F-axis points upward. The toe angle δ can then be calculated from

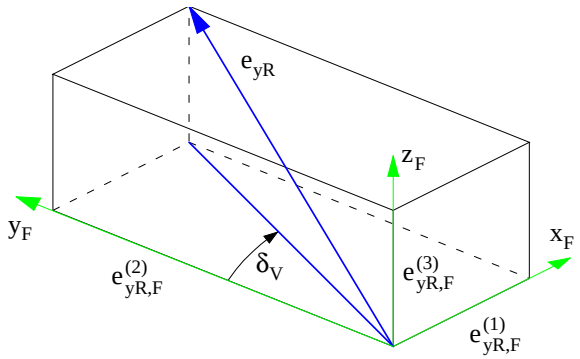

Figure 1.11: Toe Angle

$$\tan\delta \;=\; \frac{e^{(1)}_{yR,F}}{e^{(2)}_{yR,F}}\,. \tag{1.2}$$

The real camber angle γ follows from the scalar product between the unit vectors in the direction of the wheel rotation axis e_{yR} and in the direction of the track normal e_n,

$$\sin\gamma = -e_n^T\, e_{yR}\,. \tag{1.3}$$

The wheel camber angle can be calculated by

$$\sin\gamma \;=\; -e^{(3)}_{yR,F}\,. \tag{1.4}$$

On a flat horizontal road both definitions are equal.

1.4.3 Steering Geometry

1.4.3.1 Kingpin

At the steered front axle the McPherson-damper strut axis, the double wishbone axis and multi-link wheel suspension or dissolved double wishbone axis are frequently employed in passenger cars, Fig. 1.12 and Fig. 1.13.

The wheel body rotates around the kingpin at steering movements.

At the double wishbone axis, the ball joints A and B, which determine the kingpin, are fixed to the wheel body.

The ball joint point A is also fixed to the wheel body at the classic McPherson wheel suspension, but the point B is fixed to the vehicle body.

At a multi-link axle, the kingpin is no longer defined by real link points. Here, as well as with the McPherson wheel suspension, the kingpin changes its position against the wheel body at wheel travel and steer motions.

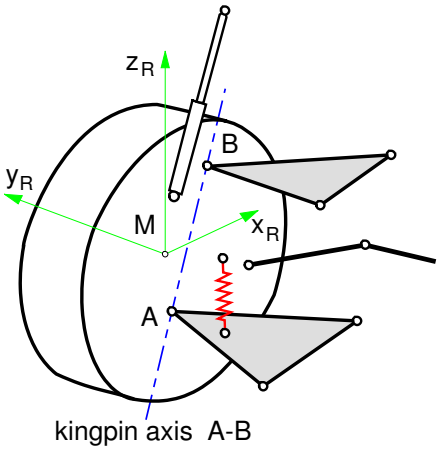

Figure 1.12: Double Wishbone Wheel Suspension

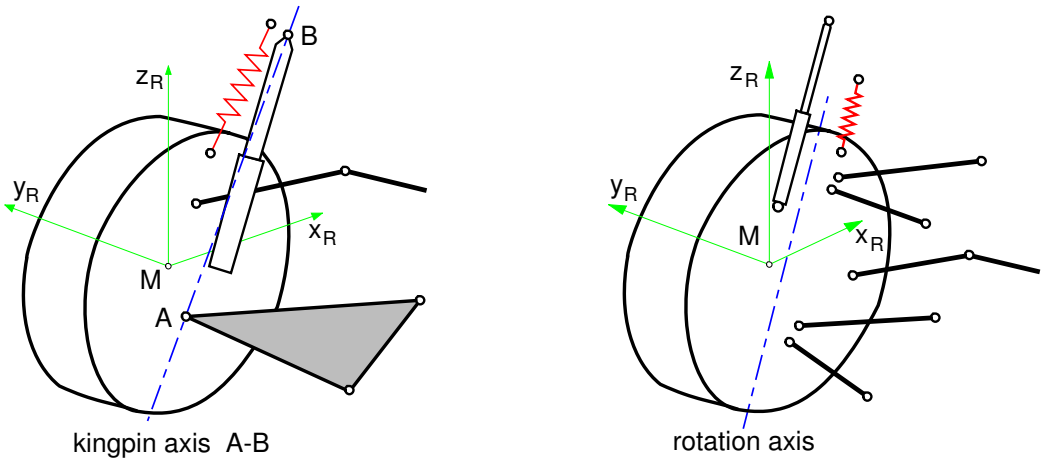

Figure 1.13: McPherson and Multi-Link Wheel Suspensions

1.4.3.2 Caster and Kingpin Angle

The current direction of the kingpin can be defined by two angles within the vehicle fixed coordinate system, Fig. 1.14.

If the kingpin is projected into the y_F-, z_F-plane, the kingpin inclination angle σ can be read as the angle between the z_F-axis and the projection of the kingpin.

The projection of the kingpin into the x_F-, z_F-plane delivers the caster angle ν with the angle between the z_F-axis and the projection of the kingpin.

With many axles the kingpin and caster angle can no longer be determined directly.

The current rotation axis at steering movements, that can be taken from kinematic calculations here delivers a virtual kingpin. The current values of the caster angle ν and the kingpin inclination angle σ can be calculated from the components of the unit vector in the direction of the

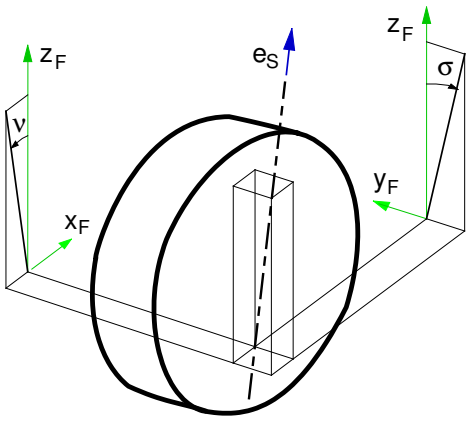

Figure 1.14: Kingpin and Caster Angle

kingpin, described in the vehicle fixed coordinate system

$$\tan\nu = \frac{-e^{(1)}_{S,F}}{e^{(3)}_{S,F}} \quad \text{and} \quad \tan\sigma = \frac{-e^{(2)}_{S,F}}{e^{(3)}_{S,F}} \tag{1.5}$$

with

$$e_{S,F} = \left[\begin{array}{ccc} e^{(1)}_{S,F} & e^{(2)}_{S,F} & e^{(3)}_{S,F} \end{array} \right]^T . \tag{1.6}$$

1.4.3.3 Disturbing Force Lever, Caster and Kingpin Offset

The distance d between the wheel center and the king pin axis is called disturbing force lever. It is an important quantity in evaluating the overall steer behavior.

In general, the point S where the kingpin runs through the track plane does not coincide with the contact point P, Fig. 1.15.

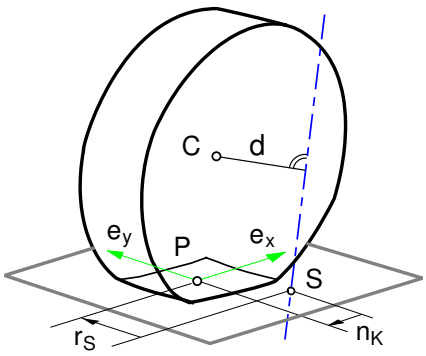

Figure 1.15: Caster and Kingpin Offset

If the kingpin penetrates the track plane before the contact point, the kinematic kingpin offset is positive, $n_K > 0$.

The caster offset is positive, $r_S > 0$, if the contact point P lies outwards of S.

2 The Tire

2.1 Introduction

2.1.1 Tire Development

The following table shows some important mile stones in the development of tires.

1839	Charles Goodyear: vulcanization
1845	Robert William Thompson: first pneumatic tire (several thin inflated tubes inside a leather cover)
1888	John Boyd Dunlop: patent for bicycle (pneumatic) tires
1893	The Dunlop Pneumatic and Tyre Co. GmbH, Hanau, Germany
1895	André and Edouard Michelin: pneumatic tires for Peugeot Paris-Bordeaux-Paris (720 Miles): 50 tire deflations, 22 complete inner tube changes
1899	Continental: longer life tires (approx. 500 Kilometer)
1904	Carbon added: black tires.
1908	Frank Seiberling: grooved tires with improved road traction
1922	Dunlop: steel cord thread in the tire bead
1943	Continental: patent for tubeless tires
1946	Radial Tire
⋮	

Table 2.1: Mile Stones in the Development of Tires

2.1.2 Tire Composites

A modern tire is a mixture of steel, fabric, and rubber.

Reinforcements: steel, rayon, nylon	16%
Rubber: natural/synthetic	38%
Compounds: carbon, silica, chalk, ...	30%
Softener: oil, resin	10%
Vulcanization: sulfur, zinc oxide, ...	4%
Miscellaneous	2%
Tire Mass	8.5 kg

Table 2.2: Tire Composites: 195/65 R 15 ContiEcoContact, Data from `www.felge.de`

2.1.3 Forces and Torques in the Tire Contact Area

In any point of contact between tire and track normal and friction forces are delivered. According to the tire's profile design the contact area forms a not necessarily coherent area.

The effect of the contact forces can be fully described by a vector of force and a torque in reference to a point in the contact patch. The vectors are described in a track-fixed coordinate system. The z-axis is normal to the track, the x-axis is perpendicular to the z-axis and perpendicular to the wheel rotation axis e_{yR}. The demand for a right-handed coordinate system then also fixes the y-axis.

F_x	longitudinal or circumferential force
F_y	lateral force
F_z	vertical force or wheel load
M_x	tilting torque
M_y	rolling resistance torque
M_z	self aligning and bore torque

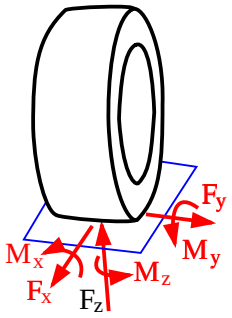

Figure 2.1: Contact Forces and Torques

The components of the contact force are named according to the direction of the axes, Fig. 2.1.

Non symmetric distributions of force in the contact patch cause torques around the x and y axes. The tilting torque M_x occurs when the tire is cambered. M_y also contains the rolling resistance of the tire. In particular the torque around the z-axis is relevant in vehicle dynamics. It consists of two parts,

$$M_z = M_B + M_S \,. \tag{2.1}$$

Rotation of the tire around the z-axis causes the bore torque M_B. The self aligning torque M_S respects the fact that in general the resulting lateral force is not applied in the center of the contact patch.

2.2 Contact Geometry

2.2.1 Dynamic Rolling Radius

At an angular rotation of $\triangle\varphi$, assuming the tread particles stick to the track, the deflected tire moves on a distance of x, Fig. 2.2.

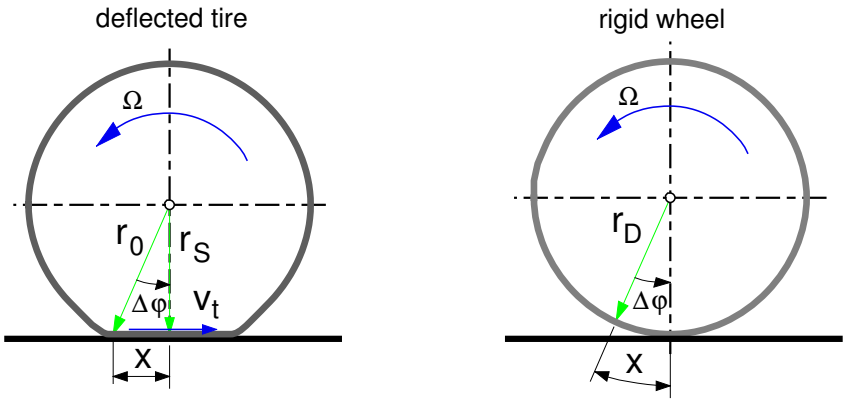

Figure 2.2: Dynamic Rolling Radius

With r_0 as unloaded and $r_S = r_0 - \triangle r$ as loaded or static tire radius

$$r_0 \sin\triangle\varphi \;=\; x \tag{2.2}$$

and

$$r_0 \cos\triangle\varphi \;=\; r_S\,. \tag{2.3}$$

hold.

If the movement of a tire is compared to the rolling of a rigid wheel, its radius r_D then has to be chosen so, that at an angular rotation of $\triangle\varphi$ the tire moves the distance

$$r_0 \sin\triangle\varphi \;=\; x \;=\; r_D\,\triangle\varphi\,. \tag{2.4}$$

Hence, the dynamic tire radius is given by

$$r_D \;=\; \frac{r_0 \sin\triangle\varphi}{\triangle\varphi}\,. \tag{2.5}$$

For $\triangle\varphi \to 0$ one gets the trivial solution $r_D = r_0$.

At small, yet finite angular rotations the sine-function can be approximated by the first terms of its Taylor-Expansion. Then, (2.5) reads as

$$r_D \;=\; r_0\,\frac{\triangle\varphi - \frac{1}{6}\triangle\varphi^3}{\triangle\varphi} \;=\; r_0\,\left(1 - \frac{1}{6}\triangle\varphi^2\right)\,. \tag{2.6}$$

With the according approximation for the cosine-function

$$\frac{r_S}{r_0} \;=\; \cos\triangle\varphi \;=\; 1-\frac{1}{2}\triangle\varphi^2 \quad \text{or} \quad \triangle\varphi^2 \;=\; 2\left(1-\frac{r_S}{r_0}\right) \tag{2.7}$$

one finally gets

$$r_D \;=\; r_0\left(1-\frac{1}{3}\left(1-\frac{r_S}{r_0}\right)\right) \quad = \quad \frac{2}{3}\,r_0+\frac{1}{3}\,r_S \tag{2.8}$$

remains.

The radius r_D depends on the wheel load F_z because of $r_S = r_S(F_z)$ and thus is named dynamic tire radius. With this first approximation it can be calculated from the undeformed radius r_0 and the steady state radius r_S.

By

$$v_t \;=\; r_D\,\Omega \tag{2.9}$$

the average velocity is given with which tread particles are transported through the contact area.

2.2.2 Contact Point

The current position of a wheel in relation to the fixed x_0-, y_0- z_0-system is given by the wheel center M and the unit vector e_{yR} in the direction of the wheel rotation axis, Fig. 2.3.

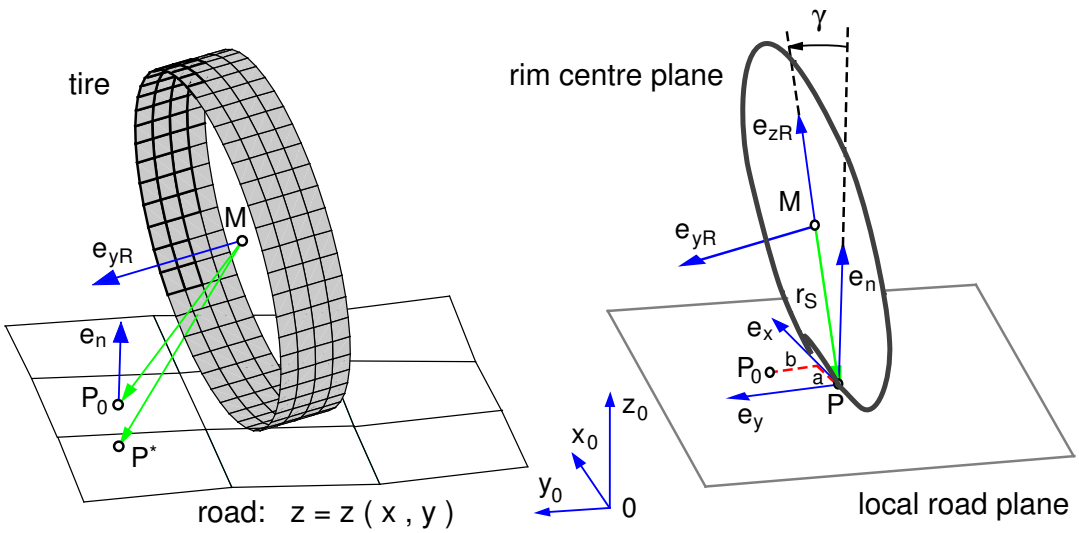

Figure 2.3: Contact Geometry

The irregularities of the track can be described by an arbitrary function of two spatial coordinates

$$z \;=\; z(x,y). \tag{2.10}$$

At an uneven track the contact point P can not be calculated directly. One can firstly get an estimated value with the vector

$$r_{MP^*} \;=\; -r_0\, e_{zB}\;, \tag{2.11}$$

where r_0 is the undeformed tire radius and e_{zB} is the unit vector in the z-direction of the body fixed reference frame.

The position of P^* with respect to the fixed system x_0, y_0, z_0 is determined by

$$r_{0P^*} \;=\; r_{0M} + r_{MP^*}, \tag{2.12}$$

where the vector r_{0M} states the position of the rim center M. Usually the point P^* lies not on the track. The corresponding track point P_0 follows from

$$r_{0P_0,0} = \begin{bmatrix} r_{0P^*,0}^{(}1) \\ r_{0P^*,0}^{(}2) \\ z(r_{0P^*,0}^{(}1),\, r_{0P^*,0}^{(}2)) \end{bmatrix}\;. \tag{2.13}$$

In the point P_0 now the track normal e_n is calculated. Then the unit vectors in the tire's circumferential direction and lateral direction can be calculated

$$e_x \;=\; \frac{e_{yR}\times e_n}{|\, e_{yR}\times e_n\,|}\;, \quad \text{and} \quad e_y \;=\; e_n \times e_x\;. \tag{2.14}$$

Calculating e_x demands a normalization, for the unit vector in the direction of the wheel rotation axis e_{yR} is not always perpendicular to the track. The tire camber angle

$$\gamma \;=\; \arcsin\left(e_{yR}^T\, e_n\right) \tag{2.15}$$

describes the inclination of the wheel rotation axis against the track normal.

The vector from the rim center M to the track point P_0 is now split into three parts

$$r_{MP_0} \;=\; -r_S\, e_{zR} + a\, e_x + b\, e_y\;, \tag{2.16}$$

where r_S names the loaded or static tire radius and a, b are displacements in circumferential and lateral direction.

The unit vector

$$e_{zR} \;=\; \frac{e_x \times e_{yR}}{|\, e_x \times e_{yR}\,|}\;. \tag{2.17}$$

is perpendicular to e_x and e_{yR}. Because the unit vectors e_x and e_y are perpendicular to e_n, the scalar multiplication of (2.16) with e_n results in

$$e_n^T\, r_{MP_0} \;=\; -r_S\, e_n^T\, e_{zR} \quad \text{or} \quad r_S \;=\; -\,\frac{e_n^T\, r_{MP_0}}{e_n^T\, e_{zR}}\;. \tag{2.18}$$

Now also the tire deflection can be calculated

$$\triangle r \;=\; r_0 - r_S\;, \tag{2.19}$$

with r_0 marking the undeformed tire radius.

The point P given by the vector

$$r_{MP} = -r_S\, e_{zR} \tag{2.20}$$

lies within the rim center plane. The transition from P^0 to P takes place according to (2.16) by terms $a\, e_x$ and $b\, e_y$, standing perpendicular to the track normal. The track normal however was calculated in the point P^0. Therefore with an uneven track P no longer lies on the track.

With the newly estimated value $P^* = P$ now the equations (2.13) to (2.20) can be recurred until the difference between P and P_0 is sufficiently small.

Tire models which can be simulated within acceptable time assume that the contact patch is even. At an ordinary passenger-car tire, the contact patch has at normal load about the size of approximately $20 \times 20\, cm$. There is obviously little sense in calculating a fictitious contact point to fractions of millimeters, when later the real track is approximated in the range of centimeters by a plane.

If the track in the contact patch is replaced by a plane, no further iterative improvement is necessary at the hereby used initial value.

2.2.3 Local Track Plane

A plane is given by three points. With the tire width b, the undeformed tire radius r_0 and the length of the contact area L_N at given wheel load, estimated values for three track points can be given in analogy to (2.12)

$$\begin{aligned} r_{ML^*} &= \tfrac{b}{2}\, e_{yR} - r_0\, e_{zB} \quad , \\ r_{MR^*} &= -\tfrac{b}{2}\, e_{yR} - r_0\, e_{zB} \quad , \\ r_{MF^*} &= \tfrac{L_N}{2}\, e_{xB} - r_0\, e_{zB} \quad . \end{aligned} \tag{2.21}$$

The points lie left, resp. right and to the front of a point below the rim center. The unit vectors e_{xB} and e_{zB} point in the longitudinal and vertical direction of the vehicle. The wheel rotation axis is given by e_{yR}. According to (2.13) the corresponding points on the track L, R and F can be calculated.

The vectors

$$r_{RF} = r_{0F} - r_{0R} \quad \text{and} \quad r_{RL} = r_{0L} - r_{0R} \tag{2.22}$$

lie within the track plane. The unit vector calculated by

$$e_n = \frac{r_{RF} \times r_{RL}}{|\, r_{RF} \times r_{RL}\,|}\, . \tag{2.23}$$

is perpendicular to the plane defined by the points L, R, and F and gives an average track normal over the contact area. Discontinuities which occur at step- or ramp-sized obstacles are smoothed that way.

Of course it would be obvious to replace L_N in (2.21) by the actual length L of the contact area and the unit vector e_{zB} by the unit vector e_{zR} which points upwards in the wheel center

plane. The values however, can only be calculated from the current track normal. Here also an iterative solution would be possible. Despite higher computing effort the model quality cannot be improved by this, because approximations in the contact calculation and in the tire model limit the exactness of the tire model.

2.2.4 Contact Point Velocity

The absolute velocity of the contact point one gets from the derivation of the position vector

$$v_{0P,0} \;=\; \dot{r}_{0P,0} \;=\; \dot{r}_{0M,0} + \dot{r}_{MP,0}\,. \tag{2.24}$$

Here $\dot{r}_{0M,0} = v_{0M,0}$ is the absolute velocity of the wheel center and $r_{MP,0}$ the vector from the wheel center M to the contact point P, expressed in the inertial frame 0. With (2.20) one gets

$$\dot{r}_{MP,0} \;=\; \frac{d}{dt}\left(-r_S\, e_{zR,0}\right) \;=\; -\dot{r}_S\, e_{zR,0} \;-\; r_S\, \dot{e}_{zR,0}\,. \tag{2.25}$$

Due to $r_0 = const.$

$$-\,\dot{r}_S \;=\; \triangle\dot{r} \tag{2.26}$$

follows from (2.19).

The unit vector e_{zR} moves with the rim but does not perform rotations around the wheel rotation axis. Its time derivative is then given by

$$\dot{e}_{zR,0} \;=\; \omega^*_{0R,0} \times e_{zR,0} \tag{2.27}$$

where ω^*_{0R} is the angular velocity of the wheel rim without components in the direction of the wheel rotation axis. Now (2.25) reads as

$$\dot{r}_{MP,0} \;=\; \triangle\dot{r}\, e_{zR,0} \;-\; r_S\, \omega^*_{0R,0} \times e_{ZR,0} \tag{2.28}$$

and the contact point velocity can be written as

$$v_{0P,0} \;=\; v_{0M,0} + \triangle\dot{r}\, e_{zR,0} - r_S\, \omega^*_{0R,0} \times e_{ZR,0}\,. \tag{2.29}$$

Because the point P lies on the track, $v_{0P,0}$ must not contain a component normal to the track

$$e_n^T\, v_{0P} \;=\; 0\,. \tag{2.30}$$

The tire deformation velocity is defined by this demand

$$\triangle\dot{r} \;=\; \frac{-e_n^T\left(v_{0M} + r_S\, \omega^*_{0R} \times e_{ZR}\right)}{e_n^T\, e_{zR}}\,. \tag{2.31}$$

Now, the contact point velocity v_{0P} and its components in longitudinal and lateral direction

$$v_x \;=\; e_x^T\, v_{0P} \tag{2.32}$$

and

$$v_y \;=\; e_y^T\, v_{0P} \tag{2.33}$$

can be calculated.

2.3 Wheel Load

The vertical tire force F_z can be calculated as a function of the normal tire deflection $\triangle z = e_n^T \triangle r$ and the deflection velocity $\triangle \dot{z} = e_n^T \triangle \dot{r}$

$$F_z \;=\; F_z(\triangle z,\, \triangle \dot{z})\,. \tag{2.34}$$

Because the tire can only deliver pressure forces to the road, the restriction $F_z \geq 0$ holds.

In a first approximation F_z is separated into a static and a dynamic part

$$F_z \;=\; F_z^S + F_z^D\,. \tag{2.35}$$

The static part is described as a nonlinear function of the normal tire deflection

$$F_z^S \;=\; a_1 \triangle z \;+\; a_2\,(\triangle z)^2\,. \tag{2.36}$$

The constants a_1 and a_2 may be calculated from the radial stiffness at nominal payload

$$c_z^N \;=\; \left.\frac{d\,F_z^S}{d\,\triangle z}\right|_{F_z^S = F_z^N} \tag{2.37}$$

and the radial stiffness at double payload

$$c_z^{2N} \;=\; \left.\frac{d\,F_z^S}{d\,\triangle z}\right|_{F_z^S = 2F_z^N}\,. \tag{2.38}$$

The dynamic part is roughly approximated by

$$F_z^D \;=\; d_R \triangle \dot{z}\,, \tag{2.39}$$

where d_R is a constant describing the radial tire damping.

2.4 Longitudinal Force and Longitudinal Slip

To get some insight into the mechanism generating tire forces in longitudinal direction we consider a tire on a flat test rig. The rim is rotating with the angular speed Ω and the flat track runs with speed v_x. The distance between the rim center an the flat track is controlled to the loaded tire radius corresponding to the wheel load F_z, Fig. 2.4.

A tread particle enters at time $t = 0$ the contact area. If we assume adhesion between the particle and the track then the top of the particle runs with the track speed v_x and the bottom with the average transport velocity $v_t = r_D\,\Omega$. Depending on the speed difference $\triangle v = r_D\,\Omega - v_x$ the tread particle is deflected in longitudinal direction

$$u \;=\; (r_D\,\Omega - v_x)\,t\,. \tag{2.40}$$

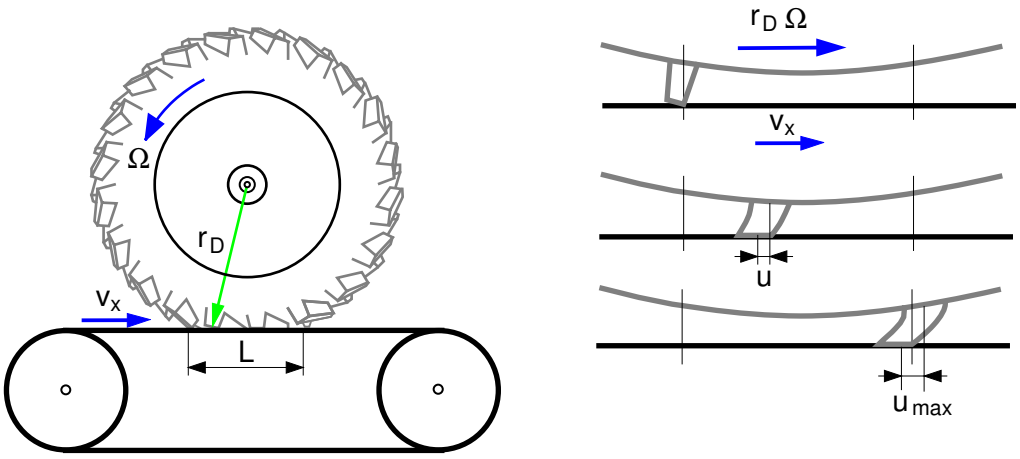

Figure 2.4: Tire on Flat Track Test Rig

The time a particle spends in the contact area can be calculated by

$$T \;=\; \frac{L}{r_D\,|\Omega|}\,, \tag{2.41}$$

where L denotes the contact length, and $T > 0$ is assured by $|\Omega|$.

The maximum deflection occurs when the tread particle leaves at $t = T$ the contact area

$$u_{max} \;=\; (r_D\,\Omega - v_x)\,T \;=\; (r_D\,\Omega - v_x)\,\frac{L}{r_D\,|\Omega|}\,. \tag{2.42}$$

The deflected tread particle applies a force to the tire. In a first approximation we get

$$F_x^t \;=\; c_x^t\,u\,, \tag{2.43}$$

where c_x^t is the stiffness of one tread particle in longitudinal direction.

On normal wheel loads more than one tread particle is in contact with the track, Fig. 2.5a. The number p of the tread particles can be estimated by

$$p \;=\; \frac{L}{s+a}\,. \tag{2.44}$$

where s is the length of one particle and a denotes the distance between the particles.

Particles entering the contact area are undeformed on exit the have the maximum deflection. According to (2.43) this results in a linear force distribution versus the contact length, Fig. 2.5b. For p particles the resulting force in longitudinal direction is given by

$$F_x \;=\; \frac{1}{2}\,p\,c_x^t\,u_{max}\,. \tag{2.45}$$

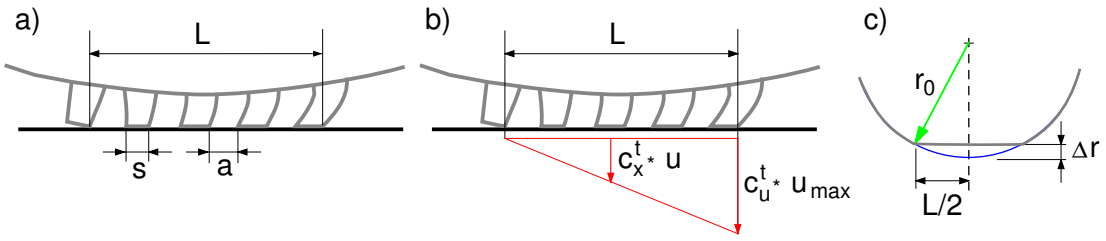

Figure 2.5: a) Particles, b) Force Distribution, c) Tire Deformation

With (2.44) and (2.42) this results in

$$F_x \;=\; \frac{1}{2}\,\frac{L}{s+a}\,c_x^t\,(r_D\,\Omega - v_x)\,\frac{L}{r_D\,|\Omega|}\;. \tag{2.46}$$

A first approximation of the contact length L is given by

$$(L/2)^2 \;=\; r_0^2 - (r_0 - \triangle r)^2\;, \tag{2.47}$$

where r_0 is the undeformed tire radius, and $\triangle r$ denotes the tire deflection, Fig. 2.5c. With $\triangle r \ll r_0$ one gets

$$L^2 \approx 8\,r_0\,\triangle r\;. \tag{2.48}$$

The tire deflection can be approximated by

$$\triangle r \;=\; F_z/c_R\;. \tag{2.49}$$

where F_z is the wheel load, and c_R denotes the radial tire stiffness. Now, (2.45) can be written as

$$F_x \;=\; 4\,\frac{r_0}{s+a}\,\frac{c_x^t}{c_R}\,F_z\,\frac{r_D\,\Omega - v_x}{r_D\,|\Omega|}\;. \tag{2.50}$$

The non-dimensional relation between the sliding velocity of the tread particles in longitudinal direction $v_x^S = v_x - r_D\,\Omega$ and the average transport velocity $r_D\,|\Omega|$ forms the longitudinal slip

$$s_x \;=\; \frac{-(v_x - r_D\,\Omega)}{r_D\,|\Omega|}\;. \tag{2.51}$$

In this first approximation the longitudinal force F_x is proportional to the wheel load F_z and the longitudinal slip s_x

$$F_x \;=\; k\,F_z\,s_x\;, \tag{2.52}$$

where the constant k collects the tire properties r_0, s, a, c_x^t and c_R.

The relation (2.52) holds only as long as all particles stick to the track. At average slip values the particles at the end of the contact area start sliding, and at high slip values only the parts at the beginning of the contact area still stick to the road, Fig. . 2.6.

The resulting nonlinear function of the longitudinal force F_x versus the longitudinal slip s_x can be defined by the parameters initial inclination (driving stiffness) dF_x^0, location s_x^M and magnitude of the maximum F_x^M, start of full sliding s_x^G and the sliding force F_x^G, Fig. 2.7.

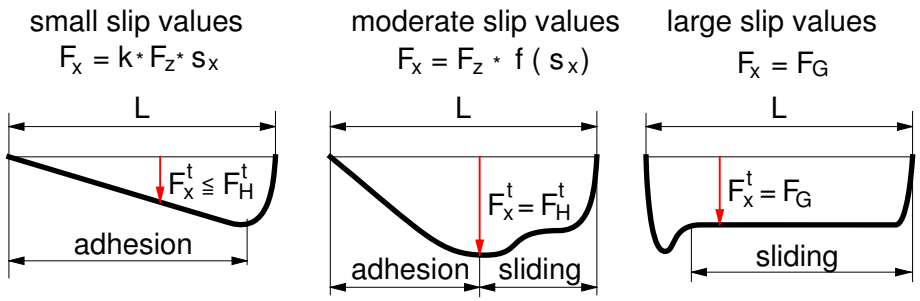

Figure 2.6: Longitudinal Force Distribution for different Slip Values

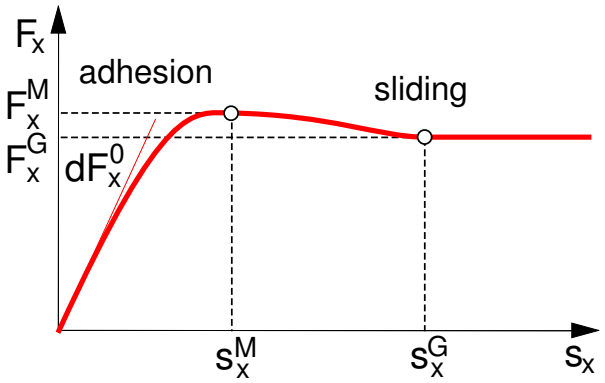

Figure 2.7: Typical Longitudinal Force Characteristics

2.5 Lateral Slip, Lateral Force and Self Aligning Torque

Similar to the longitudinal slip s_x, given by (2.51), the lateral slip can be defined by

$$s_y = \frac{-v_y^S}{r_D \, |\Omega|} , \tag{2.53}$$

where the sliding velocity in lateral direction is given by

$$v_y^S = v_y \tag{2.54}$$

and the lateral component of the contact point velocity v_y follows from (2.33).

As long as the tread particles stick to the road (small amounts of slip), an almost linear distribution of the forces along the length L of the contact area appears. At moderate slip values the particles at the end of the contact area start sliding, and at high slip values only the parts at the beginning of the contact area stick to the road, Fig. 2.8. The nonlinear characteristics of the lateral force versus the lateral slip can be described by the initial inclination (cornering stiffness) dF_y^0, location s_y^M and magnitude F_y^M of the maximum and start of full sliding s_y^G and magnitude F_y^G of the sliding force.

The distribution of the lateral forces over the contact area length also defines the acting point of the resulting lateral force. At small slip values the working point lies behind the center of

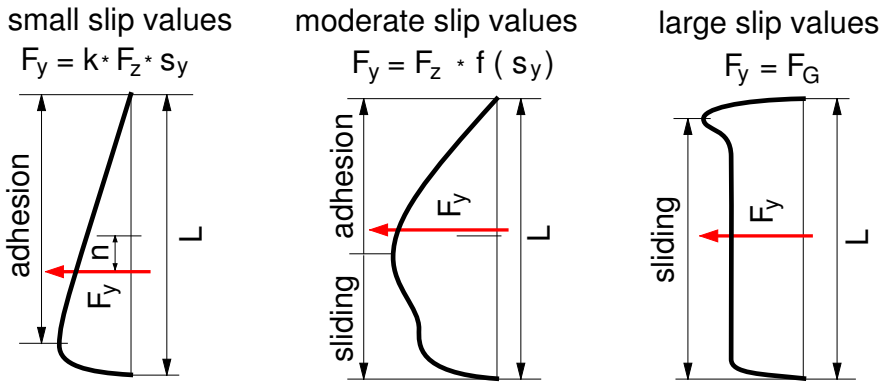

Figure 2.8: Lateral Force Distribution over Contact Area

the contact area (contact point P). With rising slip values, it moves forward, sometimes even before the center of the contact area. At extreme slip values, when practically all particles are sliding, the resulting force is applied at the center of the contact area.

The resulting lateral force F_y with the dynamic tire offset or pneumatic trail n as a lever generates the self aligning torque

$$M_S = -n\,F_y\,. \tag{2.55}$$

The lateral force F_y as well as the dynamic tire offset are functions of the lateral slip s_y. Typical plots of these quantities are shown in Fig. 2.9. Characteristic parameters for the lateral

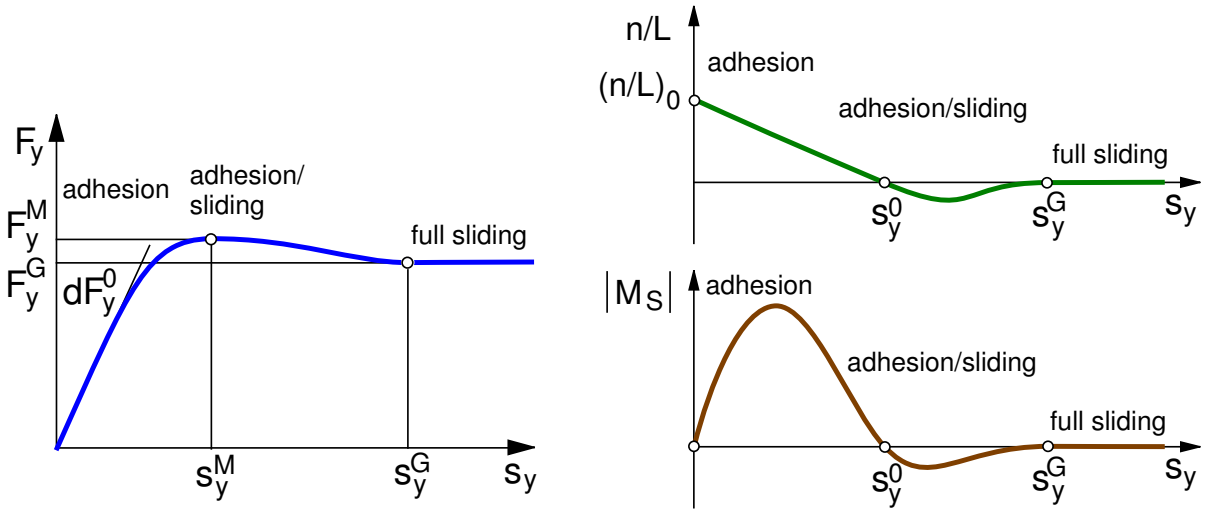

Figure 2.9: Typical Plot of Lateral Force, Tire Offset and Self Aligning Torque

force graph are initial inclination (cornering stiffness) dF_y^0, location s_y^M and magnitude of the maximum F_y^M, begin of full sliding s_y^G, and the sliding force F_y^G.

The dynamic tire offset has been normalized by the length of the contact area L. The initial value $(n/L)_0$ as well as the slip values s_y^0 and s_y^G characterize the graph sufficiently.

2.6 Camber Influence

At a cambered tire, Fig. 2.10, the angular velocity of the wheel Ω has a component normal to the road

$$\Omega_n \;=\; \Omega\,\sin\gamma\,. \tag{2.56}$$

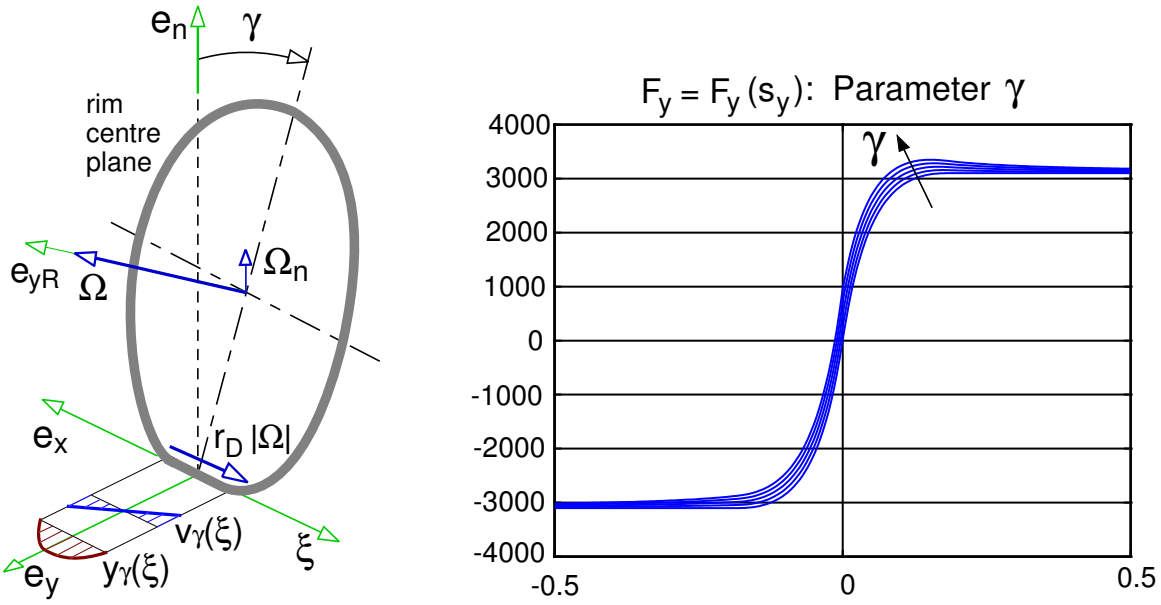

Figure 2.10: Cambered Tire $F_y(\gamma)$ at $F_z = 3.2\,kN$ and $\gamma = 0°,\ 2°\,, 4°\,, 6°\,, 8°$

Now, the tread particles in the contact area possess a lateral velocity which depends on their position ξ and is given by

$$v_\gamma(\xi) \;=\; -\Omega_n\,\frac{L}{2}\,\frac{\xi}{L/2}\,, \;=\; -\Omega\,\sin\gamma\,\xi\,, \quad -L/2 \le \xi \le L/2\,. \tag{2.57}$$

At the center of the contact area (contact point) it vanishes and at the end of the contact area it is of the same value but opposite to the value at the beginning of the contact area.

Assuming that the tread particles stick to the track, the deflection profile is defined by

$$\dot{y}_\gamma(\xi) \;=\; v_\gamma(\xi)\,. \tag{2.58}$$

The time derivative can be transformed to a space derivative

$$\dot{y}_\gamma(\xi) \;=\; \frac{d\,y_\gamma(\xi)}{d\,\xi}\,\frac{d\,\xi}{d\,t} \;=\; \frac{d\,y_\gamma(\xi)}{d\,\xi}\,r_D\,|\Omega| \tag{2.59}$$

where $r_D\,|\Omega|$ denotes the average transport velocity. Now (2.58) reads as

$$\frac{d\,y_\gamma(\xi)}{d\,\xi}\,r_D\,|\Omega| \;=\; -\Omega\,\sin\gamma\,\xi\,, \tag{2.60}$$

which results in the parabolic deflection profile

$$y_\gamma(\xi) \;=\; \frac{1}{2}\,\frac{\Omega\,\sin\gamma}{r_D\,|\Omega|}\,\left(\frac{L}{2}\right)^2\,\left[1-\left(\frac{\xi}{L/2}\right)^2\right]\,. \tag{2.61}$$

Similar to the lateral slip s_y which is by (2.53) we now can define a camber slip

$$s_\gamma \;=\; \frac{-\Omega\,\sin\gamma}{r_D\,|\Omega|}\,\frac{L}{2}\,. \tag{2.62}$$

The lateral deflection of the tread particles generates a lateral force

$$F_{y\gamma} \;=\; -c_y\,\bar{y}_\gamma\,, \tag{2.63}$$

where c_y denotes the lateral stiffness of the tread particles and

$$\bar{y}_\gamma \;=\; \frac{1}{2}\,(-s_\gamma)\,\frac{L}{2}\,\frac{1}{L}\int\limits_{-L/2}^{L/2}\left[1-\left(\frac{x}{L/2}\right)^2\right]\,d\xi \;=\; -\frac{1}{6}\,s_\gamma\,L \tag{2.64}$$

is the average value of the parabolic deflection profile.

A purely lateral tire movement without camber results in a linear deflexion profile with the average deflexion

$$\bar{y}_y \;=\; -\frac{1}{2}\,s_y\,L\,. \tag{2.65}$$

A comparison of (2.64) to (2.65) shows, that with

$$s_y^\gamma \;=\; \frac{1}{3}\,s_\gamma \tag{2.66}$$

the lateral camber slip s_γ can be converted to an equivalent lateral slip s_y^γ.

In normal driving operation, the camber angle and thus the lateral camber slip are limited to small values. So the lateral camber force can be approximated by

$$F_y^\gamma \;\approx\; dF_y^0\,s_y^\gamma\,. \tag{2.67}$$

If the “global” inclination $dF_y = F_y/s_y$ is used instead of the initial inclination dF_y^0, one gets the camber influence on the lateral force as shown in Fig. 2.10.

The camber angle influences the distribution of pressure in the lateral direction of the contact area, and changes the shape of the contact area from rectangular to trapezoidal. It is thus extremely difficult if not impossible to quantify the camber influence with the aid of such simple models. But this approach turns out to be a quit good approximation.

2.7 Bore Torque

If the angular velocity of the wheel

$$\omega_{0W} \;=\; \omega_{0R}^{*} + \Omega\, e_{yR} \tag{2.68}$$

has a component in direction of the track normal e_n

$$\omega_n \;=\; e_n^T\, \omega_{0W} \;\neq\; 0\,. \tag{2.69}$$

a very complicated deflection profile of the tread particles in the contact area occurs. By a simple approach the resulting bore torque can be approximated by the parameter of the longitudinal force characteristics.

Fig. 2.11 shows the contact area at zero camber, $\gamma = 0$ and small slip values, $s_x \approx 0$, $s_y \approx 0$. The contact area is separated into small stripes of width dy. The longitudinal slip in a stripe at position y is then given by

$$s_x(y) \;=\; \frac{-\,(-\omega_n\, y)}{r_D\,|\Omega|}\,. \tag{2.70}$$

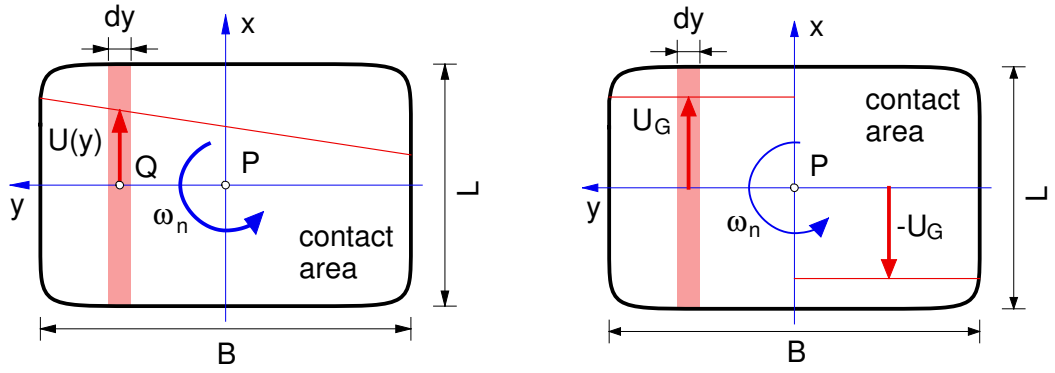

Figure 2.11: Bore Torque generated by Longitudinal Forces

For small slip values the nonlinear tire force characteristics can be linearized. The longitudinal force in the stripe can then be approximated by

$$F_x(y) \;=\; \left.\frac{d\,F_x}{d\,s_x}\right|_{s_x=0} \frac{d\,s_x}{d\,y}\,y\,. \tag{2.71}$$

With (2.70) one gets

$$F_x(y) \;=\; \left.\frac{d\,F_x}{d\,s_x}\right|_{s_x=0} \frac{\omega_n}{r_D\,|\Omega|}\,y\,. \tag{2.72}$$

The forces $F_x(y)$ generate a bore torque in the contact point P

$$\begin{aligned} M_B \;&=\; -\frac{1}{B}\int_{-\frac{B}{2}}^{+\frac{B}{2}} y\,F_x(y)\,dy \;&&=\; -\frac{1}{B}\int_{-\frac{B}{2}}^{+\frac{B}{2}} y\,\left.\frac{d\,F_x}{d\,s_x}\right|_{s_x=0}\frac{\omega_n}{r_D\,|\Omega|}\,y\,dy \\ &=\; \frac{1}{12}\,B^2\,\left.\frac{d\,F_x}{d\,s_x}\right|_{s_x=0}\frac{-\omega_n}{r_D\,|\Omega|} \;&&=\; \frac{1}{12}\,B\,\left.\frac{d\,F_x}{d\,s_x}\right|_{s_x=0}\frac{B}{r_D}\,\frac{-\omega_n}{|\,\Omega\,|}\,, \end{aligned} \tag{2.73}$$

where

$$s_B \;=\; \frac{-\omega_n}{|\,\Omega\,|} \tag{2.74}$$

can be considered as bore slip. Via dF_x/ds_x the bore torque takes into account the actual friction and slip conditions.

The bore torque calculated by (2.73) is only a first approximation. At large bore slips the longitudinal forces in the stripes are limited by the sliding values. Hence, the bore torque is limited by

$$|\,M_B\,| \;\leq\; M_B^{max} \;=\; 2\,\frac{1}{B}\int_0^{+\frac{B}{2}} y\,F_x^G\,dy \;=\; \frac{1}{4}\,B\,F_x^G\,, \tag{2.75}$$

where F_x^G denotes the longitudinal sliding force.

2.8 Typical Tire Characteristics

The tire model TMeasy[1] which is based on this simple approach can be used for passenger car tires as well as for truck tires. It approximates the characteristic curves $F_x = F_x(s_x)$, $F_y = F_y(\alpha)$ and $M_z = M_z(\alpha)$ quite well even for different wheel loads F_z, Fig. 2.12 and Fig. 2.13.

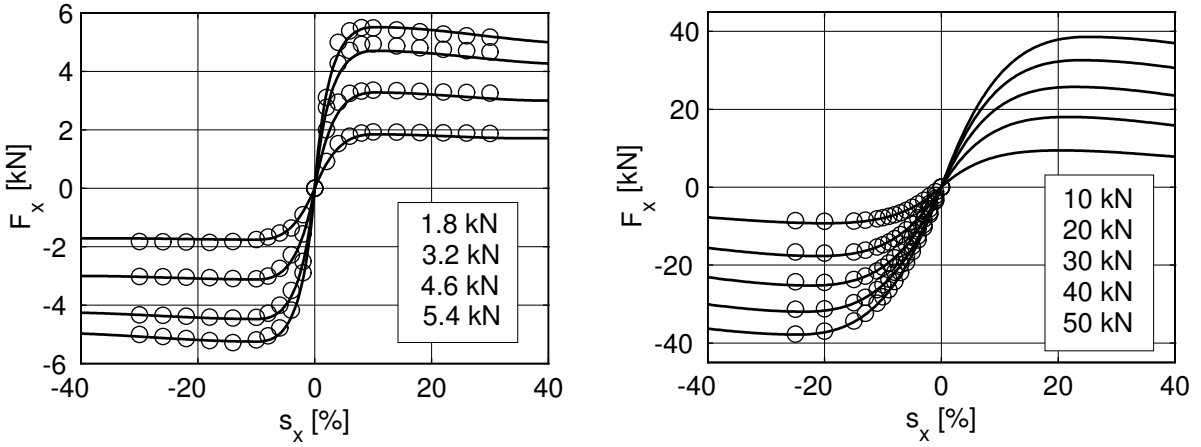

Figure 2.12: Longitudinal Force Characteristics: ○ Meas., – TMeasy

Within TMeasy the one-dimensional characteristics are automatically converted to a two-dimensional combination characteristics, Fig. 2.14.

[1] Hirschberg, W; Rill, G. Weinfurter, H.: User-Appropriate Tyre-Modelling for Vehicle Dynamics in Standard and Limit Situations. Vehicle System Dynamics 2002, Vol. 38, No. 2, pp. 103-125. Lisse: Swets & Zeitlinger.

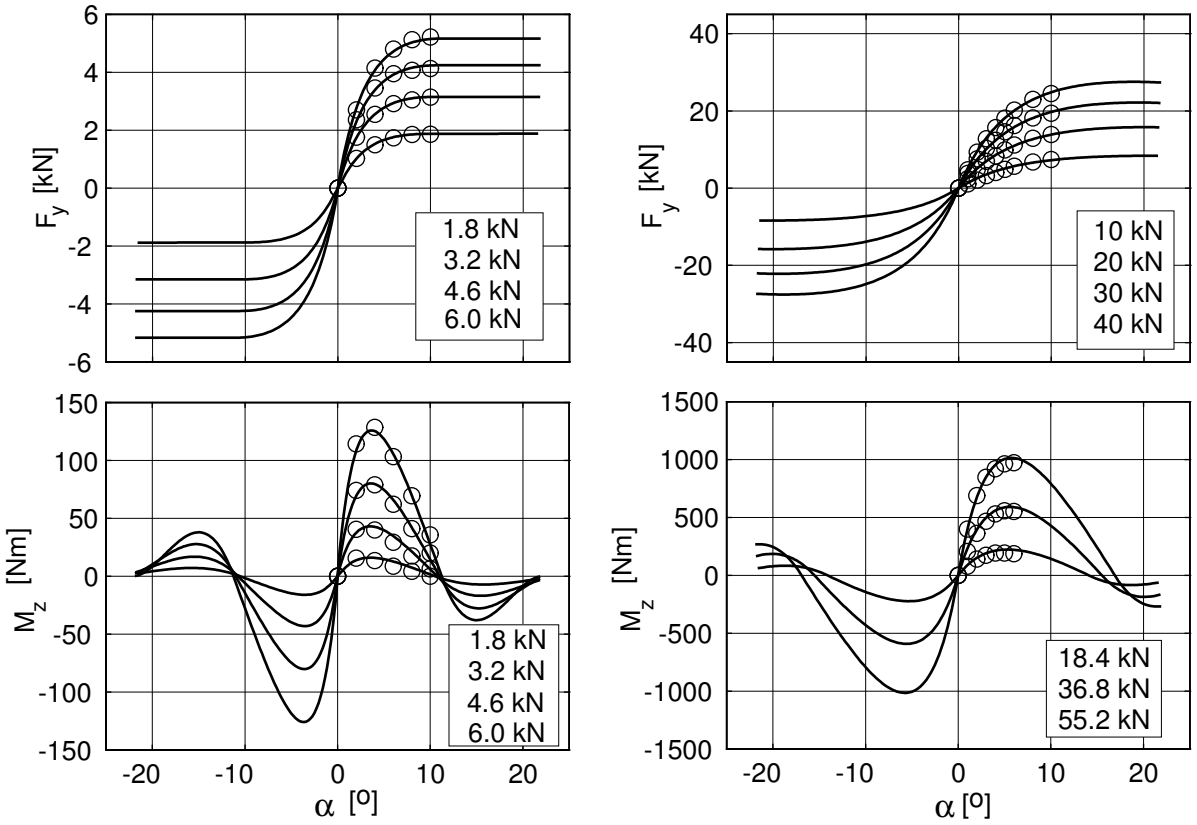

Figure 2.13: Lateral Force and Self Aligning Torque: ○ Meas., — TMeasy

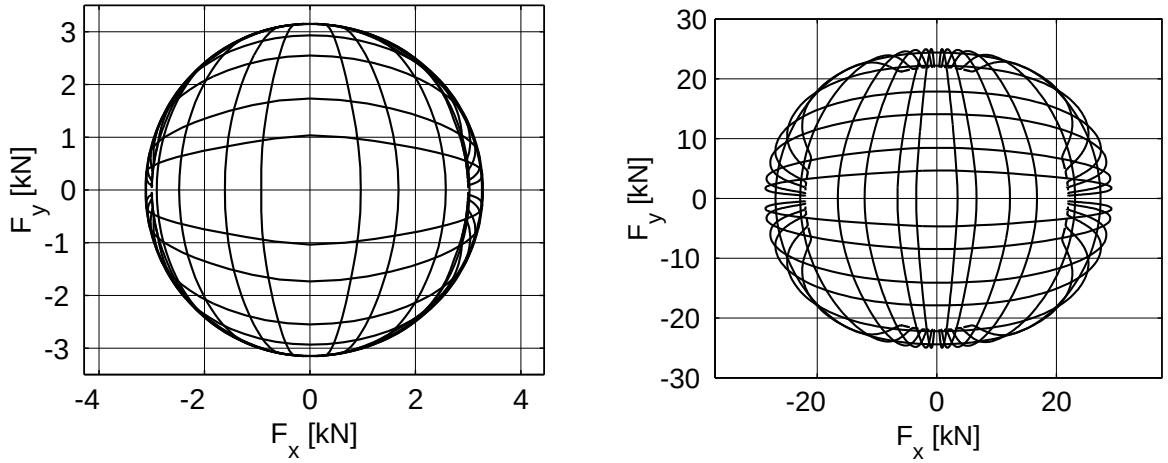

$|s_x| = 1,\ 2,\ 4,\ 6,\ 10,\ 15\,\%; \qquad |\alpha| = 1,\ 2,\ 4,\ 6,\ 10,\ 14°$

Figure 2.14: Two-dimensional Tire Characteristics at $F_z = 3.2\,kN$ / $F_z = 35\,kN$

3 Longitudinal Dynamics

3.1 Dynamic Wheel Loads

3.1.1 Simple Vehicle Model

The vehicle is considered as one rigid body which moves along an ideally even and horizontal road. At each axle the forces in the wheel contact points are combined into one normal and one longitudinal force.

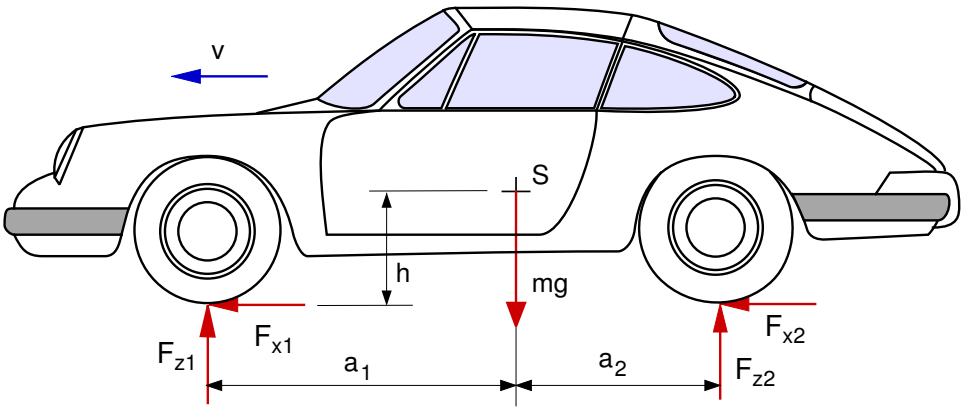

Figure 3.1: Simple Vehicle Model

If aerodynamic forces (drag, positive and negative lift) are neglected at first, then the equations of motions in the x-, z-plane read as

$$m\,\dot{v} \;=\; F_{x1} + F_{x2}\;, \tag{3.1}$$

$$0 \;=\; F_{z1} + F_{z2} - m\,g \tag{3.2}$$

and

$$0 \;=\; F_{z1}\,a_1 - F_{z2}\,a_2 + (F_{x1} + F_{x2})\,h\;, \tag{3.3}$$

where $\dot{v}$ indicates the vehicle's acceleration, m is the mass of the vehicle, $a_1 + a_2$ is the wheel base, and h is the height of the center of gravity.

This are only three equations for the four unknown forces F_{x1}, F_{x2}, F_{z1}, F_{z2}. But, if we insert (3.1) in (3.3) we can eliminate two unknowns by one stroke

$$0 \;=\; F_{z1}\, a_1 - F_{z2}\, a_2 + m\, \dot{v}\, h\,. \tag{3.4}$$

The equations (3.2) and (3.4) can now be resolved for the axle loads

$$F_{z1} = m\, g \left[\; \frac{a_2}{a_1 + a_2} - \frac{h}{a_1 + a_2}\, \frac{\dot{v}}{g} \; \right] \tag{3.5}$$

and

$$F_{z2} = m\, g \left[\; \frac{a_1}{a_1 + a_2} + \frac{h}{a_1 + a_2}\, \frac{\dot{v}}{g} \; \right] . \tag{3.6}$$

The weight of the vehicle mg is distributed among the axles according to position of the center of gravity. When accelerating $\dot{v} > 0$, the front axle is relieved, as is the rear axle when decelerating $\dot{v} < 0$.

3.1.2 Influence of Grade

For a vehicle on a grade, Fig.3.2, the equations of motions (3.1) to (3.3) can easily be extended to

$$\begin{aligned} m\, \dot{v} &= F_{x1} + F_{x2} - m\, g\, \sin\alpha\,, \\ 0 &= F_{z1} + F_{z2} - m\, g\, \cos\alpha\,, \\ 0 &= F_{z1}\, a_1 - F_{z2}\, a_2 + (F_{x1} + F_{x2})\, h\,, \end{aligned} \tag{3.7}$$

where α denotes the grade angle.

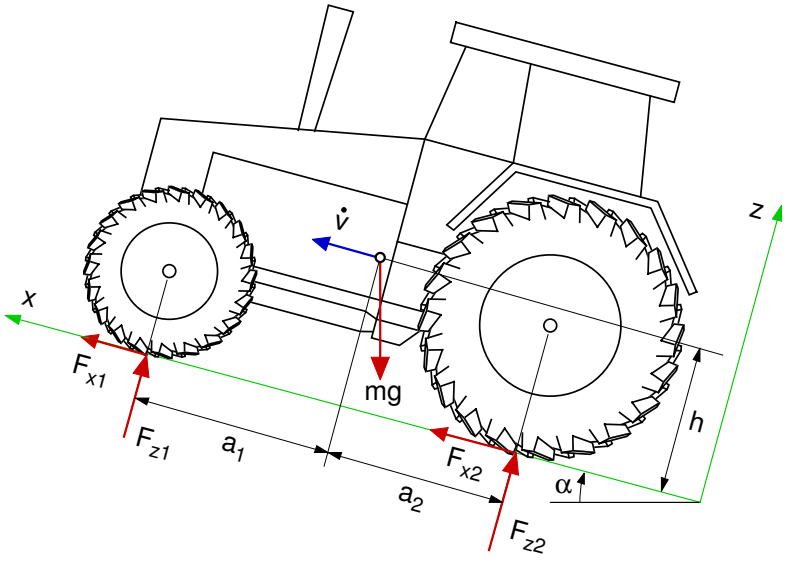

Figure 3.2: Vehicle on Grade

Now, the dynamic axle loads are given by

$$F_{z1} = m\,g\,\cos\alpha\left[\,\frac{a_2}{a_1+a_2} - \frac{h}{a_1+a_2}\left(\frac{\dot v}{g} + \tan\alpha\right)\,\right] \tag{3.8}$$

and

$$F_{z2} = m\,g\,\cos\alpha\left[\,\frac{a_1}{a_1+a_2} + \frac{h}{a_1+a_2}\left(\frac{\dot v}{g} + \tan\alpha\right)\,\right]\,. \tag{3.9}$$

A grade angle $\alpha \neq 0$ reduces the static load, $mg \rightarrow mg\cos\alpha$, and generates an additional acceleration term, $\frac{\dot v}{g} \rightarrow \frac{\dot v}{g} + \tan\alpha$.

3.1.3 Aerodynamic Forces

The shape of most vehicles or specific wings mounted at the vehicle produce aerodynamic forces and torques. The effect of this aerodynamic forces and torques can be represented by a resistant force applied at the center of gravity and ”down forces” acting at the front and rear axle, Fig. 3.3.

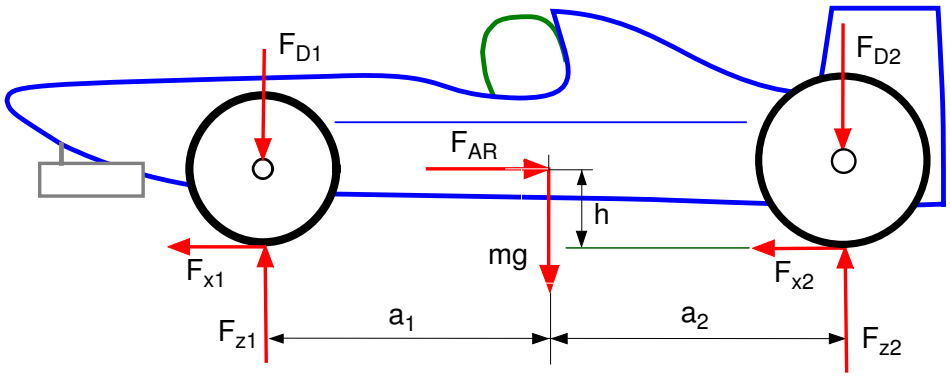

Figure 3.3: Vehicle with Aerodynamic Forces

If we assume a positive driving speed, $v >$, then the equations of motion read as

$$\begin{aligned} m\,\dot v &= F_{x1} + F_{x2} - F_{AR}\,, \\ 0 &= F_{z1} - F_{D1} + F_{z2} - F_{D2} - m\,g\,, \\ 0 &= (F_{z1} - F_{D1})\;a_1 - (F_{z2} - F_{D2})\;a_2 + (F_{x1} + F_{x2})\;h\,, \end{aligned} \tag{3.10}$$

where F_{AR} and F_{D1}, F_{D2} describe the air resistance and the down forces. For the dynamic axle loads we get

$$F_{z1} = F_{D1} + m\,g\left[\,\frac{a_2}{a_1+a_2} - \frac{h}{a_1+a_2}\left(\frac{\dot v}{g} + \frac{F_{AR}}{m\,g}\right)\,\right] \tag{3.11}$$

and

$$F_{z2} = F_{D2} + m\,g\left[\,\frac{a_1}{a_1+a_2} + \frac{h}{a_1+a_2}\left(\frac{\dot v}{g} + \frac{F_{AR}}{m\,g}\right)\,\right]\,. \tag{3.12}$$

The down forces F_{D1}, F_{D2} increase the axle loads, and the air resistance F_{AR} generates an additional acceleration term, $\frac{\dot v}{g} \rightarrow \frac{\dot v}{g} + \frac{F_{AR}}{m\,g}$.

3.2 Maximum Acceleration

3.2.1 Tilting Limits

Ordinary automotive vehicles can only deliver pressure forces to the road. If we apply the demands $F_{z1} \geq 0$ and $F_{z2} \geq 0$ to (3.8) and (3.9) we get

$$-\frac{a_1}{h} \quad \leq \quad \frac{\dot{v}}{g} + \tan\alpha \quad \leq \quad \frac{a_2}{h}\,. \tag{3.13}$$

This tilting condition limits the acceleration $\dot{v}$ and by the grade angle α the climbing capacity of the vehicle.

The presence of aerodynamic forces complicates the tilting condition. Aerodynamic forces become important only at high speeds. Here the vehicle acceleration normally is limited by the engine power.

3.2.2 Friction Limits

The maximum acceleration is also limited by the friction conditions

$$|F_{x1}| \leq \mu\, F_{z1} \quad \text{and} \quad |F_{x2}| \leq \mu\, F_{z2} \tag{3.14}$$

where the same friction coefficient μ has been assumed at front and rear axle.

In the limit case

$$F_{x1} = \pm\,\mu\, F_{z1} \quad \text{and} \quad F_{x2} = \pm\,\mu\, F_{z2} \tag{3.15}$$

the first equation in (3.7) can be written as

$$m\,\dot{v}_{max} \;=\; \pm\,\mu\;(F_{z1} + F_{z2}) - m\,g\,\sin\alpha\,. \tag{3.16}$$

Using (3.8) and (3.9) one gets

$$\left(\frac{\dot{v}}{g}\right)_{max} \quad = \quad \pm\,\mu\,\cos\alpha \;-\; \sin\alpha\,. \tag{3.17}$$

That means climbing ($\dot{v} > 0$, $\alpha > 0$) or downhill stopping ($\dot{v} < 0$, $\alpha < 0$) requires at least a friction coefficient $\mu \geq \tan\alpha$.

According to the vehicle dimensions and the friction values the maximal acceleration or deceleration is restricted either by (3.13) or by (3.17).

If we take aerodynamic forces into account the maximum acceleration on a horizontal road is limited by

$$-\,\mu\left(1 + \frac{F_{D1}}{mg} + \frac{F_{D2}}{mg}\right) - \frac{F_{AR}}{mg} \quad \leq \quad \frac{\dot{v}}{g} \quad \leq \quad \mu\left(1 + \frac{F_{D1}}{mg} + \frac{F_{D2}}{mg}\right) - \frac{F_{AR}}{mg}\,. \tag{3.18}$$

In particular the aerodynamic forces enhance the braking performance of the vehicle.

3.3 Driving and Braking

3.3.1 Single Axle Drive

With the rear axle driven in limit situations $F_{x1} = 0$ and $F_{x2} = \mu F_{z2}$ holds. Then, using (3.6) the linear momentum (3.1) results in

$$m \dot{v}_{RWD} = \mu m g \left[\frac{a_1}{a_1 + a_2} + \frac{h}{a_1 + a_2} \frac{\dot{v}_{RWD}}{g} \right] , \tag{3.19}$$

where the subscript $_{RWD}$ indicates the rear wheel drive. Hence, the maximum acceleration for a rear wheel driven vehicle is given by

$$\frac{\dot{v}_{RWD}}{g} = \frac{\mu}{1 - \mu \dfrac{h}{a_1 + a_2}} \frac{a_1}{a_1 + a_2} . \tag{3.20}$$

By setting $F_{x1} = \mu F_{z1}$ and $F_{x2} = 0$ the maximum acceleration for a front wheel driven vehicle can be calculated in a similar way. One gets

$$\frac{\dot{v}_{FWD}}{g} = \frac{\mu}{1 + \mu \dfrac{h}{a_1 + a_2}} \frac{a_2}{a_1 + a_2} , \tag{3.21}$$

where the subscript $_{FWD}$ denotes front wheel drive. Depending on the parameter μ, a_1, a_2 and h the accelerations may be limited by the tilting condition $\frac{\dot{v}}{g} \leq \frac{a_2}{h}$.

The maximum accelerations of a single axle driven vehicle are plotted in Fig. 3.4.

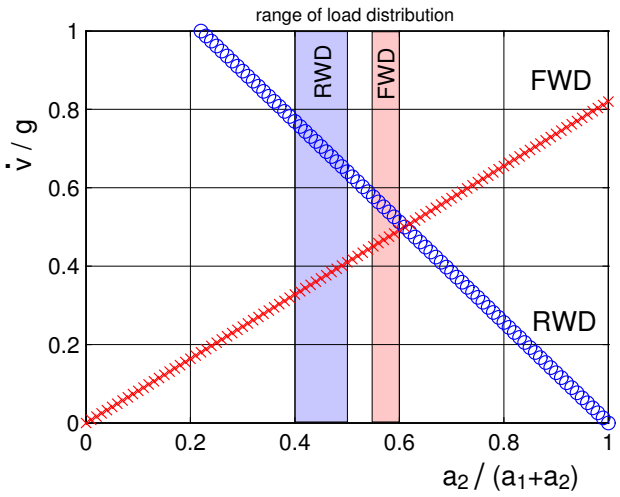

Figure 3.4: Single Axle Driven Passenger Car: $\mu = 1$, $h = 0.55\,m$, $a_1 + a_2 = 2.5\,m$

For rear wheel driven passenger cars the parameter $a_2/(a_1+a_2)$ which describes the static axle load distribution is in the range of $0.4 \leq a_2/(a_1+a_2) \leq 0.5$. For $\mu = 1$ and $h = 0.55$ this results

in maximum accelerations in between $0.77 \geq \dot{v}/g \geq 0.64$. Front wheel driven passenger cars usually cover the range $0.55 \leq a_2/(a_1{+}a_2) \leq 0.60$ which produces accelerations in the range of $0.45 \leq \dot{v}/g \geq 0.49$. Hence, rear wheel driven vehicles can accelerate much faster than front wheel driven vehicles.

3.3.2 Braking at Single Axle

If only the front axle is braked then in the limit case $F_{x1} = -\mu\, F_{z1}$ and $F_{x2} = 0$ holds. With (3.5) one gets from (3.1)

$$m\,\dot{v}_{FWB} \;=\; -\mu\, m\, g \left[\; \frac{a_2}{a_1+a_2} - \frac{h}{a_1+a_2}\,\frac{\dot{v}_{FWB}}{g} \;\right] \tag{3.22}$$

where the subscript $_{FWB}$ indicates front wheel braking. The maximum deceleration is then given by

$$\frac{\dot{v}_{FWB}}{g} \;=\; -\,\frac{\mu}{1-\mu\,\dfrac{h}{a_1+a_2}}\,\frac{a_2}{a_1+a_2}\,. \tag{3.23}$$

If only the rear axle is braked ($F_{x1} = 0$, $F_{x2} = -\mu\, F_{z2}$) one gets the maximal deceleration

$$\frac{\dot{v}_{RWB}}{g} \;=\; -\,\frac{\mu}{1+\mu\,\dfrac{h}{a_1+a_2}}\,\frac{a_1}{a_1+a_2}\,, \tag{3.24}$$

where the subscript $_{RWB}$ indicates a braked rear axle. Depending on the parameter μ, a_1, a_2 and h the decelerations may be limited by the tilting condition $\frac{\dot{v}}{g} \geq -\frac{a_1}{h}$.

The maximum decelerations of a single axle braked vehicle are plotted in Fig. 3.5.

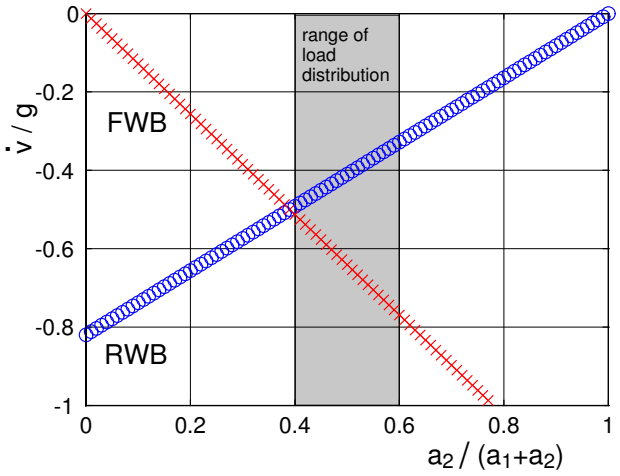

Figure 3.5: Single Axle Braked Passenger Car: $\mu = 1$, $h = 0.55\,m$, $a_1{+}a_2 = 2.5\,m$

For passenger cars the load distribution parameter $a_2/(a_1{+}a_2)$ usually covers the range from 0.4 to 0.6. If only the front axle is braked then decelerations from $\dot{v}/g = -0.51$ to $\dot{v}/g = -0.77$

can be achieved. This is pretty much compared to the deceleration range of a braked rear axle which is in the range from $\dot{v}/g = -0.49$ to $\dot{v}/g = -0.33$.

That is why the braking system at the front axle has a redundant design.

3.3.3 Optimal Distribution of Drive and Brake Forces

The sum of the longitudinal forces accelerates or decelerates the vehicle. In dimensionless style (3.1) reads

$$\frac{\dot{v}}{g} = \frac{F_{x1}}{m\,g} + \frac{F_{x2}}{m\,g}\,. \tag{3.25}$$

A certain acceleration or deceleration can only be achieved by different combinations of the longitudinal forces F_{x1} and F_{x2}. According to (3.15) the longitudinal forces are limited by wheel load and friction.

The optimal combination of F_{x1} and F_{x2} is achieved, when front and rear axle have the same skid resistance.

$$F_{x1} = \pm\,\nu\,\mu\,F_{z1} \quad \text{and} \quad F_{x2} = \pm\,\nu\,\mu\,F_{z2}\,. \tag{3.26}$$

With (3.5) and (3.6) one gets

$$\frac{F_{x1}}{m\,g} = \pm\,\nu\,\mu\left(\frac{a_2}{h} - \frac{\dot{v}}{g}\right)\frac{h}{a_1+a_2} \tag{3.27}$$

and

$$\frac{F_{x2}}{m\,g} = \pm\,\nu\,\mu\left(\frac{a_1}{h} + \frac{\dot{v}}{g}\right)\frac{h}{a_1+a_2}\,. \tag{3.28}$$

With (3.27) and (3.28) one gets from (3.25)

$$\frac{\dot{v}}{g} = \pm\,\nu\,\mu\,, \tag{3.29}$$

where it has been assumed that F_{x1} and F_{x2} have the same sign.

With (3.29 inserted in (3.27) and (3.28) one gets

$$\frac{F_{x1}}{m\,g} = \frac{\dot{v}}{g}\left(\frac{a_2}{h} - \frac{\dot{v}}{g}\right)\frac{h}{a_1+a_2} \tag{3.30}$$

and

$$\frac{F_{x2}}{m\,g} = \frac{\dot{v}}{g}\left(\frac{a_1}{h} + \frac{\dot{v}}{g}\right)\frac{h}{a_1+a_2}\,. \tag{3.31}$$

remain.

Depending on the desired acceleration $\dot{v} > 0$ or deceleration $\dot{v} < 0$ the longitudinal forces that grant the same skid resistance at both axles can now be calculated.

Fig.3.6 shows the curve of optimal drive and brake forces for typical passenger car values. At

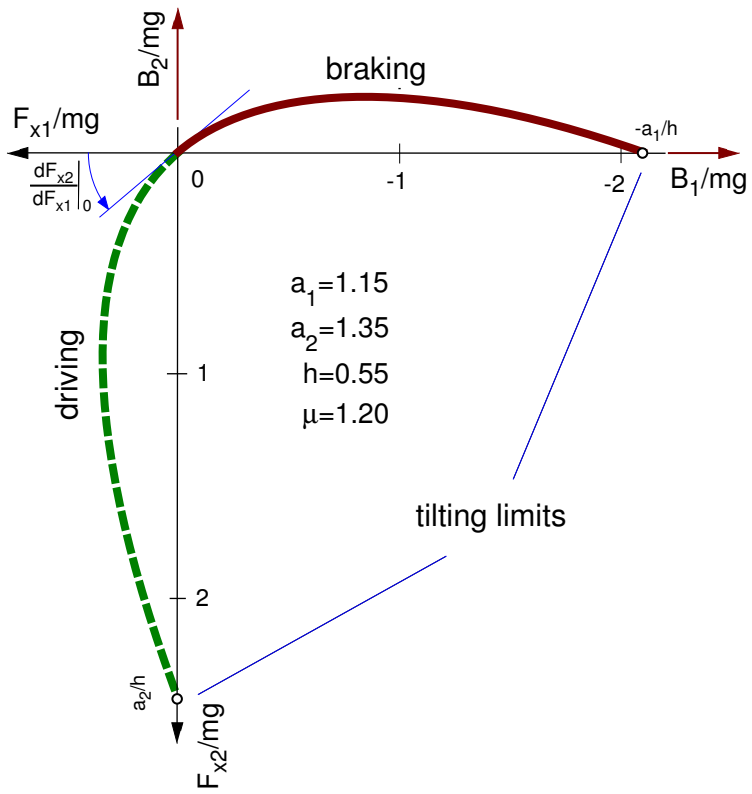

Figure 3.6: Optimal Distribution of Drive and Brake Forces

the tilting limits $\dot{v}/g = -a_1/h$ and $\dot{v}/g = +a_2/h$ no longitudinal forces can be delivered at the lifting axle.

The initial gradient only depends on the steady state distribution of wheel loads. From (3.30) and (3.31) it follows

$$\frac{d\,\dfrac{F_{x1}}{m\,g}}{d\,\dfrac{\dot{v}}{g}} = \left(\frac{a_2}{h} - 2\,\frac{\dot{v}}{g}\right)\frac{h}{a_1 + a_2} \tag{3.32}$$

and

$$\frac{d\,\dfrac{F_{x2}}{m\,g}}{d\,\dfrac{\dot{v}}{g}} = \left(\frac{a_1}{h} + 2\,\frac{\dot{v}}{g}\right)\frac{h}{a_1 + a_2}\,. \tag{3.33}$$

For $\dot{v}/g = 0$ the initial gradient remains as

$$\left.\frac{d\,F_{x2}}{d\,F_{x1}}\right|_0 = \frac{a_1}{a_2}\,. \tag{3.34}$$

3.3.4 Different Distributions of Brake Forces

In practice it is tried to approximate the optimal distribution of brake forces by constant distribution, limitation or reduction of brake forces as good as possible. Fig. 3.7.

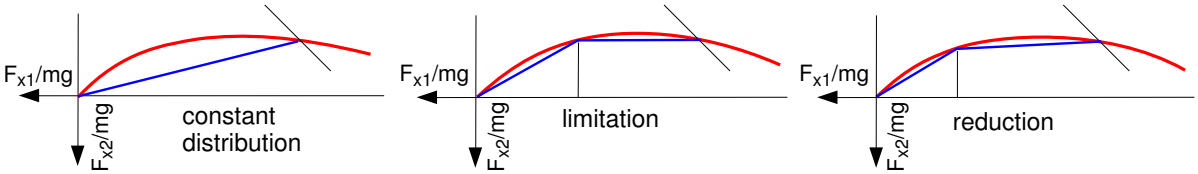

Figure 3.7: Different Distributions of Brake Forces

When braking, the vehicle's stability is dependent on the potential of lateral force (cornering stiffness) at the rear axle. In practice, a greater skid (locking) resistance is thus realized at the rear axle than at the front axle. Because of this, the brake force balances in the physically relevant area are all below the optimal curve. This restricts the achievable deceleration, specially at low friction values.

Because the optimal curve is dependent on the vehicle's center of gravity additional safeties have to be installed when designing real distributions of brake forces.

Often the distribution of brake forces is fitted to the axle loads. There the influence of the height of the center of gravity, which may also vary much on trucks, remains unrespected and has to be compensated by a safety distance from the optimal curve.

Only the control of brake pressure in anti-lock-systems provides an optimal distribution of brake forces independent from loading conditions.

3.3.5 Anti-Lock-Systems

Lateral forces can only be scarcely transmitted, if high values of longitudinal slip occur when decelerating a vehicle. Stability and/or steerability is then no longer given.

By controlling the brake torque, respectively brake pressure, the longitudinal slip can be restricted to values that allow considerable lateral forces.

The angular wheel acceleration $\dot{\Omega}$ is used here as control variable. Angular wheel accelerations are derived from the measured angular wheel speeds by differentiation. With a longitudinal slip of $s_L = 0$ the rolling condition is fulfilled. Then

$$r_D \, \dot{\Omega} \; = \; \ddot{x} \tag{3.35}$$

holds, where r_D labels the dynamic tyre radius and $\ddot{x}$ is the vehicle's acceleration. According to (3.17), the maximum acceleration/deceleration of a vehicle is dependent on the friction coefficient, $|\ddot{x}| = \mu \, g$. With a known friction coefficient μ a simple control law can be realized for every wheel

$$|\dot{\Omega}| \; \leq \; \frac{1}{r_D} \, |\ddot{x}| \, . \tag{3.36}$$

Because until today no reliable possibility to determine the local friction coefficient between tyre and road has been found, useful information can only be gained from (3.36) at optimal conditions on dry road. Therefore the longitudinal slip is used as a second control variable.

In order to calculate longitudinal slips, a reference speed is estimated from all measured wheel speeds which is then used for the calculation of slip at all wheels. This method is too imprecise at low speeds. Below a limit velocity no control occurs therefore. Problems also occur when for example all wheels lock simultaneously which may happen on icy roads.

The control of the brake torque is done via the brake pressure which can be $increased$, $held$ or $decreased$ by a three-way valve. To prevent vibrations, the decrement is usually made slower than the increment.

To prevent a strong yaw reaction, the $select\ low$ principle is often used with μ-split braking at the rear axle. The break pressure at both wheels is controlled the wheel running on lower friction. Thus the brake forces at the rear axle cause no yaw torque. The maximally achievable deceleration however is reduced by this.

3.4 Drive and Brake Pitch

3.4.1 Vehicle Model

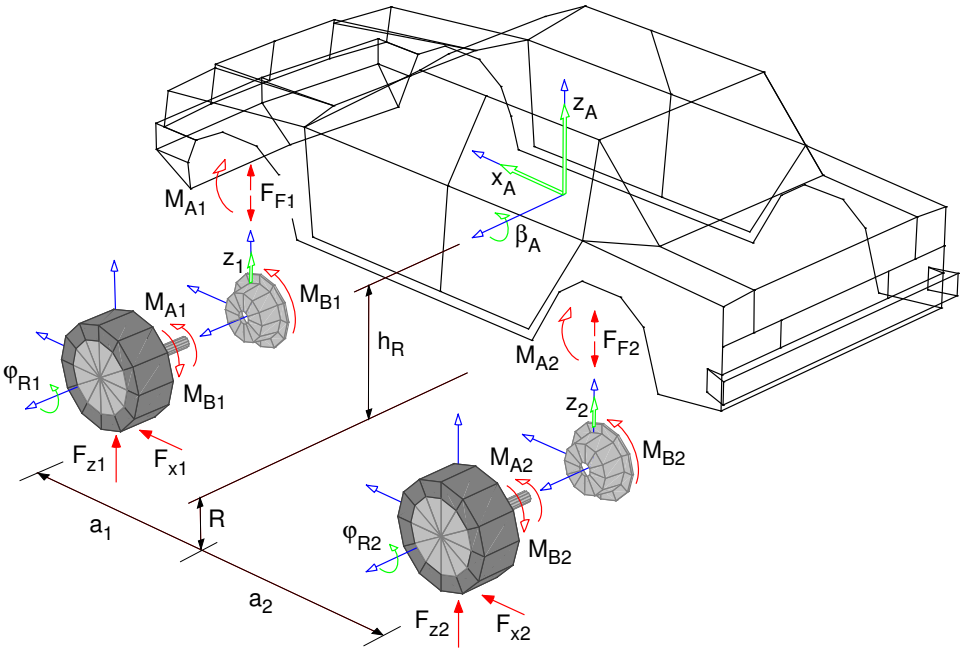

Figure 3.8: Plane Vehicle Model

The vehicle model drawn in Fig. 3.8 consists of five rigid bodies. The body has three degrees of freedom: Longitudinal motion x_A, vertical motion z_A and pitch β_A. The coordinates z_1 and z_2

describe the vertical motions of wheel and axle bodies relative to the body. The longitudinal and rotational motions of the wheel bodies relative to the body can be described via suspension kinematics as functions of the vertical wheel motion:

$$\begin{aligned} x_1 &= x_1(z_1)\,, \quad \beta_1 = \beta_1(z_1)\,; \\ x_2 &= x_2(z_2)\,, \quad \beta_2 = \beta_2(z_2)\,. \end{aligned} \tag{3.37}$$

The rotation angles φ_{R1} and φ_{R2} describe the wheel rotations relative to the wheel bodies.

The forces between wheel body and vehicle body are labelled F_{F1} and F_{F2}. At the wheels drive torques M_{A1}, M_{A2} and brake torques M_{B1}, M_{B2}, longitudinal forces F_{x1}, F_{x2} and the wheel loads F_{z1}, F_{z2} apply. The brake torques are supported directly by the wheel bodies, the drive torques are transmitted by the drive shafts to the vehicle body. The forces and torques that apply to the single bodies are listed in the last column of the tables 3.1 and 3.2.

The velocity of the vehicle body and its angular velocity is given by

$$v_{0A,0} = \begin{bmatrix} \dot{x}_A \\ 0 \\ 0 \end{bmatrix} + \begin{bmatrix} 0 \\ 0 \\ \dot{z}_A \end{bmatrix}; \qquad \omega_{0A,0} = \begin{bmatrix} 0 \\ \dot{\beta}_A \\ 0 \end{bmatrix}. \tag{3.38}$$

At small rotational motions of the body one gets for the speed of the wheel bodies and wheels

$$v_{0RK_1,0} = v_{0R_1,0} = \begin{bmatrix} \dot{x}_A \\ 0 \\ 0 \end{bmatrix} + \begin{bmatrix} 0 \\ 0 \\ \dot{z}_A \end{bmatrix} + \begin{bmatrix} -h_R\,\dot{\beta}_A \\ 0 \\ -a_1\,\dot{\beta}_A \end{bmatrix} + \begin{bmatrix} \frac{\partial x_1}{\partial z_1}\,\dot{z}_1 \\ 0 \\ \dot{z}_1 \end{bmatrix}; \tag{3.39}$$

$$v_{0RK_2,0} = v_{0R_2,0} = \begin{bmatrix} \dot{x}_A \\ 0 \\ 0 \end{bmatrix} + \begin{bmatrix} 0 \\ 0 \\ \dot{z}_A \end{bmatrix} + \begin{bmatrix} -h_R\,\dot{\beta}_A \\ 0 \\ +a_2\,\dot{\beta}_A \end{bmatrix} + \begin{bmatrix} \frac{\partial x_2}{\partial z_2}\,\dot{z}_2 \\ 0 \\ \dot{z}_2 \end{bmatrix}. \tag{3.40}$$

The angular velocities of the wheel bodies and wheels are given by

$$\omega_{0RK_1,0} = \begin{bmatrix} 0 \\ \dot{\beta}_A \\ 0 \end{bmatrix} + \begin{bmatrix} 0 \\ \dot{\beta}_1 \\ 0 \end{bmatrix} \quad \text{and} \quad \omega_{0R_1,0} = \begin{bmatrix} 0 \\ \dot{\beta}_A \\ 0 \end{bmatrix} + \begin{bmatrix} 0 \\ \dot{\beta}_1 \\ 0 \end{bmatrix} + \begin{bmatrix} 0 \\ \dot{\varphi}_{R1} \\ 0 \end{bmatrix} \tag{3.41}$$

as well as

$$\omega_{0RK_2,0} = \begin{bmatrix} 0 \\ \dot{\beta}_A \\ 0 \end{bmatrix} + \begin{bmatrix} 0 \\ \dot{\beta}_2 \\ 0 \end{bmatrix} \quad \text{and} \quad \omega_{0R_2,0} = \begin{bmatrix} 0 \\ \dot{\beta}_A \\ 0 \end{bmatrix} + \begin{bmatrix} 0 \\ \dot{\beta}_2 \\ 0 \end{bmatrix} + \begin{bmatrix} 0 \\ \dot{\varphi}_{R2} \\ 0 \end{bmatrix} \tag{3.42}$$

Introducing a vector of generalized velocities

$$z = \begin{bmatrix} \dot{x}_A & \dot{z}_A & \dot{\beta}_A & \dot{\beta}_1 & \dot{\varphi}_{R1} & \dot{\beta}_2 & \dot{\varphi}_{R2} \end{bmatrix}^T \tag{3.43}$$

the velocities and angular velocities (3.38), (3.39), (3.40), (3.41), (3.42) can be written as

$$v_{0i} = \sum_{j=1}^{7} \frac{\partial v_{0i}}{\partial z_j}\, z_j \quad \text{and} \quad \omega_{0i} = \sum_{j=1}^{7} \frac{\partial \omega_{0i}}{\partial z_j}\, z_j \tag{3.44}$$

3.4.2 Equations of Motion

The partial velocities $\frac{\partial v_{0i}}{\partial z_j}$ and partial angular velocities $\frac{\partial \omega_{0i}}{\partial z_j}$ for the five bodies $i = 1(1)5$ and for the seven generalized speeds $j = 1(1)7$ are arranged in the tables 3.1 and 3.2. With the

bodies	partial velocities $\partial v_{0i}/\partial z_j$							applied forces
	$\dot{x}_A$	$\dot{z}_A$	$\dot{\beta}_A$	$\dot{z}_1$	$\dot{\varphi}_{R1}$	$\dot{z}_2$	$\dot{\varphi}_{R2}$	F_i^e
chassis m_A	1	0	0	0	0	0	0	0
	0	0	0	0	0	0	0	0
	0	1	0	0	0	0	0	$F_{F1}+F_{F2}-m_A g$
wheel body front m_{RK1}	1	0	$-h_R$	$\frac{\partial x_1}{\partial z_1}$	0	0	0	0
	0	0	0	0	0	0	0	0
	0	1	$-a_1$	1	0	0	0	$-F_{F1}-m_{RK1} g$
wheel front m_{R1}	1	0	$-h_R$	$\frac{\partial x_1}{\partial z_1}$	0	0	0	F_{x1}
	0	0	0	0	0	0	0	0
	0	1	$-a_1$	1	0	0	0	$F_{z1}-m_{R1} g$
wheel body rear m_{RK2}	1	0	$-h_R$	0	0	$\frac{\partial x_2}{\partial z_2}$	0	0
	0	0	0	0	0	0	0	0
	0	1	a_2	0	0	1	0	$-F_{F2}-m_{RK2} g$
wheel rear m_{R2}	1	0	$-h_R$	0	0	$\frac{\partial x_2}{\partial z_2}$	0	F_{x2}
	0	0	0	0	0	0	0	0
	0	1	a_2	0	0	1	0	$F_{z2}-m_{R2} g$

Table 3.1: Partial Velocities and Applied Forces

bodies	partial angular velocities $\partial \omega_{0i}/\partial z_j$							applied torques
	$\dot{x}_A$	$\dot{z}_A$	$\dot{\beta}_A$	$\dot{z}_1$	$\dot{\varphi}_{R1}$	$\dot{z}_2$	$\dot{\varphi}_{R2}$	M_i^e
chassis Θ_A	0	0	0	0	0	0	0	0
	0	0	1	0	0	0	0	$-M_{A1}-M_{A2}-a_1 F_{F1}+a_2 F_{F2}$
	0	0	0	0	0	0	0	0
wheel body front Θ_{RK1}	0	0	0	0	0	0	0	0
	0	0	1	$\frac{\partial \beta_1}{\partial z_1}$	0	0	0	M_{B1}
	0	0	0	0	0	0	0	0
wheel front Θ_{R1}	0	0	0	0	0	0	0	0
	0	0	1	$\frac{\partial \beta_1}{\partial z_1}$	1	0	0	$M_{A1}-M_{B1}-R F_{x1}$
	0	0	0	0	0	0	0	0
wheel body rear Θ_{RK2}	0	0	0	0	0	0	0	0
	0	0	1	0	0	$\frac{\partial \beta_2}{\partial z_2}$	0	M_{B2}
	0	0	0	0	0	0	0	0
wheel rear Θ_{R2}	0	0	0	0	0	0	0	0
	0	0	1	0	0	$\frac{\partial \beta_2}{\partial z_2}$	1	$M_{A2}-M_{B2}-R F_{x2}$
	0	0	0	0	0	0	0	0

Table 3.2: Partial Angular Velocities and Applied Torques

aid of the partial velocities and partial angular velocities the elements of the mass matrix M and the components of the vector of generalized forces and torques Q can be calculated.

$$M(i,j) \;=\; \sum_{k=1}^{5} \left(\frac{\partial v_{0k}}{\partial z_i} \right)^T m_k \, \frac{\partial v_{0k}}{\partial z_j} \;+\; \sum_{k=1}^{5} \left(\frac{\partial \omega_{0k}}{\partial z_i} \right)^T \Theta_k \, \frac{\partial \omega_{0k}}{\partial z_j} \,; \quad i,j = 1(1)7 \,; \tag{3.45}$$

$$Q(i) \;=\; \sum_{k=1}^{5} \left(\frac{\partial v_{0k}}{\partial z_i} \right)^T F_k^e \;+\; \sum_{k=1}^{5} \left(\frac{\partial \omega_{0k}}{\partial z_i} \right)^T M_k^e \,; \quad i = 1(1)7 \,. \tag{3.46}$$

The equations of motion for the plane vehicle model are then given by

$$M \, \dot{z} \;=\; Q \,. \tag{3.47}$$

3.4.3 Equilibrium

With the abbreviations

$$m_1 = m_{RK1} + m_{R1} \,; \quad m_2 = m_{RK2} + m_{R2} \,; \quad m_G = m_A + m_1 + m_2 \tag{3.48}$$

and

$$h \;=\; h_R \;+\; R \tag{3.49}$$

The components of the vector of generalized forces and torques read as

$$\begin{aligned} Q(1) &= F_{x1} + F_{x2} \,; \\ Q(2) &= F_{z1} + F_{z2} - m_G \, g \,; \\ Q(3) &= -a_1 F_{z1} + a_2 F_{z2} - h(F_{x1} + F_{x2}) + a_1 \, m_1 \, g - a_2 \, m_2 \, g \,; \end{aligned} \tag{3.50}$$

$$\begin{aligned} Q(4) &= F_{z1} - F_{F1} + \tfrac{\partial x_1}{\partial z_1} \, F_{x1} - m_1 \, g + \tfrac{\partial \beta_1}{\partial z_1} (M_{A1} - R \, F_{x1}) \,; \\ Q(5) &= M_{A1} - M_{B1} - R \, F_{x1} \,; \end{aligned} \tag{3.51}$$

$$\begin{aligned} Q(6) &= F_{z2} - F_{F2} + \tfrac{\partial x_2}{\partial z_2} \, F_{x2} - m_2 \, g + \tfrac{\partial \beta_2}{\partial z_2} (M_{A_2} - R \, F_{x2}) \,; \\ Q(7) &= M_{A_2} - M_{B_2} - R \, F_{x2} \,. \end{aligned} \tag{3.52}$$

Without drive and brake forces

$$M_{A1} = 0 \,; \quad M_{A2} = 0 \,; \quad M_{B1} = 0 \,; \quad M_{B2} = 0 \tag{3.53}$$

from (3.50), (3.51) and (3.52) one gets the steady state longitudinal forces, the spring preloads and the wheel loads

$$\begin{aligned} F_{x1}^0 &= 0 \,; & F_{x2}^0 &= 0 \,; \\ F_{F1}^0 &= \tfrac{b}{a+b} \, m_A \, g \,; & F_{F2}^0 &= \tfrac{a}{a+b} \, m_A \, g \,; \\ F_{z1}^0 &= m_1 g + \tfrac{b}{a+b} \, m_A \, g \,; & F_{z2}^0 &= m_2 g + \tfrac{a}{a+b} \, m_A \, g \,. \end{aligned} \tag{3.54}$$

3.4.4 Driving and Braking

Assuming that on accelerating or decelerating the vehicle $\ddot{x}_A \neq 0$ the wheels neither slip nor lock,

$$\begin{aligned} R\,\dot{\varphi}_{R1} &= \dot{x}_A - h_R\,\dot{\beta}_A + \tfrac{\partial x_1}{\partial z_1}\,\dot{z}_1\,; \\ R\,\dot{\varphi}_{R2} &= \dot{x}_A - h_R\,\dot{\beta}_A + \tfrac{\partial x_2}{\partial z_2}\,\dot{z}_2\,. \end{aligned} \tag{3.55}$$

holds. In steady state the pitch motion of the body and the vertical motion of the wheels reach constant values

$$\beta_A = \beta_A^{st} = const.\,; \quad z_1 = z_1^{st} = const.\,; \quad z_2 = z_2^{st} = const. \tag{3.56}$$

and (3.55) simplifies to

$$R\,\dot{\varphi}_{R1} \;=\; \dot{x}_A\,; \quad R\,\dot{\varphi}_{R2} \;=\; \dot{x}_A\,. \tag{3.57}$$

With(3.56), (3.57) and (3.49) the equation of motion (3.47) results in

$$\begin{aligned} m_G\,\ddot{x}_A &= F_{x1}^a + F_{x2}^a\,; \\ 0 &= F_{z1}^a + F_{z2}^a\,; \\ -h_R(m_1{+}m_2)\,\ddot{x}_A + \Theta_{R1}\,\tfrac{\ddot{x}_A}{R} + \Theta_{R2}\,\tfrac{\ddot{x}_A}{R} &= -a\,F_{z1}^a + b\,F_{z2}^a - (h_R+R)(F_{x1}^a + F_{x2}^a)\,; \end{aligned} \tag{3.58}$$

$$\begin{aligned} \tfrac{\partial x_1}{\partial z_1}\,m_1\,\ddot{x}_A + \tfrac{\partial \beta_1}{\partial z_1}\,\Theta_{R1}\,\tfrac{\ddot{x}_A}{R} &= F_{z1}^a - F_{F1}^a + \tfrac{\partial x_1}{\partial z_1}\,F_{x1}^a + \tfrac{\partial \beta_1}{\partial z_1}(M_{A1} - R\,F_{x1}^a)\,; \\ \Theta_{R1}\,\tfrac{\ddot{x}_A}{R} &= M_{A1} - M_{B1} - R\,F_{x1}^a\,; \end{aligned} \tag{3.59}$$

$$\begin{aligned} \tfrac{\partial x_2}{\partial z_2}\,m_2\,\ddot{x}_A + \tfrac{\partial \beta_2}{\partial z_2}\,\Theta_{R2}\,\tfrac{\ddot{x}_A}{R} &= F_{z2}^a - F_{F2}^a + \tfrac{\partial x_2}{\partial z_2}\,F_{x2}^a + \tfrac{\partial \beta_2}{\partial z_2}(M_{A_2} - R\,F_{x2}^a)\,; \\ \Theta_{R2}\,\tfrac{\ddot{x}_A}{R} &= M_{A_2} - M_{B_2} - R\,F_{x2}^a\,; \end{aligned} \tag{3.60}$$

where the steady state spring forces, longitudinal forces and wheel loads have been separated into initial and acceleration-dependent terms

$$F_{xi}^{st} \;=\; F_{xi}^0 + F_{xi}^a\,; \quad F_{zi}^{st} \;=\; F_{zi}^0 + F_{zi}^a\,; \quad F_{Fi}^{st} \;=\; F_{Fi}^0 + F_{Fi}^a\,; \quad i{=}1,2\,. \tag{3.61}$$

With given torques of drive and brake the vehicle acceleration $\ddot{x}_A$, the wheel forces F_{x1}^a, F_{x2}^a, F_{z1}^a, F_{z2}^a and the spring forces F_{F1}^a, F_{F2}^a can be calculated from (3.58), (3.59) and (3.60)

Via the spring characteristics which have been assumed as linear the acceleration-dependent forces also cause a vertical displacement and pitch motion of the body

$$\begin{aligned} F_{F1}^a &= c_{A1}\,z_1^a\,, \\ F_{F2}^a &= c_{A2}\,z_2^a\,, \\ F_{z1}^a &= -c_{R1}\,(z_A^a - a\,\beta_A^a + z_1^a)\,, \\ F_{z2}^a &= -c_{R2}\,(z_A^a + b\,\beta_A^a + z_2^a)\,. \end{aligned} \tag{3.62}$$

besides the vertical motions of the wheels.

Especially the pitch of the vehicle $\beta_A^a \neq 0$, caused by drive or brake is, if too distinct, felt as annoying.

By an axle kinematics with 'anti dive' and/or 'anti squat' properties the drive and/or brake pitch angle can be reduced by rotating the wheel body and moving the wheel center in longitudinal direction during jounce and rebound.

3.4.5 Brake Pitch Pole

For real suspension systems the brake pitch pole can be calculated from the motions of the wheel contact points in the x-, z-plane, Fig. 3.9.

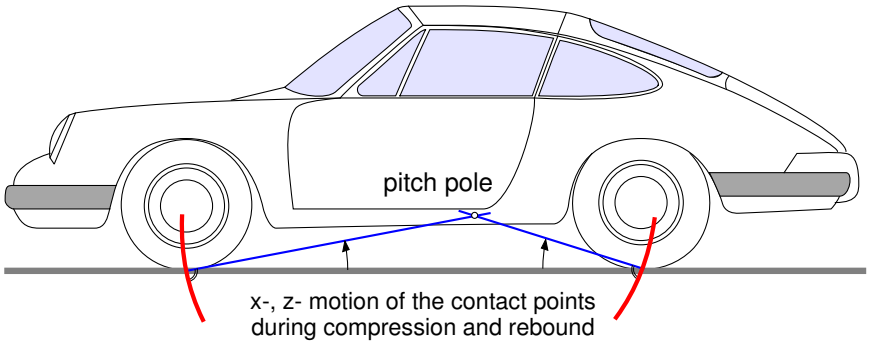

Figure 3.9: Brake Pitch Pole

Increasing the pitch pole height above the track level means a decrease in the brake pitch angle.

4 Lateral Dynamics

4.1 Kinematic Approach

4.1.1 Kinematic Tire Model

When a vehicle drives through the curve at low lateral acceleration, low lateral forces are needed for course holding. At the wheels then hardly lateral slip occurs. In the ideal case, with vanishing lateral slip, the wheels only move in circumferential direction. The speed component of the contact point in the tire's lateral direction then vanishes

$$v_y \;=\; e_y^T\, v_{0P} \;=\; 0\,. \tag{4.1}$$

This kinematic constraint equation can be used for course calculation of slowly moving vehicles.

4.1.2 Ackermann Geometry

Within the validity limits of the kinematic tire model the necessary steering angle of the front wheels can be constructed via given momentary turning center M, Fig. 4.1.

At slowly moving vehicles the lay out of the steering linkage is usually done according to the Ackermann geometry. With given steering angle of a wheel, e.g. δ_2, the wheel base a fixes the momentarily driven curve radius

$$\tan\delta_2 \;=\; \frac{a}{R} \qquad \text{or} \qquad R = \frac{a}{\tan\delta_2}\,. \tag{4.2}$$

For the second wheel however

$$\tan\delta_1 \;=\; \frac{a}{R+b} \tag{4.3}$$

holds, with b describing the track width. Combining (4.2) and (4.3) we get

$$\tan\delta_1 \;=\; \frac{a}{\dfrac{a}{\tan\delta_2}+b} \qquad \text{or} \qquad \tan\delta_1 \;=\; \frac{\tan\delta_2}{1+\dfrac{b}{a}\,\tan\delta_2}\,. \tag{4.4}$$

The deviations $\triangle\delta_1 = \delta_1^a - \delta_1^A$ of the actual steering angle δ_1^a from the Ackermann steering angle δ_1^A, which follows from (4.4), are used to judge a steering system.

At a rotation around the momentary pole M the direction of the velocity is fixed for every point of the vehicle. The angle β between the velocity vector v and the vehicle's longitudinal axis is called side slip angle.

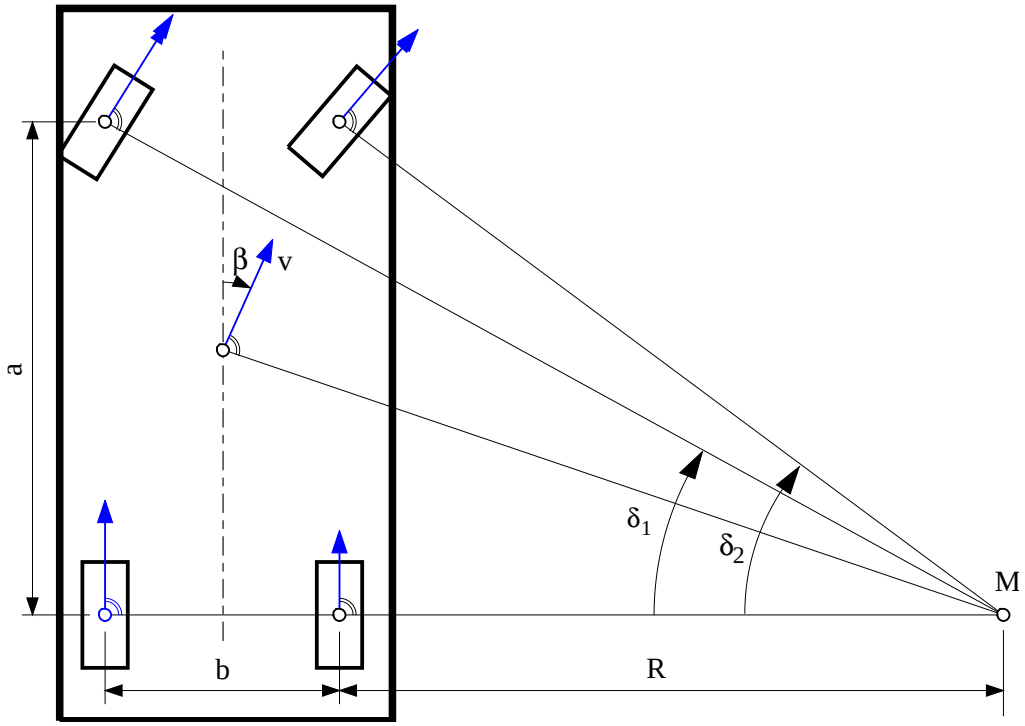

Figure 4.1: Ackermann Steering Geometry at a two-axled Vehicle

4.1.3 Space Requirement

The Ackermann approach can also be used to calculate the space requirement of a vehicle during cornering, Fig. 4.2.

If the front wheels of a two-axled vehicle are steered according to the Ackermann geometry the outer point of the vehicle front runs on the maximum radius R_{max} and a point on the inner side of the vehicle at the location of the rear axle runs on the minimum radius R_{min}. We get

$$R_{max}^2 \;=\; (R_{min} + b)^2 + (a + f)^2 \;, \tag{4.5}$$

where a, b are the wheel base and the width of the vehicle, and f specifies the distance of the vehicle front to the front axle. Hence, the space requirement

$$\triangle R \;=\; R_{max} - R_{min} \;=\; \sqrt{(R_{min} + b)^2 + (a + f)^2} \;-\; R_{min} \;, \tag{4.6}$$

can be calculated as a function of the cornering radius R_{min}.

The space requirement $\triangle R$ of a typical passenger car and a bus is plotted in Fig. 4.3 versus the minimum cornering radius.

In narrow curves $R_{min} = 5.0\,m$ a bus requires a space of 2.5 the width, whereas a passenger car needs only 1.5 the width.

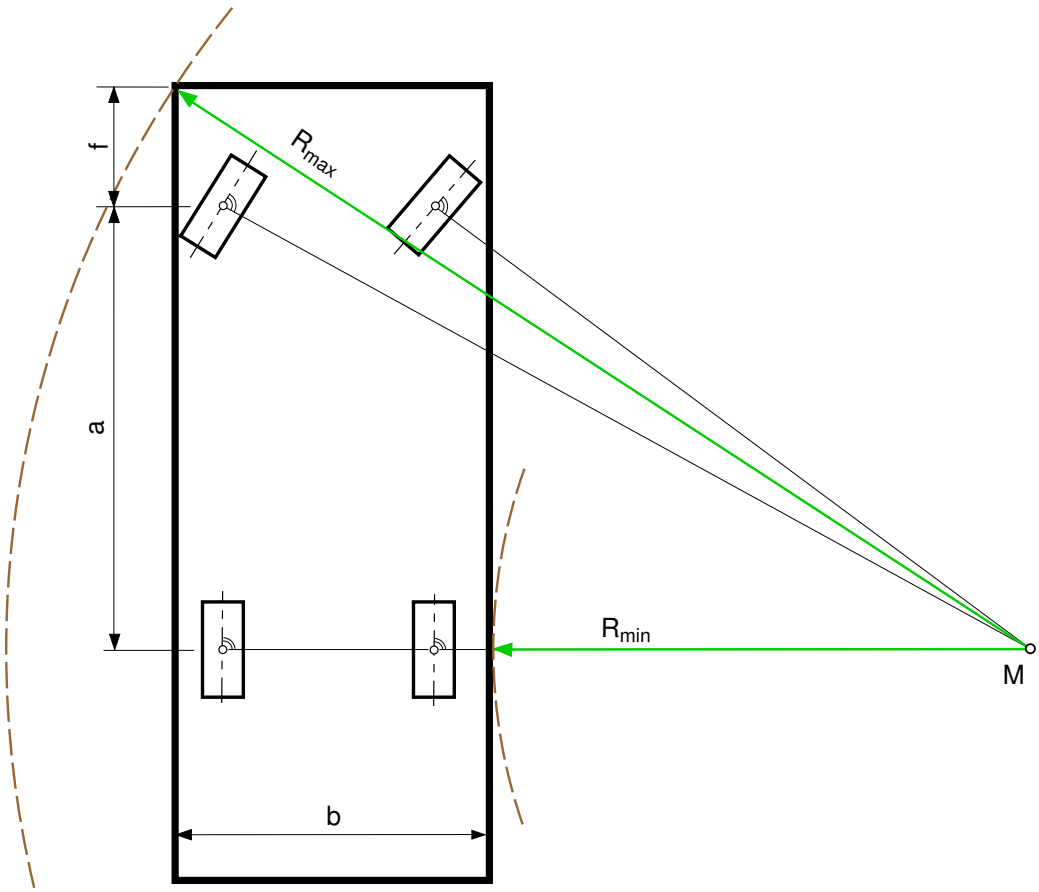

Figure 4.2: Space Requirement

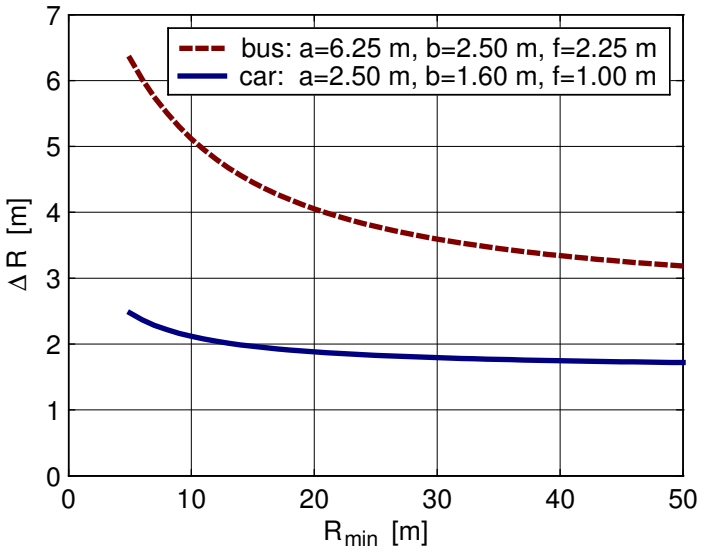

Figure 4.3: Space Requirement of typical Passenger Car and Bus

4.1.4 Vehicle Model with Trailer

4.1.4.1 Position

Fig. 4.4 shows a simple lateral dynamics model for a two-axled vehicle with a single-axled trailer. Vehicle and trailer move on a horizontal track. The position and the orientation of the

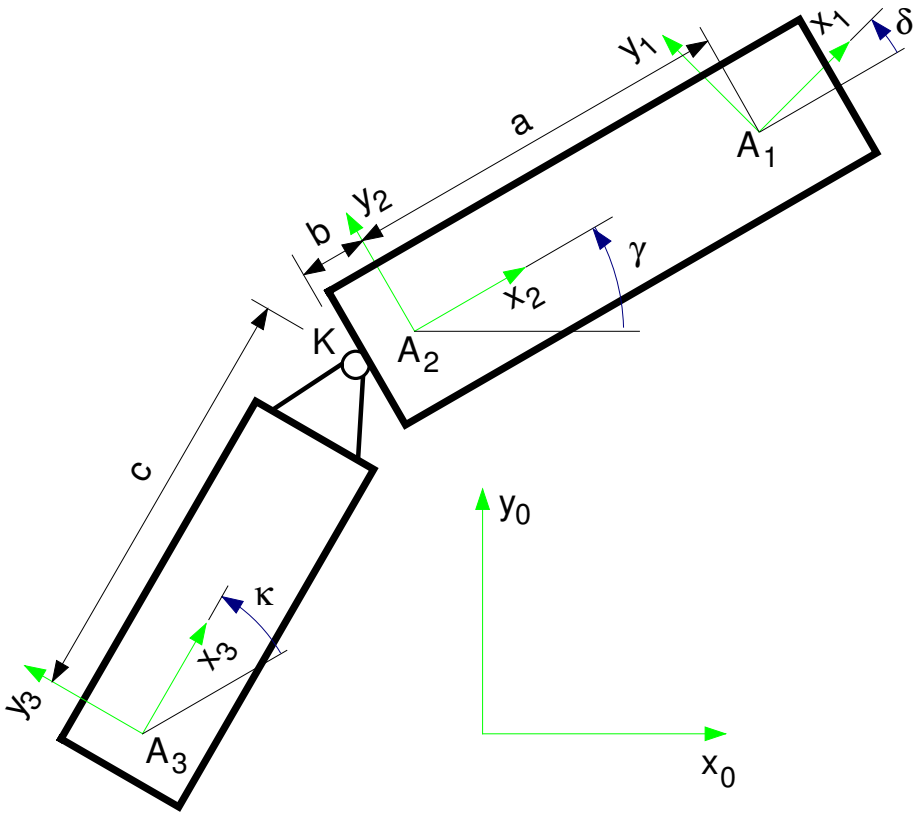

Figure 4.4: Kinematic Model with Trailer

vehicle relative to the track fixed frame x_0, y_0, z_0 is defined by the position vector to the rear axle center

$$r_{0A_2,0} = \begin{bmatrix} x_F \\ y_F \\ R \end{bmatrix} \tag{4.7}$$

and the rotation matrix

$$A_{02} = \begin{bmatrix} \cos\gamma & -\sin\gamma & 0 \\ \sin\gamma & \cos\gamma & 0 \\ 0 & 0 & 1 \end{bmatrix} . \tag{4.8}$$

Here, the tire radius R is considered to be constant, and x_F, y_F as well as γ are generalized coordinates.

The position vector

$$r_{0A_1,0} \;=\; r_{0A_2,0} \;+\; A_{02}\, r_{A_2A_1,2} \quad \text{mit} \quad r_{A_2A_1,2} = \begin{bmatrix} a \\ 0 \\ 0 \end{bmatrix} \tag{4.9}$$

and the rotation matrix

$$A_{01} \;=\; A_{02}\, A_{21} \quad \text{mit} \quad A_{21} \;=\; \begin{bmatrix} \cos\delta & -\sin\delta & 0 \\ \sin\delta & \cos\delta & 0 \\ 0 & 0 & 1 \end{bmatrix} \tag{4.10}$$

describe the position and the orientation of the front axle, where $a = const$ labels the wheel base and δ the steering angle.

The position vector

$$r_{0A_3,0} \;=\; r_{0A_2,0} + A_{02}\left(r_{A_2K,2} + A_{23}\, r_{KA_3,3}\right) \tag{4.11}$$

with

$$r_{A_2K,2} = \begin{bmatrix} -b \\ 0 \\ 0 \end{bmatrix} \quad \text{and} \quad r_{KA_3,2} = \begin{bmatrix} -c \\ 0 \\ 0 \end{bmatrix} \tag{4.12}$$

and the rotation matrix

$$A_{03} \;=\; A_{02}\, A_{23} \quad \text{mit} \quad A_{23} \;=\; \begin{bmatrix} \cos\kappa & -\sin\kappa & 0 \\ \sin\kappa & \cos\kappa & 0 \\ 0 & 0 & 1 \end{bmatrix} \tag{4.13}$$

define the position and the orientation of the trailer axis, with κ labelling the bend angle between vehicle and trailer and b, c marking the distances from the rear axle A_2 to the coupling point K and from the coupling point K to the trailer axis A_3.

4.1.4.2 Vehicle

According to the kinematic tire model, cf. section 4.1.1, the velocity at the rear axle can only have a component in the vehicle's longitudinal direction

$$v_{0A_2,2} \;=\; \begin{bmatrix} v_{x2} \\ 0 \\ 0 \end{bmatrix} . \tag{4.14}$$

The time derivative of (4.7) results in

$$v_{0A_2,0} \;=\; \dot{r}_{0A_2,0} \;=\; \begin{bmatrix} \dot{x}_F \\ \dot{y}_F \\ 0 \end{bmatrix} . \tag{4.15}$$

With the transformation of (4.14) into the system 0

$$v_{0A_2,0} \;=\; A_{02}\, v_{0A_2,2} \;=\; A_{02} \begin{bmatrix} v_{x2} \\ 0 \\ 0 \end{bmatrix} \;=\; \begin{bmatrix} \cos\gamma\, v_{x2} \\ \sin\gamma\, v_{x2} \\ 0 \end{bmatrix} \tag{4.16}$$

one gets by equalizing with (4.15) two first order differential equations for the position coordinates x_F and y_F

$$\boxed{\begin{aligned} \dot{x}_F &= \cos\gamma\, v_{x2}\,, \\ \dot{y}_F &= \sin\gamma\, v_{x2}\,. \end{aligned}} \tag{4.17}$$

The velocity at the front axis follows from (4.9)

$$v_{0A_1,0} \;=\; \dot{r}_{0A_1,0} \;=\; \dot{r}_{0A_2,0} \;+\; \omega_{02,0} \times A_{02}\, r_{A_2A_1,2}\,. \tag{4.18}$$

Transformed into the vehicle fixed system x_2, y_2, z_2

$$v_{0A_1,2} \;=\; \underbrace{\begin{bmatrix} v_{x2} \\ 0 \\ 0 \end{bmatrix}}_{v_{0A_2,2}} + \underbrace{\begin{bmatrix} 0 \\ 0 \\ \dot{\gamma} \end{bmatrix}}_{\omega_{02,2}} \times \underbrace{\begin{bmatrix} a \\ 0 \\ 0 \end{bmatrix}}_{r_{A_2A_1,2}} \;=\; \begin{bmatrix} v_{x2} \\ a\,\dot{\gamma} \\ 0 \end{bmatrix}\,. \tag{4.19}$$

remains. The unit vectors

$$e_{x1,2} \;=\; \begin{bmatrix} \cos\delta \\ \sin\delta \\ 0 \end{bmatrix} \quad \text{and} \quad e_{y1,2} \;=\; \begin{bmatrix} -\sin\delta \\ \cos\delta \\ 0 \end{bmatrix} \tag{4.20}$$

define the longitudinal and lateral direction at the front axle.

According to (4.1) the velocity component lateral to the wheel must vanish,

$$e_{y1,2}^T\, v_{0A_1,2} \;=\; -\sin\delta\, v_{x2} \;+\; \cos\delta\, a\,\dot{\gamma} \;=\; 0\,. \tag{4.21}$$

In longitudinal direction then

$$e_{x1,2}^T\, v_{0A_1,2} \;=\; \cos\delta\, v_{x2} \;+\; \sin\delta\, a\,\dot{\gamma} \;=\; v_{x1} \tag{4.22}$$

remains.

From (4.21) a first order differential equation follows for the yaw angle

$$\boxed{\dot{\gamma} \;=\; \frac{v_{x2}}{a}\, \tan\delta\,.} \tag{4.23}$$

4.1.4.3 Entering a Curve

In analogy to (4.2) the steering angle δ can be related to the current track radius R or with $k = 1/R$ to the current track curvature

$$\tan\delta \;=\; \frac{a}{R} \;=\; a\,k\,. \tag{4.24}$$

The differential equation for the yaw angle then reads as

$$\dot{\gamma} \;=\; v_{x2}\,k\,. \tag{4.25}$$

With the curvature gradient

$$k \;=\; k(t) \;=\; k_C\,\frac{t}{T} \tag{4.26}$$

The entering of a curve is described as a continuous transition from a line with the curvature $k = 0$ into a circle with the curvature $k = k_C$.

The yaw angle of the vehicle can now be calculated by simple integration

$$\gamma(t) \;=\; \frac{v_{x2}\,k_C}{T}\;\frac{t^2}{2}\,, \tag{4.27}$$

where at time $t = 0$ a vanishing yaw angle, $\gamma(t{=}0) = 0$, has been assumed.

The vehicle's position then follows with (4.27) from the differential equations (4.17)

$$x_F \;=\; v_{x2}\int_{t=0}^{t=T}\cos\left(\frac{v_{x2}\,k_C}{T}\,\frac{t^2}{2}\right)\,dt\,,\qquad y_F \;=\; v_{x2}\int_{t=0}^{t=T}\sin\left(\frac{v_{x2}\,k_C}{T}\,\frac{t^2}{2}\right)\,dt\,. \tag{4.28}$$

At constant vehicle speed $v_{x2} = const.$ (4.28) is the parameterized form of a clothoide.

From (4.24) the necessary steering angle can be calculated, too. If only small steering angles are necessary for driving through the curve, the $\tan$-function can be approximated by its argument, and

$$\delta \;=\; \delta(t) \;\approx\; a\,k \;=\; a\,k_C\,\frac{t}{T} \tag{4.29}$$

holds, i.e. the driving through a clothoide is manageable by continuous steer motion.

4.1.4.4 Trailer

The velocity of the trailer axis can be received by differentiation of the position vector (4.11)

$$v_{0A_3,0} \;=\; \dot{r}_{0A_3,0} \;=\; \dot{r}_{0A_2,0} \;+\; \omega_{02,0}\times A_{02}\,r_{A_2A_3,2} \;+\; A_{02}\,\dot{r}_{A_2A_3,2}\,. \tag{4.30}$$

With

$$r_{A_2A_3,2} \;=\; r_{A_2K,2} \;+\; A_{23}\,r_{KA_3,3} \;=\; \begin{bmatrix} -b \;-\; c\,\cos\kappa \\ -c\,\sin\kappa \\ 0 \end{bmatrix} \tag{4.31}$$

and

$$\dot{r}_{A_2A_3,2} = \underbrace{\begin{bmatrix} 0 \\ 0 \\ \dot{\kappa} \end{bmatrix}}_{\omega_{23,2}} \times \underbrace{\begin{bmatrix} -c\,\cos\kappa \\ -c\,\sin\kappa \\ 0 \end{bmatrix}}_{A_{23}\,r_{KA_3,3}} = \begin{bmatrix} c\,\sin\kappa\,\dot{\kappa} \\ -c\,\cos\kappa\,\dot{\kappa} \\ 0 \end{bmatrix} \tag{4.32}$$

it remains, if (4.30) is transformed into the vehicle fixed frame x_2, y_2, z_2

$$v_{0A_3,2} = \underbrace{\begin{bmatrix} v_{x2} \\ 0 \\ 0 \end{bmatrix}}_{v_{0A_2,2}} + \underbrace{\begin{bmatrix} 0 \\ 0 \\ \dot{\gamma} \end{bmatrix}}_{\omega_{02,2}} \times \underbrace{\begin{bmatrix} -b\,-c\,\cos\kappa \\ -c\,\sin\kappa \\ 0 \end{bmatrix}}_{r_{A_2A_3,2}} + \underbrace{\begin{bmatrix} c\,\sin\kappa\,\dot{\kappa} \\ -c\,\cos\kappa\,\dot{\kappa} \\ 0 \end{bmatrix}}_{\dot{r}_{A_2A_3,2}} = \begin{bmatrix} v_{x2} + c\,\sin\kappa\,(\dot{\kappa}+\dot{\gamma}) \\ -b\,\dot{\gamma} - c\,\cos\kappa\,(\dot{\kappa}+\dot{\gamma}) \\ 0 \end{bmatrix} . \tag{4.33}$$

The longitudinal and lateral direction at the trailer axis are defined by the unit vectors

$$e_{x3,2} = \begin{bmatrix} \cos\kappa \\ \sin\kappa \\ 0 \end{bmatrix} \quad \text{and} \quad e_{y3,2} = \begin{bmatrix} -\sin\kappa \\ \cos\kappa \\ 0 \end{bmatrix} . \tag{4.34}$$

At the trailer axis the lateral velocity must also vanish

$$e_{y3,2}^T\,v_{0A_3,2} = -\sin\kappa\,\left(v_{x2} + c\,\sin\kappa\,(\dot{\kappa}+\dot{\gamma})\right) + \cos\kappa\,\left(-b\,\dot{\gamma} - c\,\cos\kappa\,(\dot{\kappa}+\dot{\gamma})\right) = 0\,. \tag{4.35}$$

In longitudinal direction

$$e_{x3,2}^T\,v_{0A_3,2} = \cos\kappa\,\left(v_{x2} + c\,\sin\kappa\,(\dot{\kappa}+\dot{\gamma})\right) + \sin\kappa\,\left(-b\,\dot{\gamma} - c\,\cos\kappa\,(\dot{\kappa}+\dot{\gamma})\right) = v_{x3} \tag{4.36}$$

remains.

When (4.23) is inserted into (4.35), one gets a differential equation of first order for the bend angle

$$\dot{\kappa} = -\frac{v_{x2}}{a}\,\left(\frac{a}{c}\,\sin\kappa + \left(\frac{b}{c}\,\cos\kappa + 1\right)\tan\delta\right) . \tag{4.37}$$

The differential equations (4.17) and (4.23) describe position and orientation within the x_0, y_0 plane. The position of the trailer relative to the vehicle follows from (4.37).

4.1.4.5 Course Calculations

For a given set of vehicle parameters a, b, c, and predefined time functions of the vehicle speed, $v_{x2} = v_{x2}(t)$ and the steering angle, $\delta = \delta(t)$ the course of vehicle and trailer can be calculated by numerical integration of the differential equations (4.17), (4.23) and (4.37).

If the steering angle is slowly increased at constant driving speed, then the vehicle drives figure which is similar to a clothoide, Fig. 4.5.

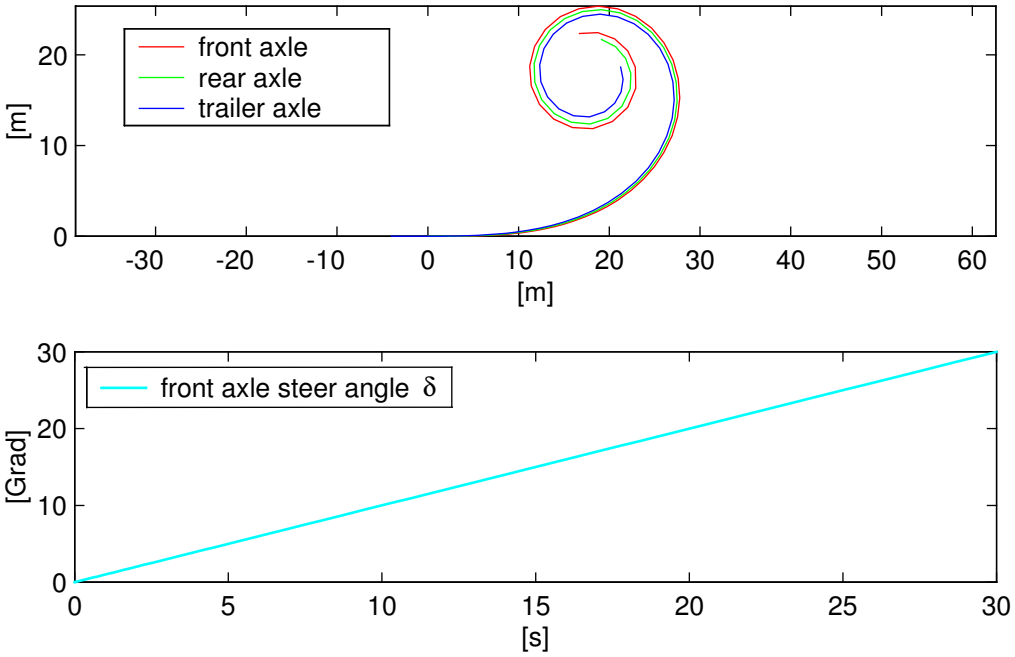

Figure 4.5: Entering a Curve

4.2 Steady State Cornering

4.2.1 Overturning Limit

The overturning hazard of a vehicle is primarily determined by the track width and the height of the center of gravity. With trucks however, also the tire deflection and the body roll have to be respected., Fig. 4.6.

The balance of torques at the already inclined vehicle delivers for small angles $\alpha_1 \ll 1$, $\alpha_2 \ll 1$

$$(F_{zL} - F_{zR})\,\frac{s}{2} \;=\; m\,a_y\,(h_1 + h_2) \;+\; m\,g\,[(h_1 + h_2)\alpha_1 + h_2\alpha_2]\;, \tag{4.38}$$

where a_y indicates the lateral acceleration and m is the sprung mass.

On a left-hand tilt, the right tire raises

$$F_{zR}^K \;=\; 0 \tag{4.39}$$

and the left tire carries all the vehicle weight

$$F_{zL}^K \;=\; m\,g\;. \tag{4.40}$$

Using (4.39) and (4.40) one gets from (4.38)

$$\frac{a_y^K}{g} \;=\; \frac{\frac{s}{2}}{h_1 + h_2} \;-\; \alpha_1^K \;-\; \frac{h_2}{h_1 + h_2}\,\alpha_2^K\;. \tag{4.41}$$

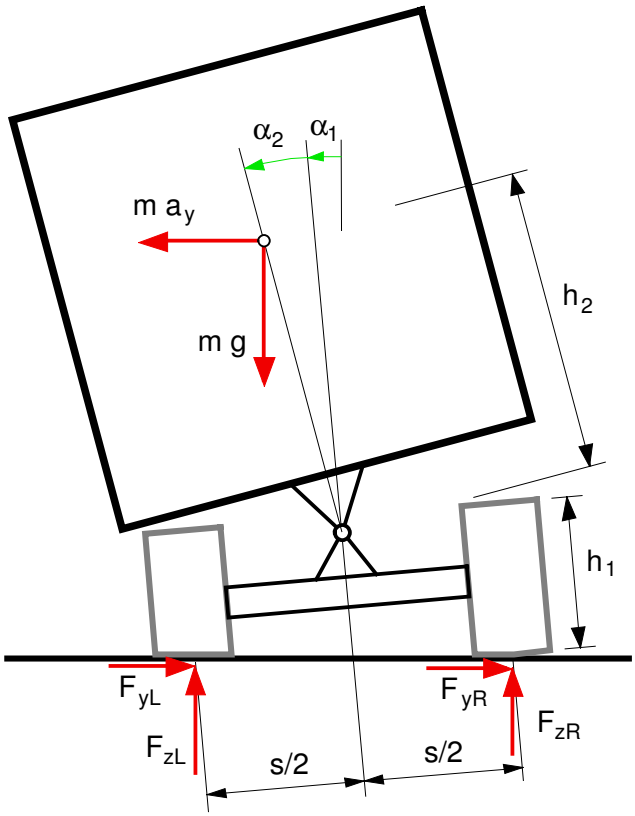

Figure 4.6: Overturning Hazard on Trucks

The vehicle turns over, when the lateral acceleration a_y rises above the limit a_y^K

Roll of axle and body reduce the overturning limit. The angles α_1^K and α_2^K can be calculated from the tire stiffness c_R and the body's roll stiffness.

On a straight-ahead drive, the vehicle weight is equally distributed to both tires

$$F_{zR}^{stat} = F_{zL}^{stat} = \frac{1}{2} m\, g\,. \tag{4.42}$$

With

$$F_{zL}^{K} = F_{zL}^{stat} + \triangle F_z \tag{4.43}$$

and the relations (4.40), (4.42) one gets for the increase of the wheel load at the overturning limit

$$\triangle F_z = \frac{1}{2} m\, g\,. \tag{4.44}$$

The resulting tire deflection then follows from

$$\triangle F_z = c_R \triangle r\,, \tag{4.45}$$

where c_R is the radial tire stiffness.

Because the right tire simultaneously rebounds for the same amount, for the roll angle of the axle

$$2 \triangle r \;=\; s\,\alpha_1^K \quad \text{or} \quad \alpha_1^K \;=\; \frac{2 \triangle r}{s} \;=\; \frac{m\,g}{s\,c_R}\,. \tag{4.46}$$

holds.

In analogy to (4.38) the balance of torques at the body delivers

$$c_W * \alpha_2 \;=\; m\,a_y\,h_2 \;+\; m\,g\,h_2\,(\alpha_1 + \alpha_2)\,, \tag{4.47}$$

where c_W names the roll stiffness of the body suspension.

Accordingly, at the overturning limit $a_y = a_y^K$

$$\alpha_2^K \;=\; \frac{a_y^K}{g}\,\frac{mgh_2}{c_W - mgh_2} \;+\; \frac{mgh_2}{c_W - mgh_2}\,\alpha_1^K \tag{4.48}$$

holds. Not allowing the vehicle to overturn already at $a_y^K \;=\; 0$ demands a minimum of roll stiffness $c_W > c_W^{min} = mgh_2$.

With (4.46) and (4.48) the overturning condition (4.41) reads as

$$(h_1 + h_2)\,\frac{a_y^K}{g} \;=\; \frac{s}{2} \;-\; (h_1 + h_2)\,\frac{1}{c_R^*} \;-\; h_2\,\frac{a_y^K}{g}\,\frac{1}{c_W^* - 1} \;-\; h_2\,\frac{1}{c_W^* - 1}\,\frac{1}{c_R*}\,, \tag{4.49}$$

where, for abbreviation purposes, the dimensionless stiffnesses

$$c_R^* \;=\; \frac{c_R}{\frac{m\,g}{s}} \quad \text{and} \quad c_W^* \;=\; \frac{c_W}{m\,g\,h_2} \tag{4.50}$$

have been used.

Resolved for the normalized lateral acceleration

$$\frac{a_y^K}{g} \;=\; \frac{\frac{s}{2}}{h_1 + h_2 + \frac{h_2}{c_W^* - 1}} \;-\; \frac{1}{c_R^*} \tag{4.51}$$

remains.

At heavy trucks, a twin tire axle can be loaded with $m = 13\,000\;kg$. The radial stiffness of one tire is $c_R = 800\,000\;N/m$ and the track with can be set to $s = 2\,m$. The values $h_1 = 0.8\,m$ and $h_2 = 1.0\;m$ hold at maximal load. This values deliver the results shown in Fig. 4.7 Even at a rigid body suspension $c_W^* \to \infty$ the vehicle turns over at a lateral acceleration of $a_y \approx 0.5\;g$. The roll angle of the vehicle then solely results from the tire deflection.

At a normalized roll stiffness of $c_W^* = 5$ the overturning limit lies at $a_y \approx 0.45\,g$ and so reaches already 90% of the maximum. The vehicle will then turn over at a roll angle of $\alpha \approx 10°$.

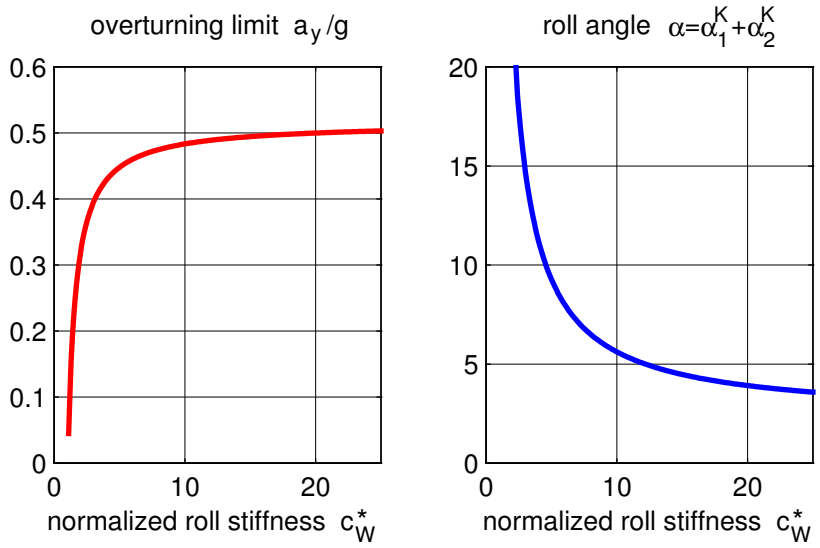

Figure 4.7: Tilting Limit for a Truck at Steady State Cornering

4.2.2 Roll Support and Camber Compensation

When a vehicle drives through a curve with the lateral acceleration a_y, centrifugal forces are delivered to the single masses. At the even roll model in Fig. 4.8 these are the forces $m_A\, a_y$ and $m_R\, a_y$, where m_A names the body mass and m_R the wheel mass.

Through the centrifugal force $m_A\, a_y$ applied to the body at the center of gravity, a roll torque is generated, that rolls the body with the angle α_A and leads to a counterwise deflection of the tires $z_1 = -z_2$.

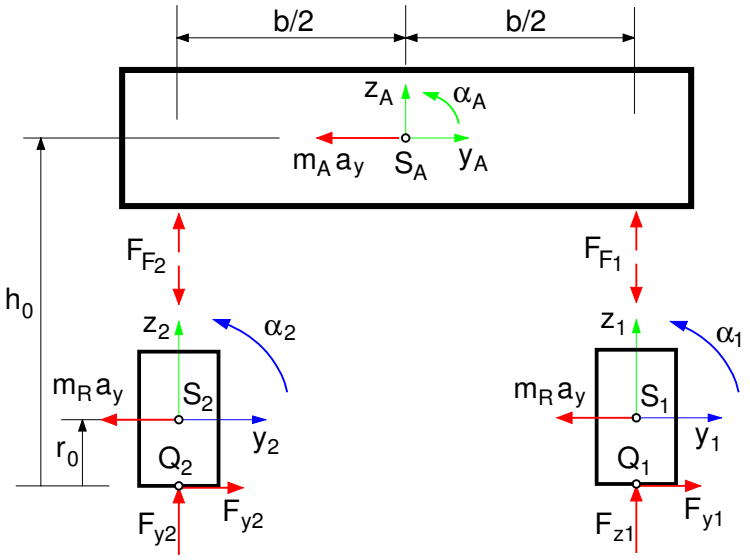

Figure 4.8: Plane Roll Model

At steady state cornering, the vehicle is balanced. With the principle of virtual work

$$\delta W \;=\; 0 \tag{4.52}$$

the equilibrium position can be calculated.

At the plane vehicle model in Fig. 4.8 the suspension forces F_{F1}, F_{F2} and tire forces F_{y1}, F_{z1}, F_{y2}, F_{z2}, are approximated by linear spring elements with the constants c_A and c_Q, c_R. The work W of these forces can be calculated directly or using $W = -V$ via the potential V. At small deflections with linearized kinematics one gets

$$\begin{aligned} W \;=\;& -m_A\, a_y\, y_A \\ & -m_R\, a_y\, \left(y_A + h_R\, \alpha_A + y_1\right)^2 \;-\; m_R\, a_y\, \left(y_A + h_R\, \alpha_A + y_2\right)^2 \\ & -\tfrac{1}{2}\, c_A\, z_1^2 \;-\; \tfrac{1}{2}\, c_A\, z_2^2 \\ & -\tfrac{1}{2}\, c_S\, \left(z_1 - z_2\right)^2 \\ & -\tfrac{1}{2}\, c_Q\, \left(y_A + h_0\, \alpha_A + y_1 + r_0\, \alpha_1\right)^2 \;-\; \tfrac{1}{2}\, c_Q\, \left(y_A + h_0\, \alpha_A + y_2 + r_0\, \alpha_2\right)^2 \\ & -\tfrac{1}{2}\, c_R\, \left(z_A + \tfrac{b}{2}\, \alpha_A + z_1\right)^2 \;-\; \tfrac{1}{2}\, c_R\, \left(z_A - \tfrac{b}{2}\, \alpha_A + z_2\right)^2 \;, \end{aligned} \tag{4.53}$$

where the abbreviation $h_R = h_0 - r_0$ has been used and c_S describes the spring constant of the anti roll bar, converted to the vertical displacement of the wheel centers.

The kinematics of the wheel suspension are symmetrical. With the linear approaches

$$y_1 \;=\; \frac{\partial y}{\partial z}\, z_1 \;, \quad \alpha_1 \;=\; \frac{\partial \alpha}{\partial z}\, \alpha_1 \quad \text{and} \quad y_2 \;=\; -\frac{\partial y}{\partial z}\, z_2 \;, \quad \alpha_2 \;=\; -\frac{\partial \alpha}{\partial z}\, \alpha_2 \tag{4.54}$$

the work W can be described as function of the position vector

$$y \;=\; \left[\, y_A,\; z_A,\; \alpha_A,\; z_1,\; z_2 \,\right]^T \;. \tag{4.55}$$

Due to

$$W = W(y) \tag{4.56}$$

principle of virtual work (4.52) leads to

$$\delta W \;=\; \frac{\partial W}{\partial y}\, \delta y \;=\; 0 \,. \tag{4.57}$$

Because of $\delta y \neq 0$ a system of linear equations in the form of

$$K\, y \;=\; b \tag{4.58}$$

results from (4.57). The matrix K and the vector b are given by

$$K = \begin{bmatrix} 2\, c_Q & 0 & 2\, c_Q\, h_0 & \frac{\partial y^Q}{\partial z} c_Q & -\frac{\partial y^Q}{\partial z} c_Q \\ 0 & 2\, c_R & 0 & c_R & c_R \\ 2\, c_Q\, h_0 & 0 & c_\alpha & \frac{b}{2} c_R + h_0 \frac{\partial y^Q}{\partial z} c_Q & -\frac{b}{2} c_R - h_0 \frac{\partial y^Q}{\partial z} c_Q \\ \frac{\partial y^Q}{\partial z} c_Q & c_R & \frac{b}{2} c_R + h_0 \frac{\partial y^Q}{\partial z} c_Q & c_A^* + c_S + c_R & -c_S \\ -\frac{\partial y^Q}{\partial z} c_Q & c_R & -\frac{b}{2} c_R - h_0 \frac{\partial y^Q}{\partial z} c_Q & -c_S & c_A^* + c_S + c_R \end{bmatrix} \tag{4.59}$$

and

$$b \;=\; -\begin{bmatrix} m_A + 2\,m_R \\ 0 \\ (m_1 + m_2)\,h_R \\ m_R\,\partial y/\partial z \\ -m_R\,\partial y/\partial z \end{bmatrix} a_y \,. \tag{4.60}$$

The following abbreviations have been used:

$$\frac{\partial y^Q}{\partial z} \;=\; \frac{\partial y}{\partial z} + r_0\,\frac{\partial \alpha}{\partial z}\,, \quad c_A^* \;=\; c_A + c_Q \left(\frac{\partial y}{\partial z}\right)^2, \quad c_\alpha \;=\; 2\,c_Q\,h_0^2 + 2\,c_R \left(\frac{b}{2}\right)^2 . \tag{4.61}$$

The system of linear equations (4.58) can be solved numerically, e.g. with MATLAB. Thus the influence of axle suspension and axle kinematics on the roll behavior of the vehicle can be investigated.

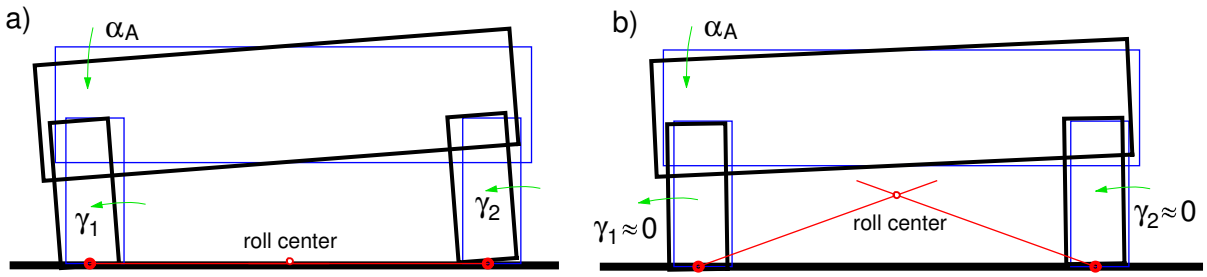

Figure 4.9: Roll Behavior at Cornering: a) without and b) with Camber Compensation

If the wheels only move vertically to the body at bound and rebound, then, at fast cornering the wheels are no longer perpendicular to the track Fig. 4.9 a.

The camber angles $\gamma_1 > 0$ and $\gamma_2 > 0$ result in an unfavorable pressure distribution in the contact area, which leads to a reduction of the maximally transmittable lateral forces.

At more sportive vehicles thus axle kinematics are employed, where the wheels are rotated around the longitudinal axis at bound and rebound, $\alpha_1 = \alpha_1(z_1)$ and $\alpha_2 = \alpha_2(z_2)$. With this, a "camber compensation" can be achieved with $\gamma_1 \approx 0$ and $\gamma_2 \approx 0$. Fig. 4.9 b. By the rotation of the wheels around the longitudinal axis on jounce, the wheel contact points are moved outwards, i.e against the lateral force. By this a 'roll support' is achieved, that reduces the body roll.

4.2.3 Roll Center and Roll Axis

The 'roll center' can be constructed from the lateral motion of the wheel contact points Q_1 and Q_2, Fig. 4.9.

The line through the roll center at the front and rear axle is called 'roll axis', Fig. 4.10.

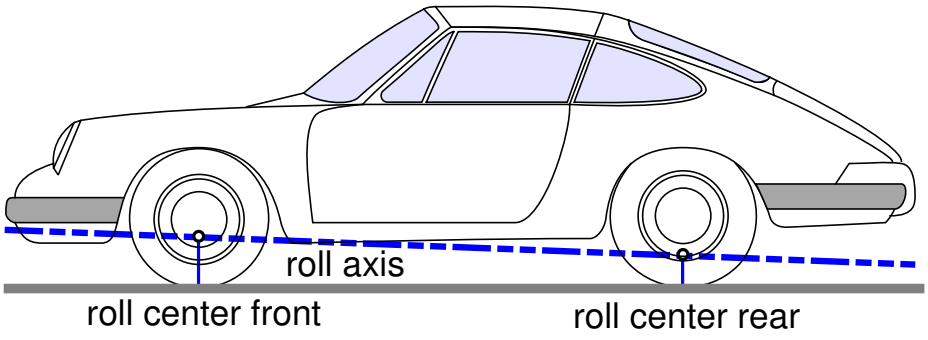

Figure 4.10: Roll Axis

4.2.4 Wheel Loads

The roll angle of a vehicle during cornering depends on the roll stiffness of the axle and on the position of the roll center.

Different axle layouts at the front and rear axle may result in different roll angles of the front and rear part of the chassis, Fig. 4.11.

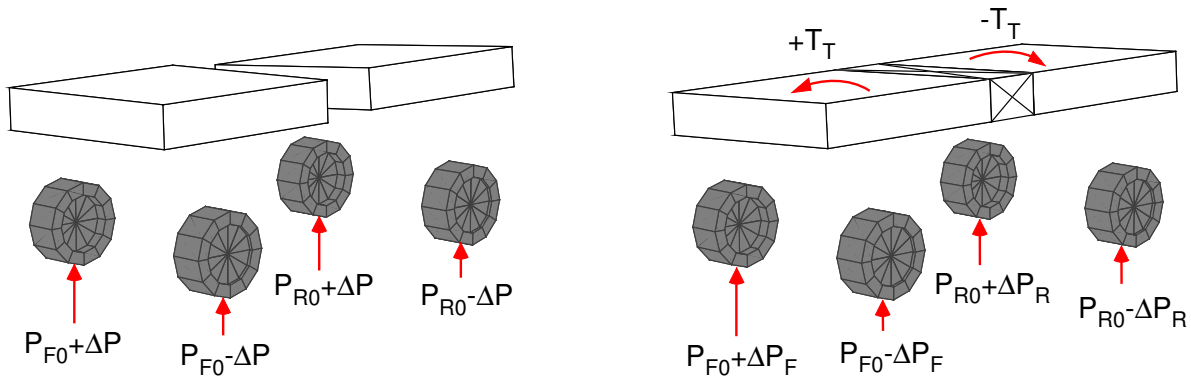

Figure 4.11: Wheel Loads for a flexible and a rigid Chassis

On most passenger cars the chassis is rather stiff. Hence, front an rear part of the chassis are forced via an internal torque to an overall chassis roll angle. This torque affects the wheel loads and generates different wheel load differences at the front and rear axle.

Due to the degressive influence of the wheel load to longitudinal and lateral tire forces the steering tendency of a vehicle can be affected.

4.2.5 Cornering Resistance

We look at a vehicle cornering with constant velocity v on an flat horizontal road, Fig. 4.12. Then, the velocity state of the vehicle can be described by

$$v_{0S,F} = \begin{bmatrix} v\,\cos\beta \\ v\,\sin\beta \\ 0 \end{bmatrix} \quad \text{und} \quad \omega_{0F,F} = \begin{bmatrix} 0 \\ 0 \\ \omega \end{bmatrix} \tag{4.62}$$

where β denotes the side slip angle of the vehicle at the center of gravity, and the subscript $_{,F}$ indicates that the vectors are expressed in the vehicle fixed reference frame F.

The angular velocity of the vehicle is given by

$$\omega = \frac{v}{R}\,, \tag{4.63}$$

where R denotes the radius of curvature.

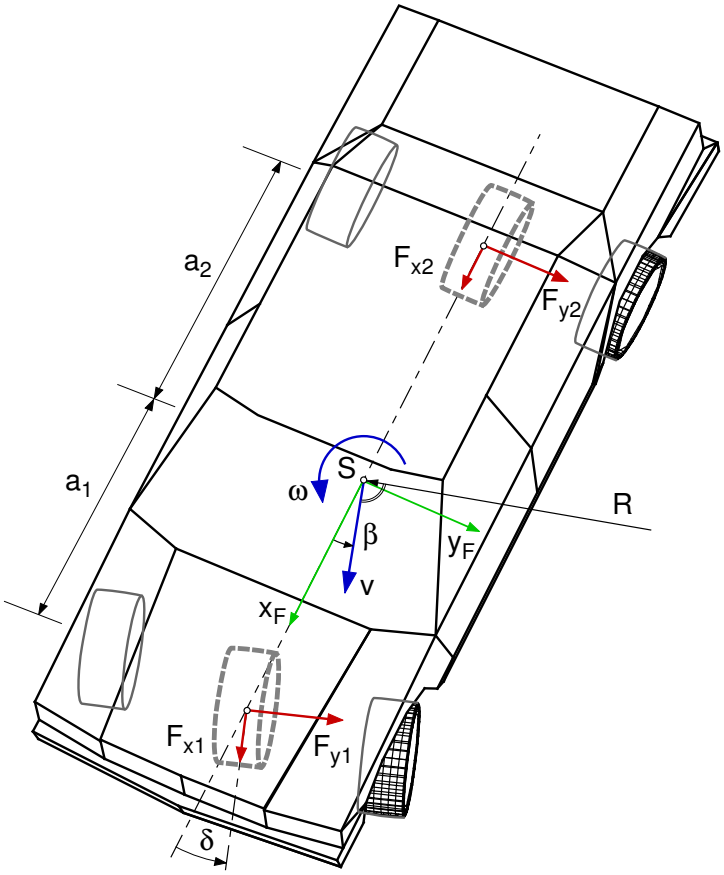

Figure 4.12: Steady State Cornering

In the body fixed reference frame linear and angular momentum result in

$$m\left(-\frac{v^2}{R}\,\sin\beta\right) \;=\; F_{x1}\cos\delta - F_{y1}\sin\delta + F_{x2}\,, \tag{4.64}$$

$$m\left(\frac{v^2}{R}\cos\beta\right) = F_{x1}\sin\delta + F_{y1}\cos\delta + F_{y2}\,, \tag{4.65}$$

$$0 = a_1\,(F_{x1}\sin\delta + F_{y1}\cos\delta) - a_2\,F_{y2}\,, \tag{4.66}$$

where m denotes the mass of the vehicle, F_{x1}, F_{x2}, F_{y1}, F_{y2} are the resulting forces in longitudinal and vertical direction applied at the front and rear axle, and δ specifies the average steer angle at the front axle.

The engine torque is distributed by the center differential to the front and rear axle. Then, in steady state condition it holds

$$F_{x1} = k\,F_D \quad \text{und} \quad F_{x2} = (1-k)\;F_D\,, \tag{4.67}$$

where F_D is the driving force and by k different driving conditions can be modelled:

$k=0$	Rear Wheel Drive	$F_{x1}=0,\;F_{x2}=F_D$
$0<k<1$	All Wheel Drive	$\dfrac{F_{x1}}{F_{x2}}=\dfrac{k}{1-k}$
$k=1$	Front Wheel Drive	$F_{x1}=F_D,\;F_{x2}=0$

If we insert (4.67) into (4.64) we get

$$\begin{aligned}
\Big(k\cos\delta+(1-k)\Big)\,F_D &- \sin\delta\,F_{y1} &&= -\frac{mv^2}{R}\sin\beta\,,\\
k\sin\delta\,F_D &+ \cos\delta\,F_{y1} + F_{y2} &&= \frac{mv^2}{R}\cos\beta\,,\\
a_1 k\sin\delta\,F_D &+ a_1\cos\delta\,F_{y1} - a_2\,F_{y2} &&= 0\,.
\end{aligned} \tag{4.68}$$

This equations can be resolved for the drive force

$$F_D = \frac{\dfrac{a_2}{a_1+a_2}\,cos\beta\,\sin\delta - \sin\beta\,cos\delta}{k+(1-k)\,\cos\delta}\,\frac{mv^2}{R}\,. \tag{4.69}$$

The drive force vanishes, if

$$\frac{a_2}{a_1+a_2}\,cos\beta\,\sin\delta = \sin\beta\,cos\delta \quad \text{oder} \quad \frac{a_2}{a_1+a_2}\,\tan\delta = \tan\beta \tag{4.70}$$

holds. This corresponds with the Ackermann geometry.

But the Ackermann geometry holds only for small lateral accelerations. In real driving situations the side slip angle of a vehicle at the center of gravity is always smaller then the Ackermann side slip angle. Then, due to $\tan\beta < \frac{a_2}{a_1+a_2}\,\tan\delta$ a drive force $F_D > 0$ is needed to overcome the 'cornering resistance' of the vehicle.

4.3 Simple Handling Model

4.3.1 Forces

The tire forces at the wheel of one axle are combined to one resulting force. Tire torques, the rolling resistance and aerodynamic forces and torques applied at the vehicle remain unrespected.

Unlike with the kinematic tire model, now small lateral motions in the contact points are permitted. At small lateral slips, the lateral force can be approximated by a linear approach

$$F_y \;=\; c_S \, s_y \tag{4.71}$$

where c_S is a constant depending on the wheel load F_z and the lateral slip s_y is defined by (2.53).

Because the vehicle is neither accelerated nor decelerated, the rolling condition is fulfilled at every wheel

$$r_D \, \Omega \;=\; e_x^T \, v_{0P} \; . \tag{4.72}$$

Here r_D is the dynamic tire radius, v_{0P} the contact point velocity and e_x the unit vector in longitudinal direction.

With the lateral tire speed

$$v_y \;=\; e_y^T \, v_{0P} \tag{4.73}$$

and the rolling condition (4.72) the lateral slip can be calculated from

$$s_y \;=\; \frac{-e_y^T \, v_{0P}}{|\, e_x^T \, v_{0P} \,|} \; , \tag{4.74}$$

with e_y labelling the unit vector in the tire's lateral direction.

So the motions of the vehicle model, Fig. 4.13, within the x_0, y_0 plane are only influenced by the lateral forces

$$F_{y1} \;=\; c_{S1} \, s_{y_{A_1}} \; ; F_{y2} \;=\; c_{S2} \, s_{y_{A_2}} \; . \tag{4.75}$$

4.3.2 Kinematics

At the single-track vehicle model, as drawn in Fig. 4.13, the yaw motion of the vehicle is described by the angle γ. The vehicle velocity at the center of gravity is given as constant

$$v \;=\; const. \tag{4.76}$$

With the side slip angle β the vehicle velocity can be expressed in the vehicle fixed frame x_F, y_F, z_F

$$v_{S_F,F} = \begin{bmatrix} v \, \cos\beta \\ v \, \sin\beta \\ 0 \end{bmatrix} \; . \tag{4.77}$$

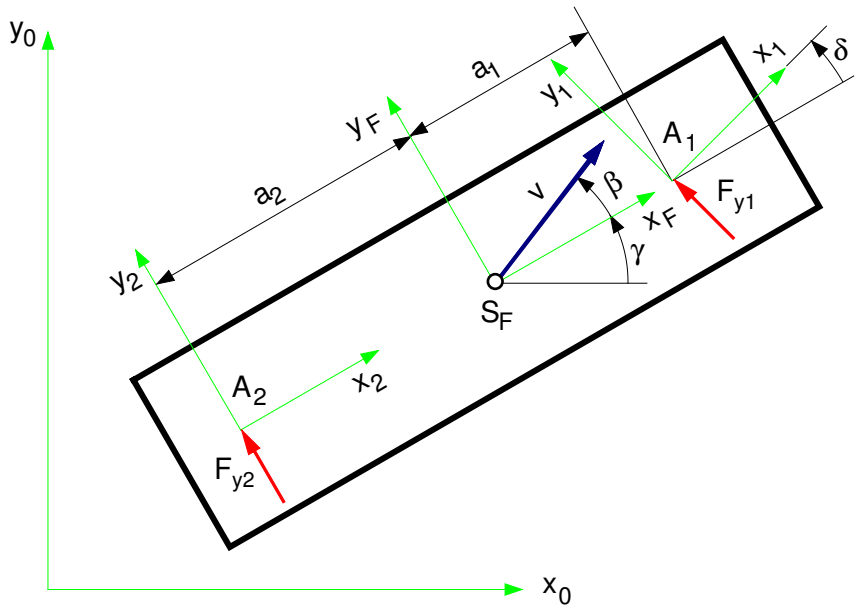

Figure 4.13: Single Track Vehicle Model

For the calculation of the lateral slips, the speed vectors and the unit vectors in longitudinal and lateral direction of the single axles are needed. One gets

$$e_{x_1,F} = \begin{bmatrix} \cos\delta \\ \sin\delta \\ 0 \end{bmatrix}, \quad e_{y_1,F} = \begin{bmatrix} -\sin\delta \\ \cos\delta \\ 0 \end{bmatrix}, \quad v_{0A_1,F} = \begin{bmatrix} v\,\cos\beta \\ v\,\sin\beta + a_1\,\dot{\gamma} \\ 0 \end{bmatrix} \tag{4.78}$$

and

$$e_{x_2,F} = \begin{bmatrix} 1 \\ 0 \\ 0 \end{bmatrix}, \quad e_{y_2,F} = \begin{bmatrix} 0 \\ 1 \\ 0 \end{bmatrix}, \quad v_{0A_2,F} = \begin{bmatrix} v\,\cos\beta \\ v\,\sin\beta - a_2\,\dot{\gamma} \\ 0 \end{bmatrix}. \tag{4.79}$$

4.3.3 Lateral Slips

With (4.79), the lateral slip at the front axle follows from (4.74):

$$s_{y_{A1}} = \frac{+\sin\delta\,(v\,\cos\beta) - \cos\delta\,(v\,\sin\beta + a_1\,\dot{\gamma})}{|\,\cos\delta\,(v\,\cos\beta) + \sin\delta\,(v\,\sin\beta + a_1\,\dot{\gamma})\,|}\,. \tag{4.80}$$

The lateral slip at the rear axle is given by

$$s_{y_{A2}} = -\frac{v\,\sin\beta - a_2\,\dot{\gamma}}{|\,v\,\cos\beta\,|}\,. \tag{4.81}$$

The yaw velocity of the vehicle $\dot{\gamma}$, the side slip angle β and the steering angle δ are considered to be small

$$|\,a_1\,\dot{\gamma}\,| \ll |v|\,; \quad |\,a_2\,\dot{\gamma}\,| \ll |v| \tag{4.82}$$

$$|\,\beta\,| \ll 1 \quad \text{and} \quad |\,\delta\,| \ll 1\,. \tag{4.83}$$

Because the side slip angle always labels the smaller angle between speed vector and vehicle longitudinal axis, instead of $v\,\sin\beta \approx v\,\beta$ the approximation

$$v\,\sin\beta \approx |v|\,\beta \tag{4.84}$$

has to be used.

Respecting (4.82), (4.83) and (4.84), from (4.80) and (4.81) then follow

$$s_{y_{A1}} \;=\; -\beta \;-\; \frac{a_1}{|v|}\,\dot{\gamma} \;+\; \frac{v}{|v|}\,\delta \tag{4.85}$$

and

$$s_{y_{A2}} \;=\; -\beta \;+\; \frac{a_2}{|v|}\,\dot{\gamma}\,. \tag{4.86}$$

4.3.4 Equations of Motion

To derive the equations of motion, the velocities, angular velocities and the accelerations are needed.

For small side slip angles $\beta \ll 1$, (4.77) can be approximated by

$$v_{S_F,F} = \begin{bmatrix} v \\ |v|\,\beta \\ 0 \end{bmatrix}\,. \tag{4.87}$$

The angular velocity is given by

$$\omega_{0F,F} \;=\; \begin{bmatrix} 0 \\ 0 \\ \dot{\gamma} \end{bmatrix}\,. \tag{4.88}$$

If the vehicle accelerations are also expressed in the vehicle fixed frame x_F, y_F, z_F, one finds at constant vehicle speed $v = const$ and with neglecting small higher order terms

$$a_{S_F,F} \;=\; \omega_{0F,F} \times v_{S_F,F} \;+\; \dot{v}_{S_F,F} \;=\; \begin{bmatrix} 0 \\ v\,\dot{\gamma} + |v|\,\dot{\beta} \\ 0 \end{bmatrix}\,. \tag{4.89}$$

The angular acceleration is given by

$$\dot{\omega}_{0F,F} \;=\; \begin{bmatrix} 0 \\ 0 \\ \dot{\omega} \end{bmatrix} \tag{4.90}$$

where the substitution

$$\dot{\gamma} \;=\; \omega \tag{4.91}$$

was used. The linear momentum in the vehicle's lateral direction reads as

$$m\,(v\,\omega + |v|\,\dot{\beta}) \;=\; F_{y1} + F_{y2}\,, \tag{4.92}$$

where, due to the small steering angle, the term $F_{y1}\,\cos\delta$ has been approximated by F_{y1} and m describes the vehicle mass.

With (4.91) the angular momentum delivers

$$\Theta\,\dot{\omega} \;=\; a_1\,F_{y1} - a_2\,F_{y2}\,, \tag{4.93}$$

where Θ names the inertia of vehicle around the vertical axis.

With the linear description of the lateral forces (4.75) and the lateral slips (4.85), (4.86) one gets from (4.92) and (4.93) two coupled, but linear first order differential equations

$$\dot{\beta} \;=\; \frac{c_{S1}}{m\,|v|}\left(\,-\beta - \frac{a_1}{|v|}\,\omega + \frac{v}{|v|}\,\delta\,\right) + \frac{c_{S2}}{m\,|v|}\left(\,-\beta + \frac{a_2}{|v|}\,\omega\,\right) - \frac{v}{|v|}\,\omega\,, \tag{4.94}$$

$$\dot{\omega} \;=\; \frac{a_1\,c_{S1}}{\Theta}\left(\,-\beta - \frac{a_1}{|v|}\,\omega + \frac{v}{|v|}\,\delta\,\right) - \frac{a_2\,c_{S2}}{\Theta}\left(\,-\beta + \frac{a_2}{|v|}\,\omega\,\right), \tag{4.95}$$

which can be written in the form of a state equation

$$\underbrace{\begin{bmatrix}\dot{\beta}\\ \dot{\omega}\end{bmatrix}}_{\dot{x}} = \underbrace{\begin{bmatrix} -\dfrac{c_{S1}+c_{S2}}{m\,|v|} & \dfrac{a_2\,c_{S2}-a_1\,c_{S1}}{m\,|v||v|} - \dfrac{v}{|v|} \\[2ex] \dfrac{a_2\,c_{S2}-a_1\,c_{S1}}{\Theta} & -\dfrac{a_1^2\,c_{S1}+a_2^2\,c_{S2}}{\Theta\,|v|} \end{bmatrix}}_{A} \underbrace{\begin{bmatrix}\beta\\ \omega\end{bmatrix}}_{x} + \underbrace{\begin{bmatrix} \dfrac{v}{|v|}\,\dfrac{c_{S1}}{m\,|v|} \\[2ex] \dfrac{v}{|v|}\,\dfrac{a_1\,c_{S1}}{\Theta} \end{bmatrix}}_{B} \underbrace{\begin{bmatrix}\delta\end{bmatrix}}_{u}\,. \tag{4.96}$$

If a system can be, at least approximatively, described by a linear state equation, then, stability, steady state solutions, transient response, and optimal controlling can be calculated with classic methods of system dynamics.

4.3.5 Stability

4.3.5.1 Eigenvalues

The homogeneous state equation

$$\dot{x} \;=\; A\,x \tag{4.97}$$

describes the eigen-dynamics. If the approach

$$x_h(t) \;=\; x_0\,e^{\lambda t} \tag{4.98}$$

is inserted into (4.97), then the homogeneous equation remains

$$(\lambda\,E \;-\; A)\;x_0 \;=\; 0\,. \tag{4.99}$$

Non-trivial solutions $x_0 \neq 0$ one gets for

$$det\,|\lambda\,E \;-\; A| \;=\; 0\,. \tag{4.100}$$

The eigenvalues λ provide information about the stability of the system.

4.3.5.2 Low Speed Approximation

The state matrix

$$A_{v\to 0} \;=\; \begin{bmatrix} -\dfrac{c_{S1}+c_{S2}}{m\,|v|} & \dfrac{a_2\,c_{S2}-a_1\,c_{S1}}{m\,|v||v|} - \dfrac{v}{|v|} \\ 0 & -\dfrac{a_1^2\,c_{S1}+a_2^2\,c_{S2}}{\Theta\,|v|} \end{bmatrix} \tag{4.101}$$

approximates at $v \to 0$ the eigen-dynamics of vehicles at low speeds.

The matrix (4.101) has the eigenvalues

$$\lambda_{1_{v\to 0}} \;=\; -\frac{c_{S1}+c_{S2}}{m\,|v|} \quad \text{and} \quad \lambda_{2_{v\to 0}} \;=\; -\frac{a_1^2\,c_{S1}+a_2^2\,c_{S2}}{\Theta\,|v|}\,. \tag{4.102}$$

The eigenvalues are real and, independent from the driving direction, always negative.

Thus, vehicles at low speed possess an asymptotically stable driving behavior!

4.3.5.3 High Speed Approximation

At highest driving velocities $v \to \infty$, the state matrix can be approximated by

$$A_{v\to\infty} \;=\; \begin{bmatrix} 0 & -\dfrac{v}{|v|} \\ \dfrac{a_2\,c_{S2}-a_1\,c_{S1}}{\Theta} & 0 \end{bmatrix}. \tag{4.103}$$

Using (4.103) one receives from (4.100) the relation

$$\lambda_{v\to\infty}^2 \;+\; \frac{v}{|v|}\,\frac{a_2\,c_{S2}-a_1\,c_{S1}}{\Theta} \;=\; 0 \tag{4.104}$$

with the solutions

$$\lambda_{1,2_{v\to\infty}} \;=\; \pm\sqrt{-\frac{v}{|v|}\,\frac{a_2\,c_{S2}-a_1\,c_{S1}}{\Theta}}\,. \tag{4.105}$$

When driving forward with $v > 0$, the root argument is positive, if

$$a_2\,c_{S2} - a_1\,c_{S1} \;<\; 0 \tag{4.106}$$

holds. Then however, one eigenvalue is positive and the system is unstable.

Two zero-eigenvalues $\lambda_1 = 0$ and $\lambda_2 = 0$ one gets for

$$a_1\,c_{S1} = a_2\,c_{S2}\,. \tag{4.107}$$

The driving behavior is then indifferent. Slight parameter variations however can lead to an unstable behavior.

With

$$a_2\, c_{S2} - a_1\, c_{S1} \;>\; 0 \quad \text{or} \quad a_1\, c_{S1} < a_2\, c_{S2} \tag{4.108}$$

and $v > 0$ the root argument in (4.105) becomes negative. The eigenvalues are then imaginary, and disturbances lead to undamped vibrations.

To avoid instability, high-speed vehicles have to satisfy the condition (4.108).

The root argument in (4.105) changes at backward driving its sign. A vehicle showing stable driving behavior at forward driving becomes unstable at fast backward driving!

4.3.6 Steady State Solution

4.3.6.1 Side Slip Angle and Yaw Velocity

With a given steering angle $\delta = \delta_0$, after a certain time, a stable system reaches steady state. With $x_{st} = const.$ or $\dot{x}_{st} = 0$, the state equation (4.96) is reduced to a linear system of equations

$$A\, x_{st} \;=\; -B\, u\;. \tag{4.109}$$

With the elements from the state matrix A and the vector B one gets from (4.109) two equations to determine the steady state side slip angle β_{st} and the steady state angular velocity ω_{st} at a constant given steering angle $\delta = \delta_0$

$$|v|\,(c_{S1} + c_{S2})\,\beta_{st} \;+\; (m\,v\,|v| + a_1\,c_{S1} - a_2\,c_{S2})\,\omega_{st} \;=\; v\,c_{S1}\,\delta_0\;, \tag{4.110}$$

$$|v|\,(a_1\,c_{S1} - a_2\,c_{S2})\,\beta_{st} \;+\; (a_1^2\,c_{S1} + a_2^2\,c_{S2})\,\omega_{st} \;=\; v\,a_1\,c_{S1}\,\delta_0\;, \tag{4.111}$$

where the first equation has been multiplied by $-m\,|v|\,|v|$ and the second with $-\Theta\,|v|$. The solution can be derived from

$$\beta_{st} \;=\; \frac{\begin{vmatrix} v\,c_{S1}\,\delta_0 & m\,v\,|v| + a_1\,c_{S1} - a_2\,c_{S2} \\ v\,a_1\,c_{S1}\,\delta_0 & a_1^2\,c_{S1} + a_2^2\,c_{S2} \end{vmatrix}}{\begin{vmatrix} |v|\,(c_{S1} + c_{S2}) & m\,v\,|v| + a_1\,c_{S1} - a_2\,c_{S2} \\ |v|\,(a_1\,c_{S1} - a_2\,c_{S2}) & a_1^2\,c_{S1} + a_2^2\,c_{S2} \end{vmatrix}} \tag{4.112}$$

and

$$\omega_{st} \;=\; \frac{\begin{vmatrix} |v|\,(c_{S1} + c_{S2}) & v\,c_{S1}\,\delta_0 \\ |v|\,(a_1\,c_{S1} - a_2\,c_{S2}) & v\,a_1\,c_{S1}\,\delta_0 \end{vmatrix}}{\begin{vmatrix} |v|\,(c_{S1} + c_{S2}) & m\,v\,|v| + a_1\,c_{S1} - a_2\,c_{S2} \\ |v|\,(a_1\,c_{S1} - a_2\,c_{S2}) & a_1^2\,c_{S1} + a_2^2\,c_{S2} \end{vmatrix}} \tag{4.113}$$

The denominator results in

$$det_D \;=\; |v|\,\big(\; c_{S1}\,c_{S2}\,(a_1 + a_2)^2 \;+\; m\,v\,|v|\,(a_2\,c_{S2} - a_1\,c_{S1})\;\big)\;. \tag{4.114}$$

For a non vanishing denominator $det_D \neq 0$ steady state solutions exist

$$\beta_{st} = \frac{v}{|v|} \frac{a_2 - m\,v\,|v| \dfrac{a_1}{c_{S2}\,(a_1+a_2)}}{a_1 + a_2 + m\,v\,|v| \dfrac{a_2\,c_{S2} - a_1\,c_{S1}}{c_{S1}\,c_{S2}\,(a_1+a_2)}}\,\delta_0\,, \tag{4.115}$$

$$\omega_{st} = \frac{v}{a_1 + a_2 + m\,v\,|v| \dfrac{a_2\,c_{S2} - a_1\,c_{S1}}{c_{S1}\,c_{S2}\,(a_1+a_2)}}\,\delta_0\,. \tag{4.116}$$

At forward driving vehicles $v > 0$ the steady state side slip angle, starts with the kinematic value

$$\beta_{st}^{v\to 0} = \frac{v}{|v|}\frac{a_2}{a_1+a_2}\,\delta_0 \quad \text{and} \quad \omega_{st}^{v\to 0} = \frac{v}{a_1+a_2}\,\delta_0 \tag{4.117}$$

and decreases with increasing speed. At speeds larger then

$$v_{\beta_{st}=0} = \sqrt{\frac{a_2\,c_{S2}\,(a_1+a_2)}{a_1\,m}} \tag{4.118}$$

the side slip angle changes the sign.

Using the kinematic value of the yaw velocity equation (4.116) can be written as

$$\omega_{st} = \frac{v}{a_1+a_2}\,\frac{1}{1 + \dfrac{|v|}{v}\left(\dfrac{v}{v_{ch}}\right)^2}\,\delta_0\,, \tag{4.119}$$

where

$$v_{ch} = \sqrt{\frac{c_{S1}\,c_{S2}\,(a_1+a_2)^2}{m\,(a_2\,c_{S2} - a_1\,c_{S1})}} \tag{4.120}$$

is called the 'characteristic' speed of the vehicle.

Because the rear wheels are not steered, higher slip angles at the rear axle can only be reached by slanting the car.

In Fig. 4.14 the side slip angle β, and the driven curve radius R are plotted versus the driving speed v. The steering angle has been set to $\delta_0 = 1.4321°$, in order to let the vehicle drive a circle with the radius $R_0 = 100\,m$ at $v \to 0$. The actually driven circle radius R has been calculated via

$$\omega_{st} = \frac{v}{R}\,. \tag{4.121}$$

Some concepts for an additional steering of the rear axle were trying to keep the vehicle's side slip angle to zero by an appropriate steering or controlling. Due to numerous problems production stage could not yet be reached.

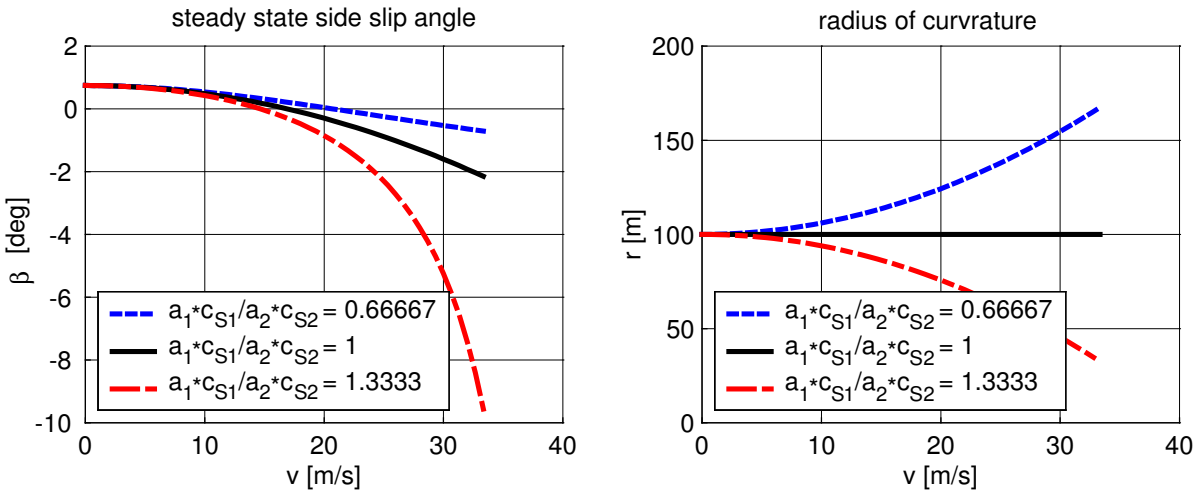

m=700 kg; a_1=1.2 m; $c_{S1} = 80\,000\ Nm$; $c_{S2} = \begin{matrix} 110\,770\ Nm \\ 73\,846\ Nm \\ 55\,385\ Nm \end{matrix}$

Θ=1000 $kg\,m^2$; a_2=1.3 m;

Figure 4.14: Steady State Cornering

4.3.6.2 Steering Tendency

After reaching the steady state solution, the vehicle moves in a circle. When inserting (4.121) into (4.116) and resolving for the steering angle, one gets

$$\delta_0 \;=\; \frac{a_1 + a_2}{R} \;+\; m\,\frac{v^2}{R}\,\frac{v}{|v|}\,\frac{a_2\,c_{S2} - a_1\,c_{S1}}{c_{S1}\,c_{S2}\,(a_1 + a_2)}\,. \tag{4.122}$$

The first term is the Ackermann steering angle, which follows from (4.2) with the wheel base $a = a_1 + a_2$ and the approximation for small steering angles $\tan\delta_0 \approx \delta_0$.

The Ackermann-steering angle provides a good approximation for slowly moving vehicles, because at $v \to 0$ the second expression in (4.122) becomes neglectably small.

At higher speeds, depending on the value of $a_2\,c_{S2} - a_1\,c_{S1}$ and the driving direction (forward: $v > 0$, backward: $v < 0$), the necessary steering angle differs from the Ackermann-steering angle. The difference is proportional to the lateral acceleration

$$a_y \;=\; \frac{v^2}{R}\,. \tag{4.123}$$

At $v > 0$ the steering tendency of a vehicle is defined by the position of the center of gravity a_1, a_2 and the cornering stiffnesses at the axles c_{S1}, c_{S2}.

The various steering tendencies are arranged in the table 4.1.

• understeer	$\delta_0 > \delta_0^A$	or	$a_1\, c_{S1} < a_2\, c_{S2}$	or	$\dfrac{a_1\, c_{S1}}{a_2\, c_{S2}} < 1$
• neutral	$\delta_0 = \delta_0^A$	or	$a_1\, c_{S1} = a_2\, c_{S2}$	or	$\dfrac{a_1\, c_{S1}}{a_2\, c_{S2}} = 1$
• oversteer	$\delta_0 < \delta_0^A$	or	$a_1\, c_{S1} > a_2\, c_{S2}$	or	$\dfrac{a_1\, c_{S1}}{a_2\, c_{S2}} > 1$

Table 4.1: Steering Tendency of a Vehicle at Forward Driving

4.3.6.3 Slip Angles

With the conditions for a steady state solution $\dot{\beta}_{st} = 0$, $\dot{\omega}_{st} = 0$ and the relation (4.121), the equations of motion (4.92) and (4.93) can be dissolved for the lateral forces

$$\begin{aligned} F_{y1_{st}} &= \frac{a_2}{a_1 + a_2}\, m\, \frac{v^2}{R}\,, \\ F_{y2_{st}} &= \frac{a_1}{a_1 + a_2}\, m\, \frac{v^2}{R} \end{aligned} \qquad \text{or} \qquad \frac{a_1}{a_2} = \frac{F_{y2_{st}}}{F_{y1_{st}}}\,. \tag{4.124}$$

With the linear tire model (4.71) one gets

$$F_{y1_{st}} = c_{S1}\, s_{y_{A1}}^{st} \quad \text{and} \quad F_{y2_{st}} = c_{S2}\, s_{y_{A2}}^{st}\,, \tag{4.125}$$

where $s_{y_{A1}}^{st}$ and $s_{y_{A2}}^{st}$ label the steady state lateral slips at the axles. From (4.124) and (4.125) now follows

$$\frac{a_1}{a_2} = \frac{F_{y2_{st}}}{F_{y1_{st}}} = \frac{c_{S2}\, s_{y_{A2}}^{st}}{c_{S1}\, s_{y_{A1}}^{st}} \qquad \text{or} \qquad \frac{a_1\, c_{S1}}{a_2\, c_{S2}} = \frac{s_{y_{A2}}^{st}}{s_{y_{A1}}^{st}}\,. \tag{4.126}$$

That means, at a vehicle with understeer tendency ($a_1\, c_{S1} < a_2\, c_{S2}$) during steady state cornering the slip angles at the front axle are larger then the slip angles at the rear axle, $s_{y_{A1}}^{st} > s_{y_{A2}}^{st}$. So, the steering tendency can also be determined from the slip angle at the axles.

4.3.7 Influence of Wheel Load on Cornering Stiffness

With identical tires at the front and rear axle, given a linear influence of wheel load on the raise of the lateral force over the lateral slip,

$$c_{S1}^{lin} = c_S\, F_{z1} \quad \text{and} \quad c_{S2}^{lin} = c_S\, F_{z2}\,. \tag{4.127}$$

holds. The weight of the vehicle $G = m\, g$ is distributed over the axles according to the position of the center of gravity

$$F_{z1} = \frac{a_2}{a_1 + a_2}\, G \quad \text{and} \quad .F_{z2} = \frac{a_1}{a_1 + a_2}\, G \tag{4.128}$$

With (4.127) and (4.128) one gets

$$a_1\, c_{S1}^{lin} \;=\; a_1\, c_S\, \frac{a_2}{a_1 + a_2}\, G \tag{4.129}$$

and

$$a_2\, c_{S2}^{lin} \;=\; a_2\, c_S\, \frac{a_1}{a_1 + a_2}\, G\,. \tag{4.130}$$

A vehicle with identical tires would thus be steering neutrally at a linear influence of wheel load on the slip stiffness, because of

$$a_1\, c_{S1}^{lin} \;=\; a_2\, c_{S2}^{lin} \tag{4.131}$$

The fact that the lateral force is applied behind the center of the contact area at the caster offset distance, leads, because of $a_1 \rightarrow a_1 - \frac{v}{|v|}\, n_{L_1}$ and $a_2 \rightarrow a_2 + \frac{v}{|v|}\, n_{L_1}$ to a stabilization of the driving behavior, independent from the driving direction.

At a real tire, a digressive influence of wheel load on the tire forces is observed, Fig. 4.15.

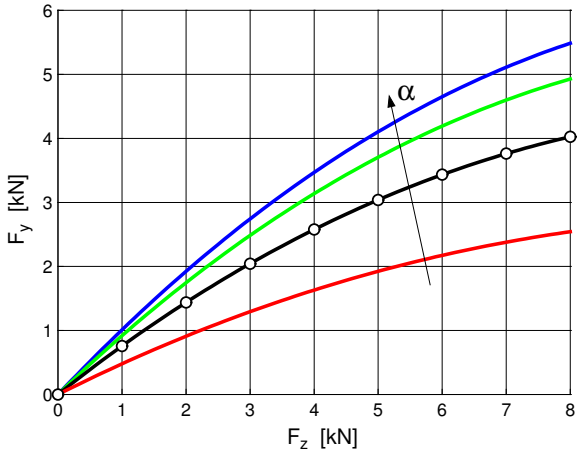

$F_z\ [N]$	$F_y\ [N]$
0	0
1000	758
2000	1438
3000	2043
4000	2576
5000	3039
6000	3434
7000	3762
8000	4025

Figure 4.15: Lateral Force F_y over Wheel Load F_z at different Slip Angles

According to (4.93) the rotation of the vehicle is stable, if the torque from the lateral forces F_{y1} and F_{y2} is aligning, i.e.

$$a_1\, F_{y1} - a_2\, F_{y2} \;<\; 0 \tag{4.132}$$

holds.

At a vehicle with the wheel base $a = 2.45\, m$ the axle loads $F_{z1} = 4000\, N$ and $F_{z2} = 3000\, N$ deliver the position of the center of gravity $a_1 = 1.05\, m$ and $a_2 = 1.40\, m$. At equal slip on front and rear axle one receives from the table in 4.15 $F_{y1} = 2576\, N$ and $F_{y2} = 2043\, N$. With this, the condition (4.132) delivers $1.05 * 2576 - 1.45 * 2043 = -257.55$. The value is significantly negative and thus stabilizing.

Vehicles with $a_1 < a_2$ have a stable, i.e. understeering driving behavior.

If the axle load at the rear axle is larger than at the front axle ($a_1 > a_2$), a stable driving behavior can generally only be achieved with different tires.

At increasing lateral acceleration the vehicle is more and more supported by the outer wheels. At a sufficiently rigid vehicle body the wheel load differences can differ, because of different kinematics (roll support) or different roll stiffnesses

Due to the digressive influence of wheel load, the deliverable lateral force at an axle decreases with increasing wheel load difference.

If the wheel load is split more strongly at the front axle than at the rear axle, the lateral force potential at the front axle decreases more than at the rear axle and the vehicle becomes more stable with increasing lateral force, i.e. more understeering.

5 Vertical Dynamics

5.1 Goals

The aim of vertical dynamics is the tuning of body suspension and damping to guarantee good driving comfort, resp. a minimal stress of the load at sufficient safety.

The stress of the load can be judged fairly well by maximal or integral values of the body accelerations.

The wheel load F_z is linked to the longitudinal F_x and lateral force F_y by the coefficient of friction. The digressive influence of F_z on F_x and F_y as well as instationary processes at the increase of F_x and F_y in the average lead to lower longitudinal and lateral forces at wheel load variations.

Maximal driving safety can therefore be achieved with minimal variations of wheel load. Small variations of wheel load also reduce the stress on the track.

The comfort of a vehicle is subjectively judged by the driver. In literature, different approaches of describing the human sense of vibrations by different metrics can be found.

Transferred to vehicle vertical dynamics, the driver primarily registers the amplitudes and accelerations of the body vibrations. These values are thus used as objective criteria in practice.

5.2 Basic Tuning

5.2.1 Simple Models

Fig. 5.1 shows simple quarter car models, that are suitable for basic investigations of body and axle vibrations.

At normal vehicles the wheel mass m is in relation to the respective body mass M much smaller $m \ll M$. The coupling of wheel and body movement can thus be neglected for basic investigations.

In describing the vertical movements of the body, the wheel movements remain unrespected. If the wheel movements are in the foreground, then body movements can be neglected.

The equations of motion for the models read as

$$M\,\ddot{z}_B \;+\; d_S\,\dot{z}_B \;+\; c_S\,z_B \;=\; d_S\,\dot{z}_R \;+\; c_S\,z_R \tag{5.1}$$

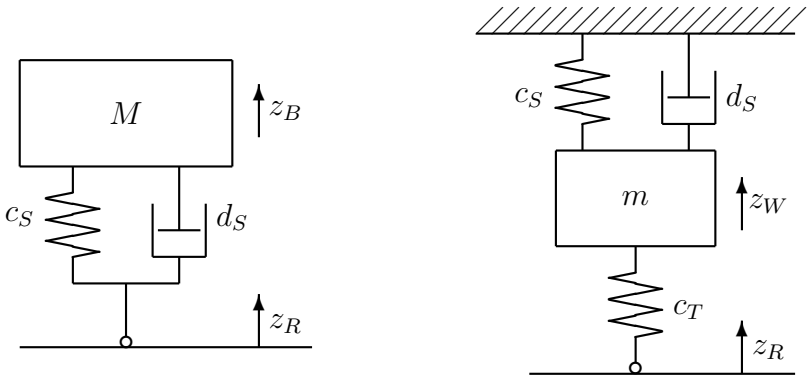

Figure 5.1: Simple Vehicle and Suspension Model

and

$$m\,\ddot{z}_W \;+\; d_S\,\dot{z}_W \;+\; (c_S + c_T)\,z_W \;=\; c_T\,z_R\,, \tag{5.2}$$

where z_B and z_W label the vertical movements of the body and the wheel mass out of the equilibrium position. The constants c_S, d_S describe the body suspension and damping, and c_T the vertical stiffness of the tire. The tire damping is hereby neglected against the body damping.

5.2.2 Track

The track is given as function in the space domain

$$z_R \;=\; z_R(x)\,. \tag{5.3}$$

In (5.1) also the time gradient of the track irregularities is necessary. From (5.3) firstly follows

$$\dot{z}_R \;=\; \frac{d\,z_R}{dx}\,\frac{dx}{dt}\,. \tag{5.4}$$

At the simple model the speed, with which the track irregularities are probed equals the vehicle speed $dx/dt = v$. If the vehicle speed is given as time function $v = v(t)$, the covered distance x can be calculated by simple integration.

5.2.3 Spring Preload

The suspension spring is loaded with the respective vehicle load. At linear spring characteristics the steady state spring deflection is calculated from

$$f_0 \;=\; \frac{M\,g}{c_S}\,. \tag{5.5}$$

At a conventional suspension without niveau regulation a load variation $M \rightarrow M + \triangle M$ leads to changed spring deflections $f_0 \rightarrow f_0 + \triangle f$. In analogy to (5.5) the additional deflection follows from

$$\triangle f \;=\; \frac{\triangle M\, g}{c_S}\,. \tag{5.6}$$

If for the maximum load variation $\triangle M^{max}$ the additional spring deflection is limited to $\triangle f^{max}$ the suspension spring rate can be estimated by a lower bound

$$c_S \;\geq\; \frac{\triangle M^{max}\, g}{\triangle f^{max}}\,. \tag{5.7}$$

5.2.4 Eigenvalues

At an ideally even track the right side of the equations of motion (5.1), (5.2) vanishes because of $z_R = 0$ and $\dot{z}_R = 0$. The remaining homogeneous second order differential equations can be written as

$$\ddot{z} \;+\; 2\,\delta\,\dot{z} \;+\; \omega_0^2\, z \;=\; 0\,. \tag{5.8}$$

The respective attenuation constants δ and the undamped natural circular frequency ω_0 for the models in Fig. 5.1 can be determined from a comparison of (5.8) with (5.1) and (5.2). The results are arranged in table 5.1.

Motions	Differential Equation	attenuation constant	undamped Eigenfrequency
Body	$M\,\ddot{z}_B \;+\; d_S\,\dot{z}_B \;+\; c_S\,z_B \;=\; 0$	$\delta_B = \dfrac{d_S}{2\,M}$	$\omega_{B_0}^2 = \dfrac{c_S}{M}$
Wheel	$m\,\ddot{z}_W \;+\; d_S\,\dot{z}_W \;+\; (c_S + c_T)\,z_W \;=\; 0$	$\delta_R = \dfrac{d_S}{2\,m}$	$\omega_{W_0}^2 = \dfrac{c_S + c_T}{m}$

Table 5.1: Attenuation Constants and undamped natural Frequencies

With

$$z \;=\; z_0\, e^{\lambda t} \tag{5.9}$$

the equation

$$(\lambda^2 + 2\,\delta\,\lambda + \omega_0^2)\, z_0\, e^{\lambda t} \;=\; 0\,. \tag{5.10}$$

follows from (5.8). For

$$\lambda^2 + 2\,\delta\,\lambda + \omega_0^2 \;=\; 0 \tag{5.11}$$

also non-trivial solutions are possible. The characteristical equation (5.11) has got the solutions

$$\lambda_{1,2} = -\delta \pm \sqrt{\delta^2 - \omega_0^2} \tag{5.12}$$

For $\delta^2 \geq \omega_0^2$ the eigenvalues $\lambda_{1,2}$ are real and, because of $\delta \geq 0$ not positive, $\lambda_{1,2} \leq 0$. Disturbances $z(t=0) = z_0$ with $\dot{z}(t=0) = 0$ then subside exponentially.

With $\delta^2 < \omega_0^2$ the eigenvalues become complex

$$\lambda_{1,2} = -\delta \pm i\,\sqrt{\omega_0^2 - \delta^2}\,. \tag{5.13}$$

The system now executes damped oscillations.

The case

$$\delta^2 \;=\; \omega_0^2\,, \qquad \text{bzw.} \qquad \delta \;=\; \omega_0 \tag{5.14}$$

describes, in the sense of stability, an optimal system behavior.

Wheel and body mass, as well as tire stiffness are fixed. The body spring rate can be calculated via load variations, cf. section 5.2.3. With the abbreviations from table 5.1 now damping parameters can be calculated from (5.14) which provide with

$$(d_S)_{opt_1} \;=\; 2\,M\,\sqrt{\frac{c_S}{M}} \;=\; 2\,\sqrt{c_S\,M} \tag{5.15}$$

optimal body vibrations and with

$$(d_S)_{opt_2} \;=\; 2\,m\,\sqrt{\frac{c_S + c_T}{m}} \;=\; 2\,\sqrt{(c_S + c_T)\,m} \tag{5.16}$$

optimal wheel vibrations.

5.2.5 Free Vibrations

Fig. 5.2 shows the time response of a damped single-mass oscillator to an initial disturbance as results from the solution of the differential equation (5.8). The system here has been started without initial speed $\dot{z}(t=0) = 0$ but with the initial disturbance $z(t=0) = z_0$. If the attenuation constant δ is increased at first the system approaches the steady state position $z_G = 0$ faster and faster, but then, a slow asymptotic behavior occurs.

Counting differences from the steady state positions as errors $\epsilon(t) = z(t) - z_G$, allows judging the quality of the vibration. The overall error is calculated by

$$\epsilon_G^2 \;=\; \int_{t=0}^{t=t_E} z(t)^2\,dt\,, \tag{5.17}$$

where the time t_E have to be chosen appropriately. If the overall error becomes a Minimum

$$\epsilon_G^2 \;\rightarrow\; Minimum \tag{5.18}$$

the system approaches the steady state position as fast as possible.

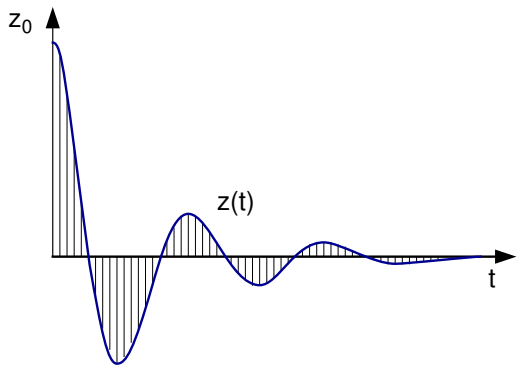

Figure 5.2: Damped Vibration

To judge driving comfort and safety the deflections z_B and accelerations $\ddot{z}_B$ of the body and the dynamic wheel load variations are used.

The system behavior is optimal if the parameters M, m, c_S, d_S, c_T result from the demands for comfort

$$\epsilon_{G_C}^2 \;=\; \int_{t=0}^{t=t_E} \Big\{ \left(g_1\, z_B \right)^2 \;+\; \left(g_2\, \ddot{z}_B \right)^2 \Big\}\, dt \;\rightarrow\; Minimum \tag{5.19}$$

and safety

$$\epsilon_{G_S}^2 \;=\; \int_{t=0}^{t=t_E} \left(c_T\, z_W \right)^2 dt \;\rightarrow\; Minimum\,. \tag{5.20}$$

With the factors g_1 and g_2 deflections and accelerations can be weighted differently. In the equations of motion for the body (5.1) the terms $M\,\ddot{z}_B$ and $c_S\, z_B$ are added. With $g_1 = M$ and $g_2 = c_S$ one gets system-fitted weighting factors.

At the damped single-mass oscillator, the integrals in (5.19) can, for $t_E \rightarrow \infty$, still be solved analytically. One gets

$$\epsilon_{G_C}^2 \;=\; z_{B_0}^2\, \frac{c_S}{M}\, \frac{1}{2} \left[\frac{d_S}{M} \;+\; 2\, \frac{c_S}{d_S} \right] \tag{5.21}$$

and

$$\epsilon_{G_S}^2 \;=\; z_{W_0}^2\, c_T^2\, \frac{1}{2} \left[\frac{d_S}{c_S + c_T} \;+\; \frac{m}{d_S} \right]. \tag{5.22}$$

Small body suspension stiffnesses $c_S \rightarrow 0$ or large body masses $M \rightarrow \infty$ make the comfort criteria (5.21) small $\epsilon_{G_C}^2 \rightarrow 0$ and so guarantee a high driving comfort.

A great body mass however is uneconomic. The body suspension stiffness cannot be reduced arbitrary low values, because then load variations would lead to too great changes in static deflection. At fixed values for c_S and M the damper can be designed in a way that minimizes the comfort criteria (5.21). From the necessary condition for a minimum

$$\frac{\partial \epsilon_{G_C}^2}{\partial d_S} \;=\; z_{B_0}^2\, \frac{c_S}{M}\, \frac{1}{2} \left[\frac{1}{M} \;-\; 2\, \frac{c_S}{d_S^2} \right] \;=\; 0 \tag{5.23}$$

the optimal damper parameter

$$(d_S)_{opt_3} = \sqrt{2\,c_S\,M}\,, \tag{5.24}$$

that guarantees optimal comfort follows.

Small tire spring stiffnesses $c_T \to 0$ make the safety criteria (5.22) small $\epsilon^2_{G_S} \to 0$ and thus reduce dynamic wheel load variations. The tire spring stiffness can however not be reduced to arbitrary low values, because this would cause too great tire deformation. Small wheel masses $m \to 0$ and/or a hard body suspension $c_S \to \infty$ also reduce the safety criteria (5.22). The use of light metal rims increases, because of wheel weight reduction, the driving safety of a car.

Hard body suspensions contradict driving comfort.

With fixed values for c_S, c_T and m here the damper can also be designed to minimize the safety criteria (5.22). From the necessary condition of a minimum

$$\frac{\partial \epsilon^2_{G_S}}{\partial d_S} = z^2_{W_0}\,c^2_T\,\frac{1}{2}\left[\frac{1}{c_S + c_T} - \frac{m}{d^2_S}\right] = 0 \tag{5.25}$$

the optimal damper parameter

$$(d_S)_{opt_4} = \sqrt{(c_S + c_T)\,m}\,, \tag{5.26}$$

follows, which guarantees optimal safety.

5.3 Nonlinear Force Elements

5.3.1 Quarter Car Model

The principal influence of nonlinear characteristics on driving comfort and safety can already be displayed on a quarter car model Fig. 5.3.

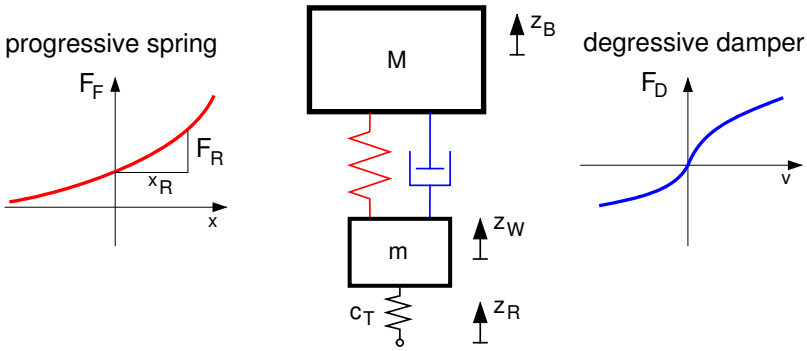

Figure 5.3: Quarter Car Model with nonlinear Characteristics

The equations of motion are given by

$$\begin{aligned} M\,\ddot{z}_B &= F - M\,g \\ m\,\ddot{z}_W &= F_z - F - m\,g\,, \end{aligned} \tag{5.27}$$

where $g = 9.81\ m/s^2$ labels the constant of gravity and M, m are the masses of body and wheel. The coordinates z_B and z_W are measured from the equilibrium position.

Thus, the wheel load F_z is calculated from the tire deflection $z_W - z_R$ via the tire stiffness c_T

$$F_z \;=\; (M+m)\,g \;+\; c_T\,(z_R - z_W)\,. \tag{5.28}$$

The first term in (5.28) describes the static part. The condition $F_z \geq 0$ takes the wheel lift off into consideration.

Body suspension and damping are described with nonlinear functions of the spring travel

$$x \;=\; z_W - z_B \tag{5.29}$$

and the spring velocity

$$v \;=\; \dot{z}_W - \dot{z}_B\,, \tag{5.30}$$

where $x > 0$ and $v > 0$ marks the spring and damper compression.

The damper characteristics are modelled as digressive functions with the parameters $p_i \geq 0$, $i = 1(1)4$

$$F_D(v) \;=\; \begin{cases} p_1\,v\,\dfrac{1}{1\;+\;p_2\,v} & v \geq 0 \quad \text{(Druck)} \\ \\ p_3\,v\,\dfrac{1}{1\;-\;p_4\,v} & v < 0 \quad \text{(Zug)} \end{cases} . \tag{5.31}$$

A linear damper with the constant d is described by $p_1 = p_3 = d$ and $p_2 = p_4 = 0$.

For the spring characteristics the approach

$$F_F(x) \;=\; M\,g \;+\; \frac{F_R}{x_R}\,x\,\frac{1-p_5}{1-p_5\,\dfrac{|x|}{x_R}} \tag{5.32}$$

is used, where $M\,g$ marks the spring preload. With parameters within the range $0 \leq p_5 < 1$, one gets differently progressive characteristics. The special case $p_5 = 0$ describes a linear spring with the constant $c = F_R/x_R$. All spring characteristics run through the operating point x_R, F_R. Thus, at a real vehicle, one gets the same roll angle, independent from the chosen progression at a certain lateral acceleration.

5.3.2 Random Road Profile

The vehicle moves with the constant speed $v_F = const$. When starting at $t = 0$ at the point $x_F = 0$, the current position of the car is given by

$$x_F(t) = v_F * t\,. \tag{5.33}$$

The irregularities of the track can thus be written as time function $z_R = z_R(x_F(t))$

The calculation of optimal characteristics, i.e. the determination of the parameters p_1 to p_5, is done for three different tracks. Each track consists of a number of single obstacles, which lengths and heights are distributed randomly. Fig. 5.4 shows the first track profile $z_{S_1}(x)$. Profiles number two and three are generated from the first by multiplication with the factors 3 and 5, $z_{S_2}(x) = 3 * z_{S_1}(x)$, $z_{S_3}(x) = 5 * z_{S_1}(x)$.

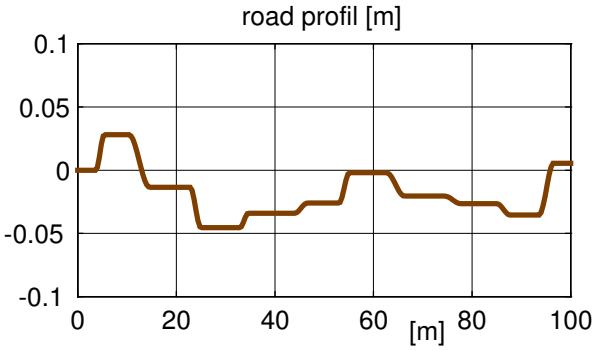

Figure 5.4: Track profile 1

5.3.3 Vehicle Data

The values, arranged in table 5.2, describe the respective body mass of a fully loaded and an empty bus over the rear axle, the mass of the rear axle and the sum of tire stiffnesses at the twin tire rear axle.

vehicle data	M [kg]	m [kg]	F_R [N]	x_R [m]	c_T [N/m]
fully loaded	11 000	800	40 000	0.100	3 200 000
unloaded	6 000	800	22 500	0.100	3 200 000

Table 5.2: Vehicle Data

The vehicle possesses niveau-regulation. Therefore also the force F_R at the reference deflection x_R has been fitted to the load.

The vehicle drives at the constant speed $v_F = 20\,m/s$.

The five parameters, p_i, $i = 1(1)5$, which describe the nonlinear spring-damper characteristics, are calculated by minimizing quality functions.

5.3.4 Quality Criteria

In a first quality function, driving comfort and safety are to be judged by body accelerations and wheel load variations

$$G_{K1} = \frac{1}{t_E - t_0} \int_{t_0}^{t_E} \left\{ \underbrace{\left(\frac{\ddot{z}_B}{g}\right)^2}_{\text{comfort}} + \underbrace{\left(\frac{F_z^D}{F_z^S}\right)^2}_{\text{safety}} \right\} \quad . \tag{5.34}$$

The body acceleration $\ddot{z}_B$ has been normalized to the constant of gravity g. The dynamic share of the normal force $F_z^D = c_T\,(z_R - z_W)$ follows from (5.28) with the static normal force $F_z^S = (M + m)\,g$.

At real cars the spring travel is limited. The quality criteria is therefore extended accordingly

$$G_{K2} = \frac{1}{t_E - t_0} \int_{t_0}^{t_E} \left\{ \underbrace{\left(\frac{\ddot{z}_B}{g}\right)^2}_{\text{comfort}} + \underbrace{\left(\frac{P_D}{P_S}\right)^2}_{\text{safety}} + \underbrace{\left(\frac{x}{x_R}\right)^2}_{\text{spring travel}} \right\} , \tag{5.35}$$

where the spring travel x, defined by (5.29), has been related to the reference travel x_r.

According to the covered distance and chosen driving speed, the times used in (5.34) and (5.35) have been set to $t_0 = 0\ s$ and $t_E = 8\ s$

5.3.5 Optimal Parameter

5.3.5.1 Linear Characteristics

Judging the driving comfort and safety after the criteria G_{K1} and restricting to linear characteristics, with $p_1 = p_3$ and $p_2 = p_4 = p_5 = 0$, one gets the results arrayed in table5.3. The spring

road	load	optimal parameter p_1	p_2	p_3	p_4	p_5	parts in quality criteria comfort	safety
1	+	35766	0	35766	0	0	0.002886	0.002669
2	+	35763	0	35763	0	0	0.025972	0.024013
3	+	35762	0	35762	0	0	0.072143	0.066701
1	−	20298	0	20298	0	0	0.003321	0.003961
2	−	20300	0	20300	0	0	0.029889	0.035641
3	−	19974	0	19974	0	0	0.083040	0.098385

Table 5.3: Linear Spring and Damper Parameter optimized via G_{K1}

constants $c = F_R/x_r$ for the fully loaded and the empty vehicle are defined by the numerical values in table 5.2. One gets:$c_{empty} = 225\,000 N/m$ and $c_{loaded} = 400\,000 N/m$.

As expected the results are almost independent from the track. The optimal value of the damping parameter $d = p_1 = p_3$ however is strongly dependent on the load state. The optimizing quasi fits the damper constant to the changed spring rate.

The loaded vehicle is more comfortable and safer.

5.3.5.2 Nonlinear Characteristics

The results of the optimization with nonlinear characteristics are arrayed in the table 5.4.

The optimizing has been started with the linear parameters from table 5.3. Only at the extreme track irregularities of profile 3, linear spring characteristics, with $p_5 = 0$, appear, Fig. 5.6. At moderate track irregularities, one gets strongly progressive springs.

road	load	optimal parameter p_1	p_2	p_3	p_4	p_5	parts in quality criteria comfort	safety
1	+	16182	0.000	20028	1.316	0.9671	0.000265	0.001104
2	+	52170	2.689	57892	1.175	0.6983	0.009060	0.012764
3	+	1875	3.048	311773	4.295	0.0000	0.040813	0.050069
1	−	13961	0.000	17255	0.337	0.9203	0.000819	0.003414
2	−	16081	0.808	27703	0.454	0.6567	0.012947	0.031285
3	−	9942	0.227	64345	0.714	0.0000	0.060992	0.090250

Table 5.4: Nonlinear Spring and Damper Characteristics optimized via G_{K1}

The dampers are digressive and differ in jounce and rebound.

In comparison to the linear model a significant improvement can be noted, especially in comfort.

While driving over profile 2 with the loaded vehicle, the body accelerations are displayed in Fig. 5.5.

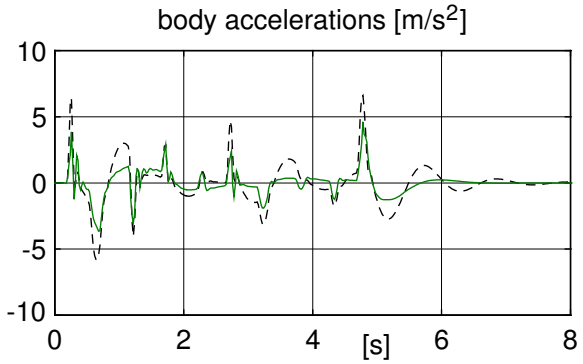

Figure 5.5: Body Accelerations optimized via G_{K1} (· · · linear, — nonlinear)

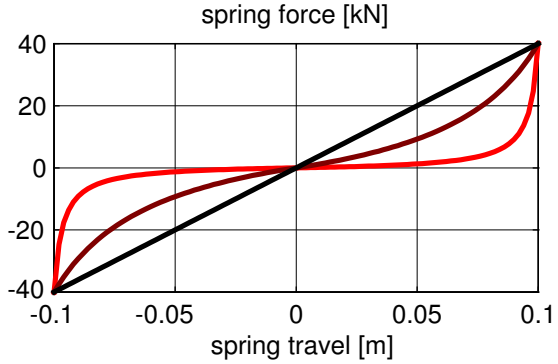

Figure 5.6: Optimal Spring Characteristics for fully loaded Vehicle; Criteria: G_{K1}

The extremely progressive spring characteristics, optimal at smooth tracks (profile 1), cannot be realize practically in that way. Due to the small spring stiffness around the equilibrium position, small disturbances cause only small aligning forces. Therefore it would take long to reach the equilibrium position again. Additionally, friction forces in the body suspension would cause a large deviation of the equilibrium position.

5.3.5.3 Limited Spring Travel

Practically relevant results can only be achieved, if additionally the spring travels are judged. Firstly, linear characteristics are assumed again, table 5.5.

road	load	optimal parameter p_1	p_2	p_3	p_4	p_5	parts in quality criteria comfort	safety	s. travel
1	$+$	68727	0	68727	0	0	0.003854	0.003673	0.006339
2	$+$	68666	0	68666	0	0	0.034657	0.033025	0.057097
3	$+$	72882	0	72882	0	0	0.098961	0.094431	0.148757
1	$-$	35332	0	35332	0	0	0.004417	0.004701	0.006638
2	$-$	35656	0	35656	0	0	0.040049	0.042507	0.059162
3	$-$	37480	0	37480	0	0	0.112143	0.116722	0.155290

Table 5.5: Linear Spring and Damper Characteristics optimized via G_{K2}

The judging numbers for comfort and safety have worsened by limiting the spring travel in comparison to the values from table 5.3.

In order to receive realistic spring characteristics, now the parameter p_5 has been limited upwards to $p_5 \leq 0.6$. Starting with the linear parameters from table 5.5, an optimization via

road	load	optimal parameter p_1	p_2	p_3	p_4	p_5	parts in quality criteria comfort	safety	s. travel
1	$+$	175530	12.89	102997	3.437	0.4722	0.001747	0.002044	0.005769
2	$+$	204674	5.505	107498	1.234	0.6000	0.015877	0.018500	0.050073
3	$+$	327864	4.844	152732	1.165	0.5140	0.064980	0.068329	0.116555
1	$-$	66391	5.244	50353	2.082	0.5841	0.002380	0.003943	0.005597
2	$-$	37246	0.601	37392	0.101	0.5459	0.024524	0.033156	0.059717
3	$-$	89007	1.668	68917	0.643	0.3614	0.085001	0.102876	0.125042

Table 5.6: Nonlinear Spring and Damper Characteristics optimized via G_{K2}

criteria G_{K2} delivers the results arranged in table 5.6.

A vehicle with G_{K2}-optimized characteristics manages the travel over uneven tracks with significantly less spring travel than a vehicle with G_{K1}-optimized characteristics, Fig. 5.7.

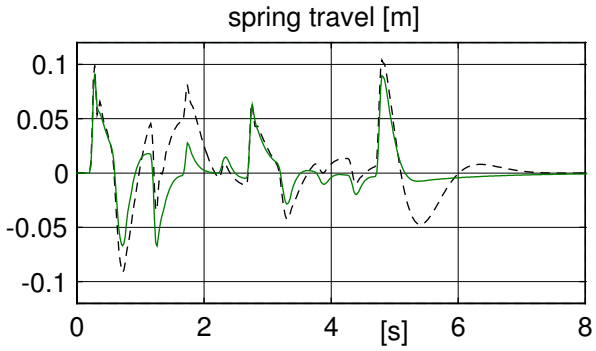

Figure 5.7: Spring Travels on Profile 2 (- - - G_{K1}, — G_{K2})

The reduced spring travel however reduces comfort and safety.

Still, in most cases, the according part of the quality criteria in table 5.6 lie even below the values of the linear model from table 5.3, where the spring travels have not been evaluated.

By the use of nonlinear characteristics, the comfort and safety of a vehicle can so be improved, despite limitation of the spring travel.

The optimal damper characteristics strongly depend on the roughness of the track, Fig. 5.8.

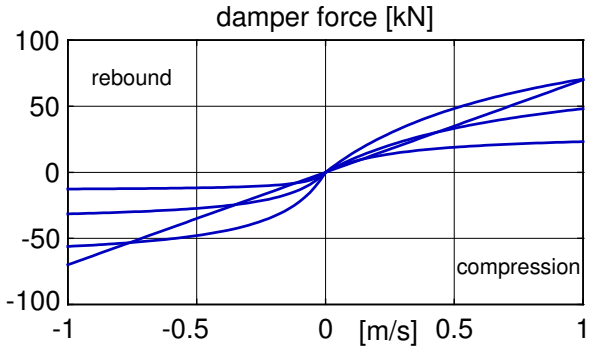

Figure 5.8: Optimal Damper Characteristics according to Table 5.6

Optimal comfort and safety are only guaranteed if the dampers are fitted to the load as well as to the roughness of the track.

5.4 Dynamic Force Elements

5.4.1 System Response in the Frequency Domain

5.4.1.1 First Harmonic Oscillation

The effect of dynamic force elements is usually judged in the frequency domain. For this, on test rigs or in simulation, the force element is periodically excited with different frequencies

$f_0 \le f_i \le f_E$ and amplitudes $A_{min} \le A_j \le A_{max}$

$$x_e(t) \;=\; A_j \,\sin(2\pi\, f_i\, t)\;. \tag{5.36}$$

Starting at $t = 0$ at $t = T_0$ with $T_0 = 1/f_0$ the system usually is in a steady state condition. Due to the nonlinear system behavior the system response is periodic, yet not harmonic. For the evaluation thus the answer, e.g. the measured or calculated force F, each within the intervals $t_{S_i} \le t \le t_{S_i}+T_i$, is approximated by harmonic functions as good as possible

$$\underbrace{F(t)}_{\substack{measured\\ or\\ calculated}} \;\approx\; \underbrace{\alpha_i\,\sin(2\pi\, f_i\, t) + \beta_i\,\cos(2\pi\, f_i\, t)}_{first\ harmonic\ approximation}\;. \tag{5.37}$$

The coefficients α_i and β_i can be calculated from the demand for a minimal overall error

$$\frac{1}{2}\int\limits_{t_{S_i}}^{t_{S_i}+T_i} \Big(\alpha_i\,\sin(2\pi\, f_i\, t)+\beta_i\,\cos(2\pi\, f_i\, t) - F(t)\Big)^2\, dt \quad\longrightarrow\quad Minimum\;. \tag{5.38}$$

The differentiation of (5.38) with respect to α_i and β_i delivers two linear equations as necessary conditions

$$\begin{aligned}
\int\limits_{t_{S_i}}^{t_{S_i}+T_i} \Big(\alpha_i\,\sin(2\pi\, f_i\, t)+\beta_i\,\cos(2\pi\, f_i\, t) - F(t)\Big)^2\,\sin(2\pi\, f_i\, t)\, dt &= 0\\
\int\limits_{t_{S_i}}^{t_{S_i}+T_i} \Big(\alpha_i\,\sin(2\pi\, f_i\, t)+\beta_i\,\cos(2\pi\, f_i\, t) - F(t)\Big)^2\,\cos(2\pi\, f_i\, t)\, dt &= 0
\end{aligned} \tag{5.39}$$

with the solutions

$$\begin{aligned}
\alpha_i &= \frac{\int F\,\sin\,dt\,\int\cos^2\,dt - \int F\,\cos\,dt\,\int \sin\,\cos\,dt}{\int\sin^2\,dt\,\int\cos^2\,dt - 2\,\int\sin\,\cos\,dt}\\
\beta_i &= \frac{\int F\,\cos\,dt\,\int\sin^2\,dt - \int F\,\sin\,dt\,\int \sin\,\cos\,dt}{\int\sin^2\,dt\,\int\cos^2\,dt - 2\,\int\sin\,\cos\,dt}
\end{aligned}\;, \tag{5.40}$$

where the integral limits and arguments of sine and cosine have no longer been written.

Because it is integrated exactly over one period $t_{S_i} \le t \le t_{S_i}+T_i$, for the integrals in (5.40)

$$\int \sin\,\cos\,dt \;=\; 0\,;\quad \int\sin^2\,dt \;=\; \frac{T_i}{2}\,;\quad \int\cos^2\,dt \;=\; \frac{T_i}{2} \tag{5.41}$$

holds, and as solution

$$\alpha_i \;=\; \frac{2}{T_i}\int F\,\sin\,dt\,,\qquad \beta_i \;=\; \frac{2}{T_i}\int F\,\cos\,dt\,. \tag{5.42}$$

remains. These however are exactly the first two coefficients of a Fourier–Approximation.

In practice, the frequency response of a system is not determined punctual, but continuous. For this, the system is excited by a sweep-sine.

5.4.1.2 Sweep-Sine Excitation

In analogy to the simple sine-function

$$x_e(t) \;=\; A\,\sin(2\pi\,f\,t)\,, \tag{5.43}$$

where the period duration $T = 1/f$ appears as pre-factor at differentiation

$$\dot{x}_e(t) \;=\; A\,2\pi\,f\,\cos(2\pi\,f\,t) \;=\; \frac{2\pi}{T}\,A\,\cos(2\pi\,f\,t)\,, \tag{5.44}$$

now a generalized sine-function can be constructed. Starting with

$$x_e(t) \;=\; A\,\sin(2\pi\,h(t)) \tag{5.45}$$

the time derivative results in

$$\dot{x}_e(t) \;=\; A\,2\pi\,\dot{h}(t)\,\cos(2\pi\,h(t))\,. \tag{5.46}$$

Now we demand, that the function $h(t)$ delivers a period, that fades linear in time, i.e:

$$\dot{h}(t) \;=\; \frac{1}{T(t)} \;=\; \frac{1}{p - q\,t}\,, \tag{5.47}$$

where $p > 0$ and $q > 0$ are constants yet to determine. From (5.47)

$$h(t) \;=\; -\,\frac{1}{q}\ln(p - q\,t) \;+\; C \tag{5.48}$$

follows. The initial condition $h(t = 0) = 0$ fixes the integration constant

$$C \;=\; \frac{1}{q}\ln p\,. \tag{5.49}$$

Inserting (5.49) in (5.48), a sine-like function follows from (5.45)

$$x_e(t) \;=\; A\,\sin\Big(\frac{2\pi}{q}\,\ln\frac{p}{p - q\,t}\Big)\,, \tag{5.50}$$

delivering linear fading period durations.

The important zero values for determining the period duration lie at

$$\frac{1}{q}\,\ln\frac{p}{p - q\,t_n} \;=\; 0,\,1,\,2, \quad \text{or} \quad \frac{p}{p - q\,t_n} \;=\; e^{n\,q}\,,\ \text{mit}\ n = 0,\,1,\,2, \tag{5.51}$$

and

$$t_n \;=\; \frac{p}{q}(1 - e^{-n\,q})\,,\ n = 0,\,1,\,2,\,. \tag{5.52}$$

The time difference between two zero points determines the period

$$\begin{aligned} T_n \;&=\; t_{n+1} - t_n \;=\; \frac{p}{q}(1 - e^{-(n+1)\,q} - 1 + e^{-n\,q}) \\ T_n \;&=\; \frac{p}{q}\,e^{-n\,q}\,(1 - e^{-q}) \end{aligned} \qquad ,\ n = 0,\,1,\,2,\,. \tag{5.53}$$

For the first $(n = 0)$ and last $(n = N)$ period one finds

$$\begin{aligned} T_0 &= \frac{p}{q}\,(1 - e^{-q}) \\ T_N &= \frac{p}{q}\,(1 - e^{-q})\,e^{-N\,q} \;=\; T_0\,e^{-N\,q} \end{aligned} \quad . \tag{5.54}$$

With the frequency range to investigate given by the initial f_0 and final f_E frequency, the parameters q and the relation q/p can be calculated from (5.54)

$$q \;=\; \frac{1}{N}\,\ln\frac{f_E}{f_0}\,, \qquad \frac{q}{p} \;=\; f_0\left\{1 - \left[\frac{f_E}{f_0}\right]^{\frac{1}{N}}\right\}, \tag{5.55}$$

with N fixing the number of frequency intervals. The passing of the whole frequency range then takes

$$t_{N+1} \;=\; \frac{1 - e^{-(N+1)\,q}}{q/p} \tag{5.56}$$

seconds.

5.4.2 Hydro-Mount

5.4.2.1 Principle and Model

For elastic suspension of engines in vehicles very often specially developed hydro-mounts are used. The dynamic nonlinear behavior of these components guarantees a good acoustic decoupling, but simultaneously provides sufficient damping.

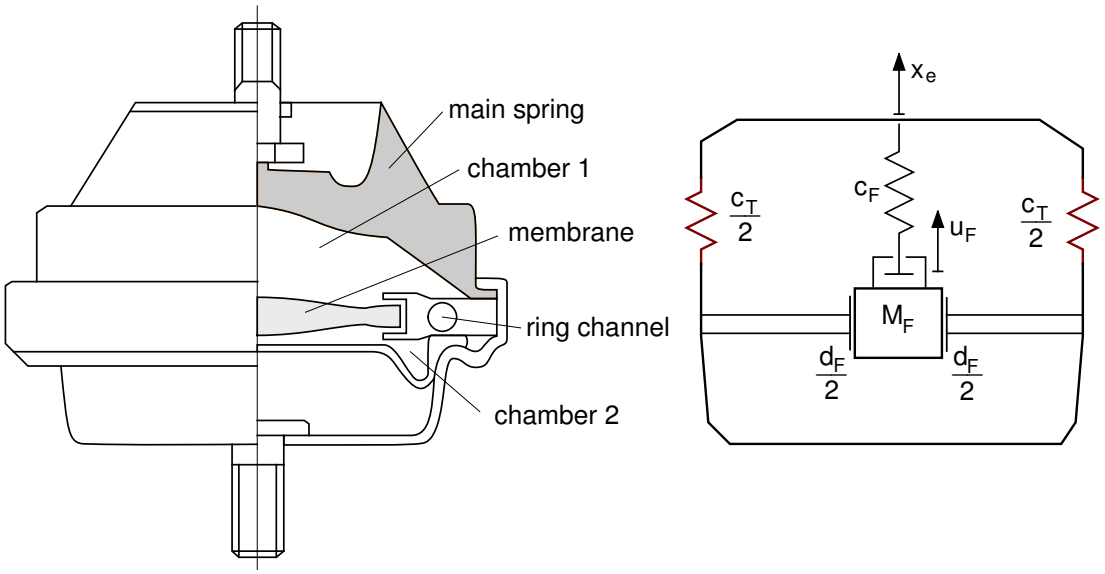

Figure 5.9: Hydro-Mount

Fig. 5.9 shows the principle and mathematical model of a hydro-mount.

At small deformations the change of volume in chamber 1 is compensated by displacements of the membrane. When the membrane reaches the stop, the liquid in chamber 1 is pressed through a ring channel into chamber 2. The relation of the chamber cross section to ring channel cross section is very large. Thus the fluid is moved through the ring channel at very high speed. From this remarkable inertia and resistance forces (damping forces) result.

The force effect of a hydro-mount is combined from the elasticity of the main spring and the volume change in chamber 1.

With u_F labelling the displacement of the generalized fluid mass M_F,

$$F_H \;=\; c_T\, x_e \;+\; F_F(x_e - u_F) \tag{5.57}$$

holds, where the force effect of the main spring has been approximated by a linear spring with the constant c_T.

With M_{FR} as actual mass in the ring channel and the cross sections A_K, A_R of chamber and ring channel the generalized fluid mass is given by

$$M_F \;=\; \left(\frac{A_K}{A_R}\right)^2 M_{FR}\,. \tag{5.58}$$

The fluid in chamber 1 is not being compressed, unless the membrane can evade no longer. With the fluid stiffness c_F and the membrane clearance s_F one gets

$$F_F(x_e - u_F) \;=\; \begin{cases} c_F\left((x_e - u_F) \;+\; s_F\right) & (x_e - u_F) \;<\; -s_F \\ 0 \qquad\qquad\qquad\qquad\quad \text{for} & |x_e - u_f| \;\leq\; s_F \\ c_F\left((x_e - u_F) \;-\; s_F\right) & (x_e - u_f) \;>\; +s_F \end{cases} \tag{5.59}$$

The hard transition from clearance $F_F = 0$ and fluid compression, resp. chamber deformation with $F_F \neq 0$ is not realistic and leads to problems, even with the numeric solution. The function (5.59) is therefore smoothed by a parable in the range $|x_e - u_f| \leq 2 * s_F$.

The motions of the fluid mass cause friction losses in the ring channel, which are, at first approximation, proportional to the speed,

$$F_D \;=\; d_F\, \dot{u}_F\,. \tag{5.60}$$

The equation of motion for the fluid mass then reads as

$$M_F\, \ddot{u}_F \;=\; -\,F_F - F_D\,. \tag{5.61}$$

The membrane clearing makes (5.61) nonlinear, and only solvable by numerical integration. The nonlinearity also affects the overall force (5.57) in the hydro-mount.

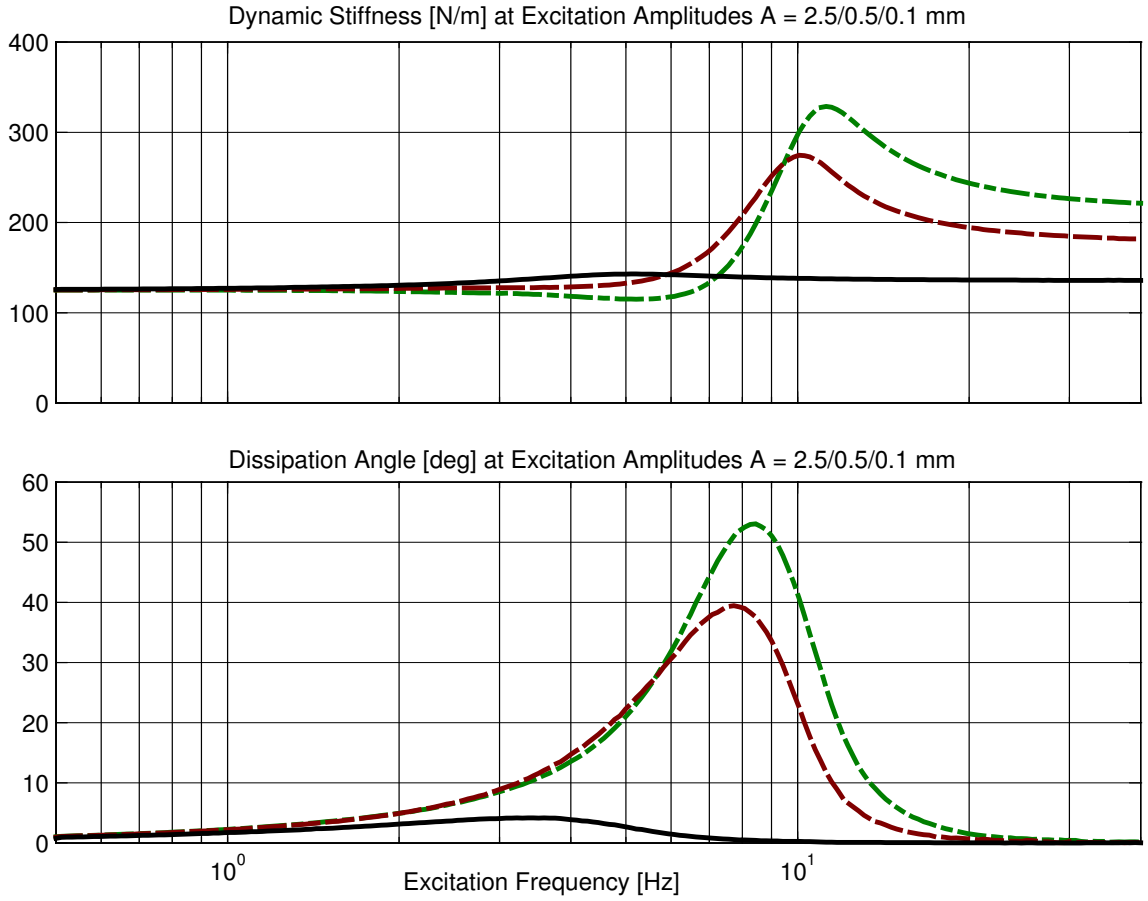

Figure 5.10: Dynamic Stiffness [N/mm] and Dissipation Angle [deg] for a Hydro-Mount

5.4.2.2 Dynamic Force Characteristics

The dynamic stiffness and the dissipation angle of a hydro bearing are displayed in Fig. 5.10 over the frequency. The dissipation angle is a measurement for the damping.

The simulation is based on the following system parameters

m_F	$=$	$25\ kg$	generalized fluid mass
c_T	$=$	$125\,000\ N/m$	stiffness of main spring
d_F	$=$	$750\ N/(m/s)$	damping constant
c_F	$=$	$100\,000\ N/m$	fluid stiffness
s_F	$=$	$0.0002\ mm$	clearance in membrane bearing

By the nonlinear and dynamic behavior a very good compromise between noise isolation and vibration damping can be achieved.

5.5 Different Influences on Comfort and Safety

5.5.1 Vehicle Model

Ford motor company uses the vehicle dynamics program `VeDynA` (Vehicle Dynamic Analysis) for comfort calculations.

The theoretical basics of the program – modelling, generating the equations of motion, and numeric solution – have been published in the book ”G.Rill: Simulation von Kraftfahrzeugen, Vieweg 1994”

Through program extensions, adaption to different operating systems, installation of interfaces to other programs and a menu-controlled in- and output, `VeDynA` has been subsequently developed to marketability by the company TESIS GmbH in Munich.

At the tire model `tmeasy`(tire model easy to use), as integrated in `VeDynA`, the tire forces are calculated dynamically with respect to the tire deformation. For every tire a contact calculation is made. The local inclination of the track is determined from three track points. From the statistic characteristics of a track, spectral density and waviness, two-dimensional, irregular tracks are calculated.

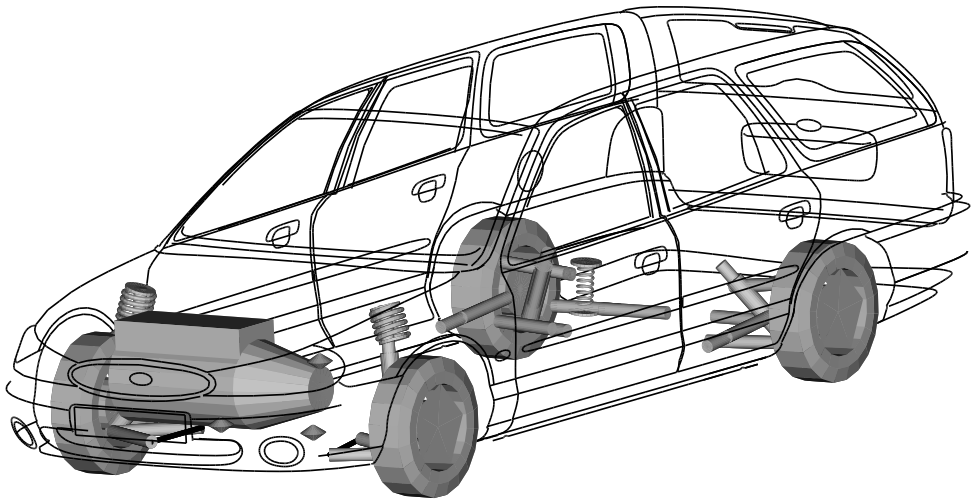

Figure 5.11: Car Model

The vehicle model is specially distinguished by the following details:

- nonlinear elastic kinematics of the wheel suspensions,
- friction-affected and elastically suspended dampers,
- fully elastic motor suspension by static and dynamic force elements (rubber elements and/or hydro-mounts,
- integrated passenger-seat models.

Beyond this, interfaces to external tire- and force element models are provided. A specially developed integration procedure allows real-time simulation on a PC.

5.5.2 Simulation Results

The vehicle, a Ford Mondeo, occupied by two persons, drives with $v = 80 km/h$ over a country road. The thereby occurring accelerations at the driver's seat rail and the wheel load variations are displayed in Fig. 5.12.

The peak values of the accelerations and the maximal wheel load variations are arranged in the tables 5.7 and 5.8 for the standard car and several modifications.

acceleration	standard	– friction	– seat model	– engine mounts	– comfort bushings
$\ddot{x}_{min}$	-0.7192	-0.7133	-0.7403	-0.5086	-0.7328
$\ddot{x}_{max}$	+0.6543	+0.6100	+0.6695	+0.5092	+0.6886
$\ddot{y}_{min}$	-1.4199	-1.2873	-1.4344	-0.7331	-1.5660
$\ddot{y}_{max}$	+1.3991	+1.2529	+1.3247	+0.8721	+1.2564
$\ddot{z}_{min}$	-4.1864	-3.9986	-4.1788	-3.6950	-4.2593
$\ddot{z}_{max}$	+3.0623	2.7769	+3.1176	+2.8114	+3.1449

Table 5.7: Peak Acceleration Values

$\triangle F_z$	standard	– friction	– seat model	– engine mounts	– comfort bushings
front left	2.3830	2.4507	2.4124	2.3891	2.2394
front right	2.4208	2.3856	2.4436	2.3891	2.4148
rear left	2.1450	2.2616	2.1600	2.1113	2.1018
rear right	2.3355	2.2726	2.3730	2.2997	2.1608

Table 5.8: Wheel Load Variations $\triangle F_z = F_z^{max} - F_z^{min}$

It can be seen, that the damper friction, the passengers, the engine suspension and the compliance of the wheel suspensions, (here:represented by comfort bushings) influence especially the accelerations and with this the driving comfort.

At fine tuning thus all these influences must be respected.

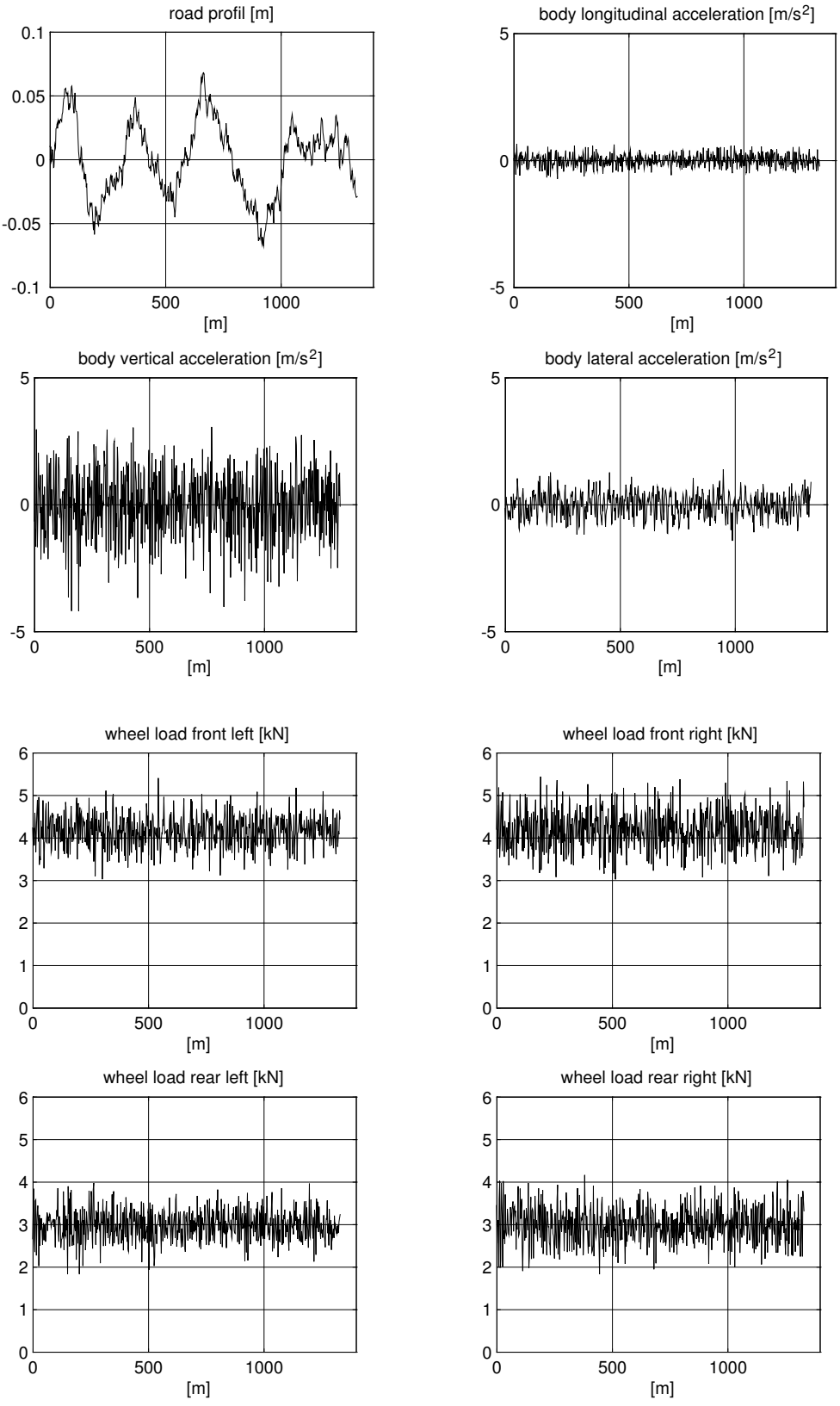

Figure 5.12: Road Profile, Accelerations and Wheel Loads

6 Driving Behavior of Single Vehicles

6.1 Standard Driving Maneuvers

6.1.1 Steady State Cornering

The steering tendency of a real vehicle is determined by the driving maneuver called steady state cornering. The maneuver is performed quasi-static. The driver tries to keep the vehicle on a circle with the given radius R. He slowly increases the driving speed v and, with this, because of $a_y = \frac{v^2}{R}$, the lateral acceleration, until reaching the limit. Typical results are displayed in Fig. 6.1.

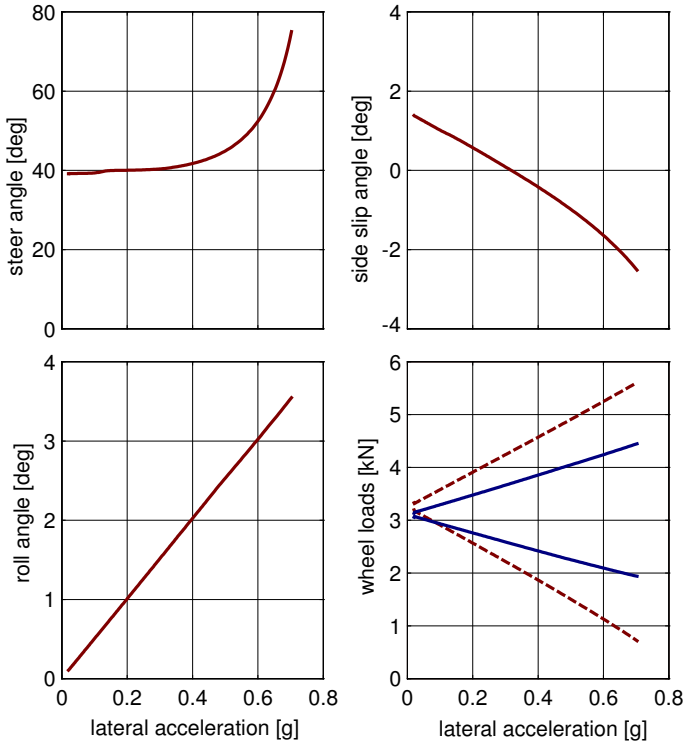

Figure 6.1: Steady State Cornering: Rear-Wheel-Driven Car on $R = 100\,m$

The vehicle is under-steering and thus stable. The inclination in the diagram steering angle over lateral velocity decides, according to (4.122) with (4.123), about the steering tendency and stability behavior.

The nonlinear influence of the wheel load on the tire performance is here used to design a vehicle that is weakly stable, but sensitive to steer input in the lower range of lateral acceleration, and is very stable but less sensitive to steer input in limit conditions.

With the increase of the lateral acceleration the roll angle becomes larger. The overturning torque is intercepted by according wheel load differences between the outer and inner wheels. With a sufficiently rigid frame the use of a anti roll bar at the front axle allows to increase the wheel load difference there and to decrease it at the rear axle accordingly.

The digressive influence of the wheel load on the tire properties, cornering stiffness and maximally possible lateral force is thus stressed more strongly at the front axle and the vehicle becomes more under-steering and stable at increasing lateral acceleration, until, in the limit situation, it drifts out of the curve over the front axle.

Problems occur at front driven vehicles, because, due to the traction, the front axle cannot be relieved at will.

Having a sufficiently large test site, the steady state cornering maneuver can also be carried out at constant speed. There the steering wheel is slowly turned until the vehicle reaches the limit range. That way also weakly motorized vehicles can be tested at high lateral accelerations.

6.1.2 Step Steer Input

The dynamic response of a vehicle is often tested with a step steer input. Methods for the calculation and evaluation of an ideal response, as used in system theory or control technics, can not be used with a real car, for a step input at the steering wheel is not possible in practice. In Fig. 6.2 a real steering angle gradient is displayed.

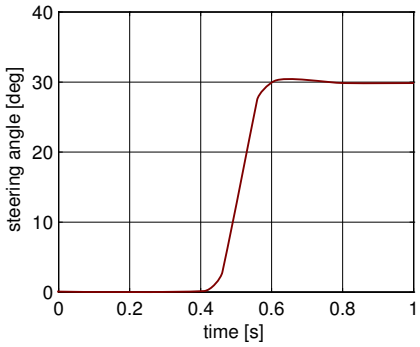

Figure 6.2: Step Steer Input

Not the angle at the steering wheel is the decisive factor for the driving behavior, but the steer angle at the wheels, which can differ from the steering wheel angle because of elasticities,

friction influences and a servo-support. At very fast steering movements also the dynamic raise of tire forces plays an important role.

In practice, a step steer input is usually only used to judge vehicles subjectively. Exceeds in yaw velocity, roll angle and especially sideslip angle are felt as annoying.

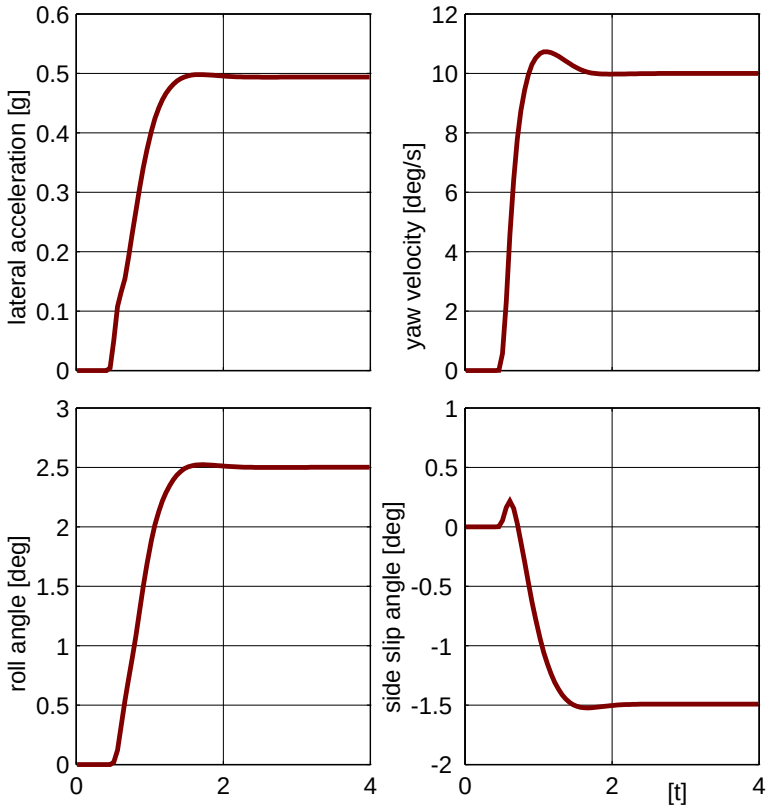

Figure 6.3: Step Steer: Passenger Car at $v = 100\ km/h$

The vehicle behaves dynamically very well, Fig. 6.3. Almost no exceeds at roll angle and lateral acceleration. Small exceeds at yaw velocity and sideslip angle.

6.1.3 Driving Straight Ahead

6.1.3.1 Random Road Profile

The irregularities of a track are of stochastic nature. Fig. 6.4 shows a country road profile in different scalings. To limit the effort at the stochastic description of a track, one usually employs simplifying models.

Instead of a fully two-dimensional description either two parallel tracks are evaluated

$$z = z(x,y) \quad \rightarrow \quad z_1 = z_1(s_1)\,, \quad \text{and} \quad z_2 = z_2(s_2) \tag{6.1}$$

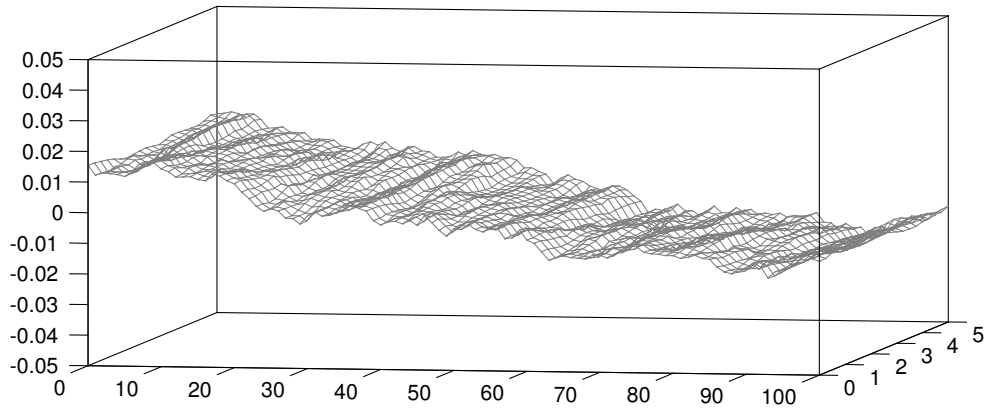

Figure 6.4: Track Irregularities

or one uses an isotropic track. At an isotropic track the statistic properties are direction-independent. Then a two-dimensional track with its stochastic properties can be described by a single random process

$$z \;=\; z(x,y) \quad \rightarrow \quad z \;=\; z(s)\,; \tag{6.2}$$

A normally distributed, stationary and ergodic random process $z = z(s)$ is completely characterized by the first two expectation values, mean value

$$m_z \;=\; \lim_{s\to\infty} \frac{1}{2s} \int_{-s}^{s} z(s)\, ds \tag{6.3}$$

and correlating function

$$R_{zz}(\delta) \;=\; \lim_{s\to\infty} \frac{1}{2s} \int_{-s}^{s} z(s)\, z(s-\delta)\, ds \tag{6.4}$$

. A vanishing mean value $m_z \;=\; 0$ can always be achieved by an appropriate coordinate transformation. The correlation function is symmetric,

$$R_{zz}(\delta) \;=\; R_{zz}(-\delta) \tag{6.5}$$

and

$$R_{zz}(0) \;=\; \lim_{s\to\infty} \frac{1}{2s} \int_{-s}^{s} \big(z(s)\big)^2\, ds \tag{6.6}$$

describes the squared average of z_s.

Stochastic track irregularities are mostly described by power spectral densities (abbreviated by psd). Correlating function and the one-sided power spectral density are linked by the Fourier-transformation

$$R_{zz}(\delta) \;=\; \int_{0}^{\infty} S_{zz}(\Omega)\, \cos(\Omega\delta)\, d\Omega \tag{6.7}$$

where Ω denotes the space circular frequency. With (6.7) follows from (6.6)

$$R_{zz}(0) \;=\; \int_0^\infty S_{zz}(\Omega)\, d\Omega \;. \tag{6.8}$$

The psd thus gives information, how the square average is compiled from the single frequency shares.

The power spectral densities of real tracks can be approximated by the relation[1]

$$S_{zz}(\Omega) \;=\; S_0 \left[\frac{\Omega}{\Omega_0}\right]^{-w} \tag{6.9}$$

Where the reference frequency is fixed to $\Omega_0 = 1\; m^{-1}$. The reference psd $S_0 = S_{zz}(\Omega_0)$ acts as a measurement for unevennes and the waviness w indicates, whether the track has notable irregularities in the short or long wave spectrum.

At real tracks reference-psd and waviness lie within the range

$$1 * 10^{-6}\, m^3 \;\leq\; S_0 \;\leq\; 100 * 10^{-6}\, m^3 \quad \text{and}$$

6.1.3.2 Steering Activity

A straightforward drive upon an uneven track makes continuous steering corrections necessary. The histograms of the steering angle at a driving speed of $v = 90\, km/h$ are displayed in Fig. 6.5.

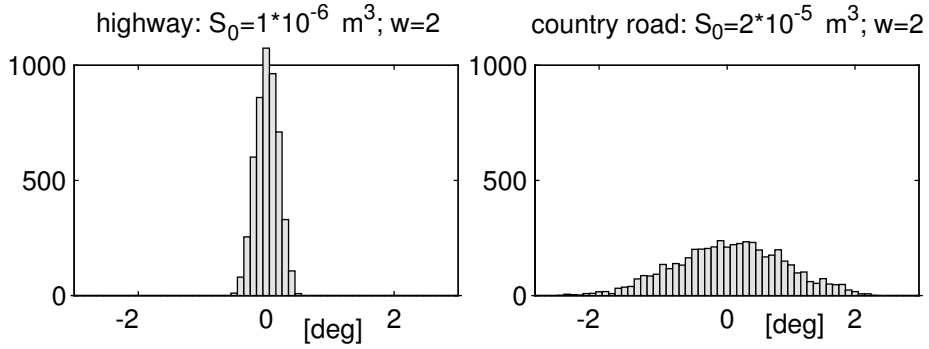

Figure 6.5: Steering Activity on different Roads

The track quality is reflected in the amount of steering actions. The steering activity is often used to judge a vehicle in practice.

[1] cf.: M. Mitschke: Dynamik der Kraftfahrzeuge (Band B), Springer-Verlag, Berlin 1984, S. 29.

6.2 Coach with different Loading Conditions

6.2.1 Data

At trucks and coaches the difference between empty and laden is sometimes very large. In the table 6.1 all relevant data of a travel coach in fully laden and empty condition are arrayed.

vehicle	mass $[kg]$	center of gravity $[m]$	inertias $[kg\,m^2]$
empty	$12\,500$	$-3.800 \mid 0.000 \mid 1.500$	$\begin{matrix} 12\,500 & 0 & 0 \\ 0 & 155\,000 & 0 \\ 0 & 0 & 155\,000 \end{matrix}$
fully laden	$18\,000$	$-3.860 \mid 0.000 \mid 1.600$	$\begin{matrix} 15\,400 & 0 & 250 \\ 0 & 200\,550 & 0 \\ 250 & 0 & 202\,160 \end{matrix}$

Table 6.1: Data for a Laden and Empty Coach

The coach has a wheel base of $a = 6.25\,m$. The front axle with the track width $s_v = 2.046\,m$ has a double wishbone single wheel suspension. The twin-tire rear axle with the track widths $s_h^o = 2.152\,m$ and $s_h^i = 1.492\,m$ is guided by two longitudinal links and an a-arm. The air-springs are fitted to load variations via a niveau-control.

6.2.2 Roll Steer Behavior

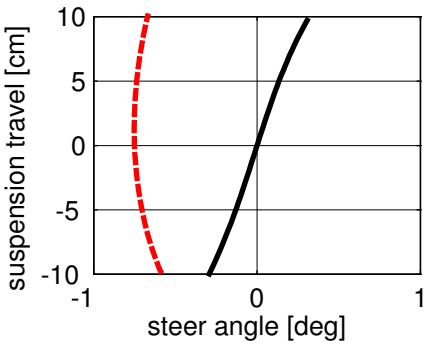

Figure 6.6: Roll Steer: - - front, — rear

While the kinematics at the front axle hardly cause steering movements at roll motions, the kinematics at the rear axle are tuned in a way to cause a notable roll steer effect, Fig. 6.6.

6.2.3 Steady State Cornering

Fig. 6.7 shows the results of a steady state cornering on a $100\ m$-Radius.

The fully occupied vehicle is slightly more understeering than the empty one. The higher wheel loads cause greater tire aligning torques and increase the digressive wheel load influence on the increase of the lateral forces. Additionally roll steering at the rear axle occurs.

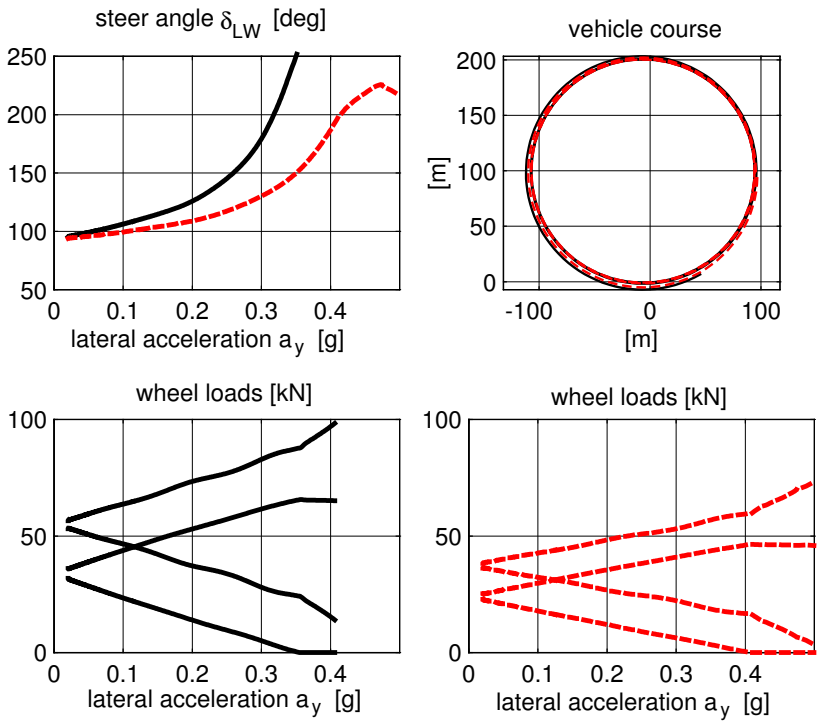

Figure 6.7: Steady State Cornering: Coach - - empty, — fully occupied

In the limit range both vehicles can not be kept on the given radius. Due to the high position of the center of gravity the maximal lateral acceleration is limited by the overturning hazard. At the empty vehicle, the inner front wheel lift off at a lateral acceleration of $a_y \approx 0.4\ g$. If the vehicle is fully occupied, this effect occurs already at $a_y \approx 0.35\ g$.

6.2.4 Step Steer Input

The results of a step steer input at the driving speed of $v = 80\ km/h$ can be seen in Fig. 6.8.

To achieve comparable acceleration values in steady state condition, the step steer input was done at the empty vehicle with $\delta = 90\ Grad$ and at the fully occupied one with $\delta = 135\ Grad$.

The steady state roll angle is at the fully occupied bus 50% larger than at the empty one.

By the niveau-control the air spring stiffness increases with the load. Because the damper effect remains unchange, the fully laden vehicle is not damped as well as the empty one. The results are higher exceeds in the lateral acceleration, the yaw speed and sideslip angle.

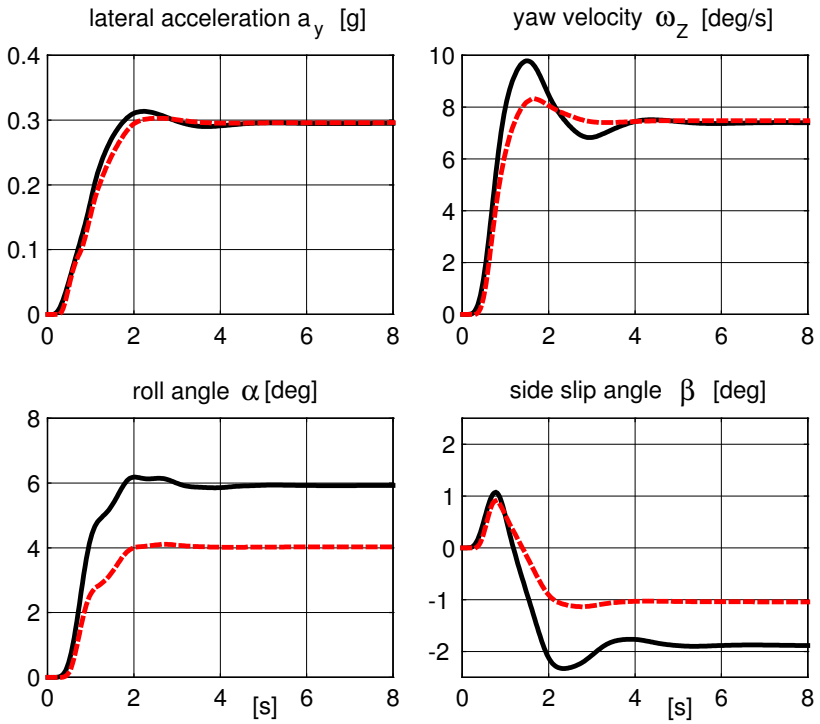

Figure 6.8: Step Steer: - - Coach empty, — Coach fully occupied

6.3 Different Rear Axle Concepts for a Passenger Car

A medium-sized passenger car is equipped in standard design with a semi-trailing rear axle. By accordingly changed data this axle can easily be transformed into a trailing arm or a single wishbone axis.

The semi-trailing axle realized in serial production represents, according to the roll support, Fig. 6.9, a compromise between the trailing arm and the single wishbone.

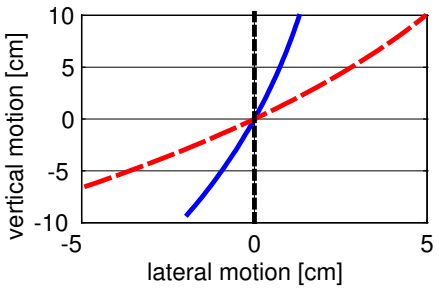

Figure 6.9: Rear Axle Kinematics: — Semi-Trailing Arm, - - Single Wishbone, · · · Trailing Arm

The influences on the driving behavior at steady state cornering on a $100\,m$ radius are shown in Fig. 6.10.

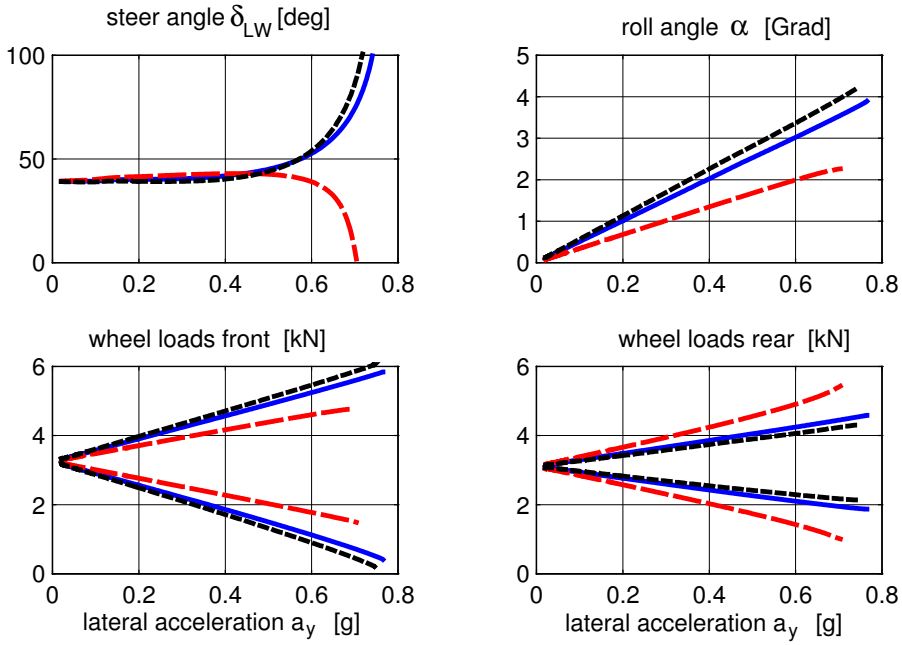

Figure 6.10: Steady State Cornering, — Semi-Trailing Arm, - - Single Wishbone, · · · Trailing Arm

Substituting the semi-trailing arm at the standard car by a single wishbone, one gets, without adaption of the other system parameters, a vehicle, which oversteers in the limit range.

The single wishbone causes, compared to the semi-trailing arm a notably higher roll support. This increases the wheel load difference at the rear axle, Fig. 6.10. Because the wheel load difference is simultaneously reduced at the front axle, the understeer tendency is reduced. In the limit range, this even leads to oversteer behavior.

The vehicle with a trailing arm rear axle is, compared to the serial car, more understeering. The lack of roll support at the rear axle also causes a larger roll angle.

Index